Conformal Printed Graphene Antennas for Wireless Communication and Applications

A thesis submitted to The University of Manchester for the degree of
Doctor of Philosophy
in the Faculty of Science and Engineering

2022

Xinyao Zhou

Faculty of Science and Engineering
Department of Electrical and Electronic Engineering

Contents

List of Figures

List of Tables

List of Abbreviations

2D	Two Dimensional
3D	Three Dimensional
5G	The Fifth Generation
ABS	Acrylonitrile Butadiene Styrene
AFM	Atomic Force Microscopy
AgNW	Silver Nanowire
BP	Black Phosphorus
CCL	Channel Capacity Loss
CNT	Carbon Nanotube
CPW	Co-Planar Waveguide
CuNW	Copper Nanowire
CVD	Chemical Vapor Deposition
DMF	Dimethylformamide
EBG	Electromagnetic Band Gap
ECC	Envelop Correlation Coefficient
EG	Ethylene Glycol
EIRP	Equivalent isotropically radiated power
GO	Graphene Oxide
h-BN	Hexagonal-Boron Nitride
HOPG	High Ordered Pyrolytic Graphite
IoE	Internet Of Everything
IoT	Internet Of Things
IPA	Isopropyl Alcohol

LAN	Local Area Network
LPE	Liquid Phase Exfoliation
LTE	Long-Term Evolution
MIMO	Multiple-Input Multiple-Output
MMIC	Microwave Integrated Circuit
NMP	N-Methyl-2-Pyrrolidone
OLED	Organic Light-Emitting Diodes
PDMS	Poly Dimethyl Sulfate
PET	Polyethylene Terephthalate
PLA	Polylactic Acid
RF	Radio Frequency
RFID	Radio Frequency Identification
SEM	Scanning Electron Microscopy
SiC	Silicon Carbide
SISO	Single-Input Single-Output
SMA	Subminiature Version A
TEM	Electron Transfer Microscopy
TMD	Transition Metal Dichalcogenides
UHF	Ultra High Frequency
UWB	Ultra Wideband
VNA	Vector Network Analyzer
VSWR	Voltage Standing Wave Ratio
WiMAX	Worldwide Interoperability For Microwave Access
WLAN	Wireless Local Area Network

Abstract

For keeping abreast with the steps of wireless communication system development, especially for 5G, antennas that can transmit signals at higher rate and are compatible for different frequency ranges, especially MIMO (multiple-input multiple-output), array and multi-band antennas, have been continuously researched with high expectations. These new generation antennas should be able to efficiently improve data rate, transmission speed and channel capacity, as well as fit in the IoE mass applications. To maximize the integration viability of 5G wireless architectures, the flexibility and conformity of next-generation electronics as well as the environmental amity of their materials and related fabrications are the essential features to achieve a more robust and reliable revolutionized end-user experience.

Among all the flexible conductive materials, graphene has surpassed others for its excellent flexibility, conductivity, low cost and strength, been proved a strong candidate for next generation indispensable soft electronics in wireless communication and sensing applications. However, the research of graphene is still at the beginning state. A number of issues still need to be addressed, such as: complicated structures of different kinds of antennas need to be specially designed to enhance the gain and cope with the loss introduced by graphene material comparing to normal metal; a more sustainable method should be investigated bypassing toxic solvents, complex fabrication, expensive materials, and high temperature annealing; the conductivity and stability of the ink should be improved; large-scale and affordable fabrication process is also in urgent need, where lies the

novelty of the work: an aggregation of different antenna technologies and graphene printing electronics, enabling cheap accessible and green antennas with high performance to be massively integrated in IoT applications.

In this thesis, different designs of antennas, i.e., MIMO, array, dual- and tri-bands, RFID tag antennas, with excellent radiation performance and flexibility have been integrated with low-cost, biodegradable printed graphene technique to conquer the most concerned surge in electronic waste caused by the mass production of antennas spurred by the significant deployment of IoE applications. These specially designed sustainable antennas provide strong support of 5G wireless communication mass data throughput and high performance IoT applications, guaranteeing high-speed data transmission and system reliability, and can be easily applied in flexible 5G front ends, various IoT systems, as well as in next-generation wearable electronic devices.

In addition, this dissertation has successfully investigated and explored a low-cost sustainable way for fabricating screen-printing graphene inks with high conductivity, presenting the novel aggregation of high-quality graphene printing technology and large-scale industrial production of flexible electronic devices in microwave region.

Declaration

No portion of the work referred to in the thesis has been submitted in support of an application for another degree or qualification of this or any other university or other institute of learning. All of the published papers that are included in this dissertation have been granted permission to be reused.

Copyright Statement

Acknowledgement

First, and foremost, I would express my deep gratitude to my supervisor Prof. Zhirun Hu for helping me out throughout the entire course of my Ph.D. dissertation. His erudition, expertise, understanding, patience, passion, and sound knowledge of my selected field assisted me beyond measures. He continuously provided me encouragement and guidance and was always willing and enthusiastic to assist in any way he could. I have been incredibly fortunate to have a mentor like him to steer me in the right direction, to get me back on track and to cheer me on for the past four years.

Next, I want to take a moment to express my appreciation to my family, especially my parents, who have always unconditionally supported me, gave me courage, and taught me to be independent and always full of hope. Thank you for the opportunity and understanding you provided so that I could grow up while exploring the world freely. Many thanks to my lovely dog Oreo who has taken the role of my therapy.

I am indebted to all my beloved friends and colleagues from whom I have learned so much: Dr. Ting Leng, Dr. Kewen Pan, Dr. Yixian Fang, Dr. Yutong Jiang, Mr. Yize Li, Mr. Yibo Ning, Mr. Xiaoyu Xiao, Miss Zizhen Zhang, Mr. Yifan Mao, I could not have done this without them. I would also like to express my deepest gratitude to all of those who had my back for all these years, supporting me with encouragement and recognition, especially in this Covid-19 period of time: Miss. Jiachen Li, Miss. Yixiu Pan, Miss. Shengnan Zhan, Miss. Siwei Liu, Mr. Keyi Wang, Mr. Sicheng Yu, Mr. Yangye Ji, etc.

Last but not least, the support from UK Engineering and Physical Sciences Research Council (EP/N010345) and the EEE Department of The University of Manchester is gratefully acknowledged.

List of Publications

[1] "Conformal screen printed graphene 4×4 wideband MIMO antenna on flexible substrate for 5G communication and IoT applications"
X. Zhou, T. Leng, K. Pan, M. Abdalla, K. Novoselov and Z. Hu,
2D Materials, vol. 8, no. 4, p. 045021, 2021.
doi: 10.1088/2053-1583/ac1959.

[2] "Graphene Printed Flexible and Conformal Array Antenna on Paper Substrate for 5.8GHz Wireless Communications"
X. Zhou, T. Leng, K. Pan, M. A. Abdalla and Z. Hu
2020 14th European Conference on Antennas and Propagation (EuCAP), pp. 1-4, 2020
doi: 10.23919/EuCAP48036.2020.9135742.

[3] "A Dual-band Flexible Printed Graphene Antenna Array for 2.4 and 5 GHz WLAN IoE Applications".
Xinyao Zhou, Ting Leng, Kewen Pan, Zhirun Hu
2021 51st European Microwave Conference (EuMC), London, UK, 2022

[4] "Graphene Printed Antenna Array for Wireless Communication Applications"
Xinyao Zhou, Ting Leng, Kewen Pan, Zhirun Hu
2021 IEEE International Symposium on Antennas and Propagation and USNC-URSI Radio Science Meeting, Singapore, 2022

[5] "Non-Volatile RF Reconfigurable Antenna On Flexible Substrate for Wireless IoT Applications"
T. Leng, K. Pan, **X. Zhou**, Y. Li, M. Abdalla and Z. Hu
IEEE Access, vol. 9, pp. 119395-119401, 2021.
doi: 10.1109/access.2021.3107486.

[6] “Soft Wireless Battery-free UHF RFID Stretchable Sensor based on Microfluidic Technology”
K. Pan, L. Teng, L. Ting, **X. Zhou**, A. Stokes and Z. Hu
IEEE Journal of Radio Frequency Identification, vol. 3, no. 4, pp. 252-258, 2019.
doi: 10.1109/jrfid.2019.2912959.

[7] “Graphene Printed UWB Monopole Antenna for Wireless communication applications”
K. Pan, T. Leng, Y. Jiang, Y. Fang, **X. Zhou**, M. A. Abdalla, H. Ouslimani, Z. Hu
2019 IEEE International Symposium on Antennas and Propagation and USNC&URSI Radio Science Meeting, Atlanta, GA, USA, 2019
doi: 10.1109/APUSNCURSINRSM.2019.8888805

Chapter 1 Introduction

1.1 Motivation

Higher data rate signal communication has always been pursued in the recent decades. With the formidable development rate of mobile networks, 5G has arrived with users' enormous demand of high-quality data exchange as well as communication processing, enabling the rapid development of IoT applications in various fields such as flexible screens, medical monitoring sensors and antennas, optical detectors, electronic paper, radio frequency identification (RFID) tags, and wearable electronics, etc.

. Many emerging multifunctional electronic platforms have been activated by

Fig. 1-1. Wearable electronics application in IoT networks [1].

recent interdisciplinary implements in flexible electronics, including materials, devices and related system designs [1-3]. These electronic platforms exhibit tremendous potential in wearable electronics and human to machine/machine to machine interface fields of application, as shown in Fig. 1-1, by applying excellent soft mechanical properties and thin, compact and conformal integrated sensing functionalities for devices. Hence, wearables are at the forefront of consumer electronics as conventional antennas made of solid metal and rigid substrate are incapable of bending or deformation with very low space utilization and high cost, which are severely limiting the huge demand brought by the blooming market of IoT applications. The flexible electronics have thus brought a revolution to electronics field, and evolved tremendously to meet the growing volume of data usage, eventually facilitating swift and secure personal, laboratorial, and commercial use of services, especially for the devices applied to implantable sensors, health monitoring system, body centric networks, etc. These intelligent products have achieved many highly effective practical implementations in various monitoring systems by generating tactile sensing and signal transmitting. By combining technologies such as wireless data transmission, self-supplied modules and signal processing circuits, flexible electronic devices applied to IoT can achieve better portability, versatile integration, on-site analysis and real-time feedback, as presented in Fig. 1-2 (a) and (b).

With the enormous demand for flexible devices, in a situation where the e-waste problem remains unresolved, there is a clear need for cheaper, greener and

lightweight portable antennas that can be twisted and bent to reinforce the

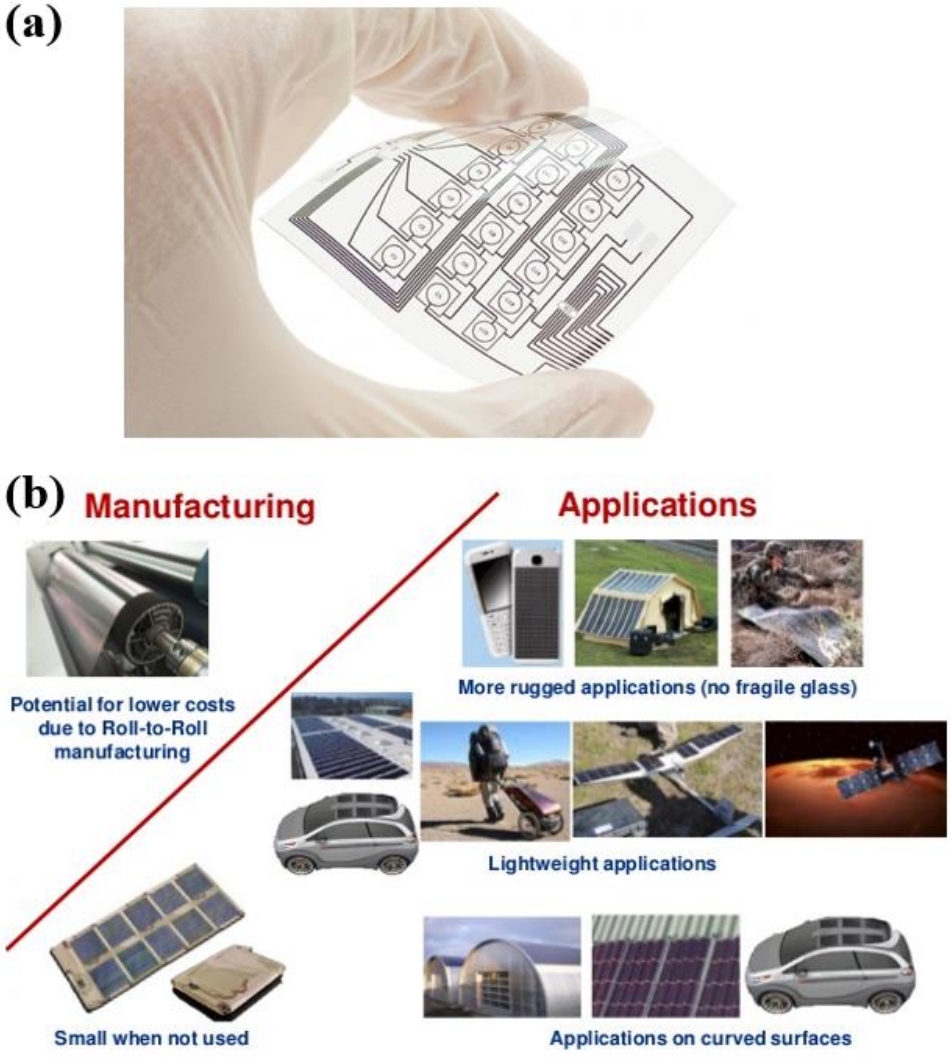

Fig. 1-2. (a) A fabricated flexible printed circuit on thin polymer substrate [4]. (b) Advantages of flexible electronics when applied in various fields [5].

integration with the systems. Graphene, a planar honeycomb atomic layer of sp2 hybridized carbon atoms, is a promising substitution of metallic materials, which can achieve excellent performance when dispersed in suitable solvents [6]. Graphene conductive inks can achieve high conductivity and sustainability, high flexibility, oxidation free, good stability and low cost.

It has been proved by previous studies that graphene conductive inks may be printed by a number of different printing techniques, such as ink-jet printing, screen printing, gravure printing, and sputtering [7-9]. For the preparation of graphene inks,

graphene flakes have to be stripped from large graphite particles using either mechanical methods such as liquid-phase bath ultrasonication exfoliation and shear mixing, or chemical approaches. In the case of the mechanical methods, the concentration of graphene ink is a concerning issue and most studies use toxic

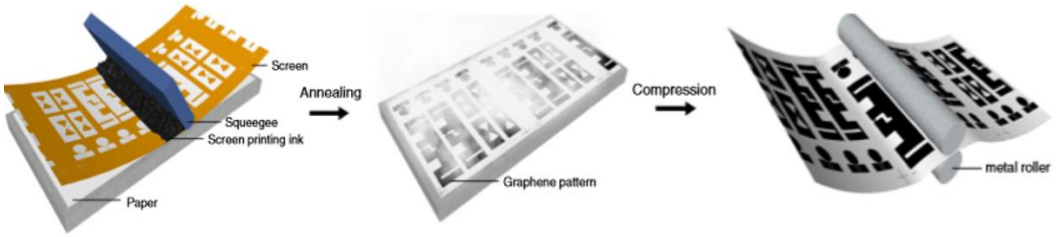

Fig. 1-3. Graphene screen printing technology [7].

solvents in order to improve electrical conductivity. Regarding the chemical approach, the presence of defects in the structure is likely to degrade its electrical conductivity [10-13]. As a result, the greatest challenge is to develop an efficient ink with environmental protection features, which is of high conductivity and stability, also can be manufactured in large-scale industrial production and applied in flexible electronics. Consequently, printing graphene on sustainable substrates, such as paper, for radiating and receiving RF signals wirelessly could be an ideal way for low cost disposal and consumable wearable electronics.

In this paper, the state-of-the-art of flexible electronics and their materials, especially graphene, are discussed and investigated, along with the resolutions to the challenges of high-speed transmission, large-scale production and world-concerning electronic waste issue. Observations on possible future research directions are also included.

1.2 Aims and Objectives

The aim of the project is to first estimate and investigate basic theories and the most recent development on flexible low-cost antennas, graphene ink production and related printing technology, array antennas, dual-band antennas and MIMO antennas suitable for massive industrial fabrications as well as their RF applications in IoE market.

The objectives of this project are:

- To gain familiarization of the graphene-printed antenna fabrication, including ink fabrication, printing process and four-needle method for measuring the sheet resistance of electroconductive films
- To develop a sustainable method of graphene ink production suitable for mass production
- To investigate the design methods of various antennas
- To integrate conventional rigid designs into flexible materials and achieve good performance
- To achieve wide operating bandwidth/dual band/tri-band, make sure it covers 2.4 GHz, 3.5 GHz, and 5 GHz commercial communication bands at the same time to fit in the complex frequency bands generated by 5G
- To balance the considerations of structure, space utilization, material properties, manufacturing process, sustainability and antenna performance
- To perform accurate measurements on the antenna performance
- To implement a flexible graphene-printed array antenna with high gain, a

MIMO antenna with excellent isolation, a tri-band and a dual-band array antenna

- To collect, collate and discuss the data obtained from experiments then analyze the performance of various antennas, such as return loss, efficiency, surface current, gain, radiation patterns, envelope correlation coefficients, channel capacity loss, etc.
- To determine the bending and pressure that flexible antenna can stand, finding the bending fatigue limit
- To minimize the mutual coupling of the planar screen printed MIMO antenna
- To research about recently developed metasurface antennas, RF reconfigurable antennas, MIMO antennas and multiple bandwidth antennas
- To estimate the performance of a non-volatile RF reconfigurable antenna on flexible substrate for wireless IoT applications
- To achieve highly conductive graphene inks and to evaluate the effect of changing the factors of different experimental parameters on the change of ink performance, to carry out measurements of an UHF RFID temperature sensor tag antenna

1.3 Thesis Outline

This dissertation contains 8 chapters. Chapter 1 introduces the aims and motivations of the work, describing the circumstances that provided the inspiration for conducting this study. Chapter 2 first elaborates the recent achievements of flexible and conformable antennas, after that, narrows down to graphene printed antennas, involving printed graphene fabrication development. Then, it moves on to some background theories of graphene properties and its modeling method. The basic knowledge of multi-band antennas, arrays, and MIMO antennas in wireless communication is also demonstrated in detail with some new designs and their applications, along with some antenna performance evaluation methods.

From Chapter 3 to Chapter 7, results of the study are presented in detail in the format of scientific journal publications.

Chapter 3 integrates MIMO technology with low-cost, biodegradable printed graphene technique to conquer the most concerned surge in electronic waste caused by the mass production of antennas spurred by the significant deployment of IoT applications, while at the same time fully supporting 5G wireless communication mass data throughput and high performance IoT applications, guaranteeing high-speed data transmission and system reliability. The major novelties in this work are: 1) flexibility brought by printing graphene technology, 2) low-cost and easily accessible fabrication process suitable for large scale sustainable manufacturing, and 3) the design of wideband flexible MIMO antenna with very low mutual coupling. The work is a novel aggregation of screen-printed graphene and MIMO technology, enabling easy integration of low-cost, flexible and green MIMO

antennas for massive IoT applications.

Chapter 4 illustrates the design, simulation, and fabrication of a high gain printed graphene compact conformal linear array antenna, which was designed for 5.8 GHz radars, portable electronic devices, and commercial wireless LAN applications. This is manufactured by screen printing specially formulated highly conductive graphene nanoflakes ink (with the use of NMP and EG solvent) on paper substrate. The bandwidth of the flexible antenna array ranges from 4.6 GHz to 7.9 GHz (52.8%) with its peak gain value 4.5 dBi at 5.8 GHz and a total radiation efficiency of 73%. The remarkable performance outcomes in the simulation and its extremely low cost imply promising potential of graphene printed electronics, notably for applications where flexibility and high-quality signal transmission are required.

Chapter 5 exhibits a novel tri-band graphene printed 1×2 planar array antenna for wireless communication use, with three clear resonances at 1.35 GHz, 3.5 GHz and 5.25 GHz, designed with meandered line and ground extensions for generating resonation at different bands. The antenna used previously mentioned graphene nanoflakes ink fabricated with NMP and EG solvent on paper substrate with a conductivity of 3.5×10^4 S/m. Whilst the peak gain of this antenna can achieve 2.14 dBi at 3.8 GHz, the gain is not guaranteed to stay above 0 dBi within all three bands it is designed for.

To maintain both high gain and multiple frequency bands features so as to realize high-quality simultaneous transmission of signals in different bands, Chapter 6 presents a dual-band flexible antenna array designed for 2.4 GHz and 5 GHz Internet of Everything (IoE) wireless local area network (WLAN) communication use, successfully achieving a gain above 2 dBi for both frequency bands. The

measured results revealed it as a good candidate for high data rate IoE system use, especially for systems require high signal transmission reliability such as health and military monitoring.

In Chapter 7, to enhance the simplicity and sustainability of graphene ink fabrication, a novel, environmental friendly and cost-effective strategy of ink production is proposed, which uses recycled Cyrene in circulations, followed only by shear mixing exfoliation, investigating the effect of recycled Cyrene on the properties of shear mixed graphene nanoflakes ink. By adopting this concept, one is finally able to avoid the necessity of extensive consumption of toxic solvents, to bypass the chemical process of graphene conductive ink production, and to tackle the critical issues associated with sustainable industrial use [7]. More importantly, the high price of Cyrene graphene inks can be dramatically reduced by at least one-tenth, the fabrication is extremely simplified, while maintaining the outstanding conductivity, defect-free, high concentration and stability of the resulting graphene inks, justifying the feasibility of recycling Cyrene for large-scale industrial production. A far-field graphene ink (made of recycled Cyrene) printed UHF RFID tag is presented and tested to prove the ink quality.

Finally, in Chapter 8, the main contributions of this dissertation are reviewed and summarized. The limitations of this study and possible future work are commented on. At the end, an objective evaluation is made, listing the merits and deficiencies of the work.

References

[1] D. Anagnostou, A. Gheethan, A. Amert and K. Whites, "A Direct-Write Printed Antenna on Paper-Based Organic Substrate for Flexible Displays and WLAN Applications", *Journal of Display Technology*, vol. 6, no. 11, pp. 558-564, 2010. Available: 10.1109/jdt.2010.2045474.

[2] F. Aieta, P. Genevet, M. Kats and F. Capasso, "Aberrations of flat lenses and aplanatic metasurfaces", *Optics Express*, vol. 21, no. 25, p. 31530, 2013. Available: 10.1364/oe.21.031530.

[3] S. Zhao and R. Zhu, "Electronic Skin: Electronic Skin with Multifunction Sensors Based on Thermosensation (Adv. Mater. 15/2017)", *Advanced Materials*, vol. 29, no. 15, 2017. Available: 10.1002/adma.201770099.

[4] A. Ono, M. Takishita, M. Sumiyoshi and V. Mizeikis, "Laser Induced Photoreduction for Metal Based Flexible Transparent Electrode", *Proceedings of the International Display Workshops*, p. 939, 2020. Available: 10.36463/idw.2020.0939.

[5] N. Ooi, H. Aoki, D. Watanabe, J. Jeong, C. Kimura and T. Sugino, "Cu Electroplating Process with Magnetic Field for Flexible Device", *Japanese Journal of Applied Physics*, vol. 48, no. 4, p. 046504, 2009. Available: 10.1143/jjap.48.046504.

[6] W. Whittow et al., "Inkjet-Printed Microstrip Patch Antennas Realized on Textile for Wearable Applications", *IEEE Antennas and Wireless Propagation Letters*, vol. 13, pp. 71-74, 2014. Available: 10.1109/lawp.2013.2295942.

[7] M. Saleh, C. Hu and R. Panat, "Three-dimensional microarchitected materials and devices using nanoparticle assembly by pointwise spatial printing", *Science Advances*, vol. 3, no. 3, 2017. Available: 10.1126/sciadv.1601986.

[8] L. Song, A. Myers, J. Adams and Y. Zhu, "Stretchable and Reversibly Deformable Radio Frequency Antennas Based on Silver Nanowires", *ACS Applied Materials & Interfaces*, vol. 6, no. 6, pp. 4248-4253, 2014. Available: 10.1021/am405972e.

[9] M. Mirzaee, S. Noghanian, L. Wiest and I. Chang, "Developing flexible 3D printed antenna using conductive ABS materials," *2015 IEEE International Symposium on Antennas and Propagation & USNC/URSI National Radio Science Meeting*, 2015, pp. 1308-1309, doi: 10.1109/APS.2015.7305043.

[10] I. M. Graz, D. P. J. Cotton, and S. P. Lacour, "Extended cyclic uniaxial loading of stretchable gold thin-films on elastomeric substrates",*Applied Physics Letters,* Vol. 94, No. 7, Feb. 2009.

[11] Hu L, Hecht DS, Gruner G. Carbon nanotube thin films: fabrication, properties, and applications. Chem Rev 2010;110:5790–844.

[12] K. Lu, R. Lago, Y. Chen, M. Green, P. Harris and S. Tsang, "Mechanical damage of carbon nanotubes by ultrasound", *Carbon*, vol. 34, no. 6, pp. 814-816, 1996. Available: 10.1016/0008-6223(96)89470-x.

[13] S. Azoubel and S. Magdassi, "The formation of carbon nanotube dispersions by high pressure homogenization and their rapid characterization by analytical centrifuge", *Carbon*, vol. 48, no. 12, pp. 3346-3352, 2010. Available: 10.1016/j.carbon.2010.05.024.

[14] T. Rai, P. Dantes, B. Bahreyni and W. Kim, "A Stretchable RF Antenna With Silver Nanowires", *IEEE Electron Device Letters*, vol. 34, no. 4, pp. 544-546, 2013. Available: 10.1109/led.2013.2245626.

[15] A. Rathmell and B. Wiley, "The Synthesis and Coating of Long, Thin Copper Nanowires to Make Flexible, Transparent Conducting Films on Plastic Substrates", *Advanced Materials*, vol. 23, no. 41, pp. 4798-4803, 2011. Available: 10.1002/adma.201102284.

[16] H. Shirakawa, E. Louis, A. MacDiarmid, C. Chiang and A. Heeger, "Synthesis of electrically conducting organic polymers: halogen derivatives of polyacetylene, (CH) x", *Journal of the Chemical Society, Chemical Communications*, no. 16, p. 578, 1977. Available: 10.1039/c39770000578.

[17] R. J. Vyas, A. Rida, L. Yang, and M. M. Tentzeris, “Design and development of the first entirely paper-based wireless sensor module,” in IEEE Antennas Propag Soc. Int. Symp., Jul. 5–11, 2008, pp. 1–4.

[18] K. Namiki, X. Cheng and H. Takahashi, "Indirectly Reactive Sputtering Coater for High Quality Optical Coatings", *IEICE Transactions on Electronics*, vol. 91-, no. 10, pp. 1673-1674, 2008. Available: 10.1093/ietele/e91-c.10.1673.

[19] T. Campbell, R. Kalia, A. Nakano, P. Vashishta, S. Ogata and S. Rodgers, "Dynamics of Oxidation of Aluminum Nanoclusters using Variable Charge Molecular-Dynamics Simulations on Parallel Computers", *Physical Review Letters*, vol. 82, no. 24, pp. 4866-4869, 1999. Available: 10.1103/physrevlett.82.4866.

[20] K. Novoselov et al., "Electric Field Effect in Atomically Thin Carbon Films", *Science*, vol. 306, no. 5696, pp. 666-669, 2004. Available: 10.1126/science.1102896.

[21] X. Huang, T. Leng, T. Georgiou, J. Abraham, R. Nair, K. S. Novoselov, and Z. Hu, “Graphene oxide dielectric permittivity at GHz and its applications for wireless humidity sensing,” *Scientific reports*, vol. 8, no. 1, p. 43, 2018.

[22] X. Huang et al., "Highly Flexible and Conductive Printed Graphene for Wireless Wearable Communications Applications", *Scientific Reports*, vol. 5, no. 1, 2015. Available: 10.1038/srep18298.

[23] T. Leng et al., "Printed graphene/WS2 battery-free wireless photosensor on

papers", *2D Materials*, vol. 7, no. 2, p. 024004, 2020. Available: 10.1088/2053-1583/ab602f.

[24] T. Leng, X. Huang, K. Chang, J. Chen, M. Abdalla and Z. Hu, "Graphene Nanoflakes Printed Flexible Meandered-Line Dipole Antenna on Paper Substrate for Low-Cost RFID and Sensing Applications", *IEEE Antennas and Wireless Propagation Letters*, vol. 15, pp. 1565-1568, 2016. Available: 10.1109/lawp.2016.2518746.

[25] K. Pan et al., "Sustainable production of highly conductive multilayer graphene ink for wireless connectivity and IoT applications", *Nature Communications*, vol. 9, no. 1, 2018. Available: 10.1038/s41467-018-07632-w.

[26] A. Lamminen et al., "Graphene-Flakes Printed Wideband Elliptical Dipole Antenna for Low-Cost Wireless Communications Applications", *IEEE Antennas and Wireless Propagation Letters*, vol. 16, pp. 1883-1886, 2017. Available: 10.1109/lawp.2017.2684907.

[27] K. Arapov et al., "Graphene screen-printed radio-frequency identification devices on flexible substrates", physica status solidi (RRL) - *Rapid Research Letters*, vol. 10, no. 11, pp. 812-818, 2016. Available: 10.1002/pssr.201600330.

[28] K. Jaakkola, H. Sandberg, M. Lahti and V. Ermolov, "Near-Field UHF RFID Transponder With a Screen-Printed Graphene Antenna", *IEEE Transactions on Components*, Packaging and Manufacturing Technology, vol. 9, no. 4, pp. 616-623, 2019. Available: 10.1109/tcpmt.2019.2902322.

[29] X. Huang, T. Leng, K. Chang, J. Chen, K. Novoselov and Z. Hu, "Graphene radio frequency and microwave passive components for low cost wearable electronics", *2D Materials*, vol. 3, no. 2, p. 025021, 2016. Available: 10.1088/2053-1583/3/2/025021.

[30] X. Huang et al., "Binder-free highly conductive graphene laminate for low cost printed radio frequency applications", *Applied Physics Letters*, vol. 106, no. 20, p. 203105, 2015. Available: 10.1063/1.4919935.

[31] R. Song et al., "A Graphene-Assembled Film Based MIMO Antenna Array with High Isolation for 5G Wireless Communication", *Applied Sciences*, vol. 11, no. 5, p. 2382, 2021. Available: 10.3390/app11052382.

[32] O.M. Slobodian, P.M. Lytvyn, A.S. Nikolenko, V.M. Naseka, O.Y. Khyzhun, A. V Vasin, S. V Sevostianov, A.N. Nazarov, Low-Temperature Reduction of Graphene Oxide: Electrical Conductance and Scanning Kelvin Probe Force Microscopy, *Nanoscale Res. Lett*. 13 (2018) 139.

[33] A. Lamminen et al., "Graphene-Flakes Printed Wideband Elliptical Dipole Antenna for Low-Cost Wireless Communications Applications", *IEEE Antennas and Wireless Propagation Letters*, vol. 16, pp. 1883-1886, 2017. Available: 10.1109/lawp.2017.2684907.

[34] A. Geim and K. Novoselov, "The rise of graphene", *Nature Materials*, vol. 6, no. 3, pp. 183-191, 2007. Available: 10.1038/nmat1849.

[35] L. Berry, " Liquids and Solids Chapter 10.," Slideplayer, 2019.

[36] H. Abutarboush and A. Shamim, "Paper-Based Inkjet-Printed Tri-Band U-Slot Monopole Antenna for Wireless Applications", *IEEE Antennas and Wireless Propagation Letters*, vol. 11, pp. 1234-1237, 2012. Available: 10.1109/lawp.2012.2223751.

[37] H. Zhu, Z. Xu, D. Xie and Y. Fang, *Graphene*. London: Academic Press, an imprint of Elsevier, 2018.

[38] K. Novoselov, "Beyond the wonder material", *Physics World*, vol. 22, no. 08, pp. 27-30, 2009. Available: 10.1088/2058-7058/22/08/33.

[39] V. Gusynin, S. Sharapov, and J. Carbotte, "Magneto-optical conductivity in graphene," J. Phys.: Condens. Matter, vol. 19, no. 2, Dec. 2006, Art. no. 026222.

[40] G. W. Hanson, "Dyadic Green's functions and guided surface waves for a surface conductivity model of graphene," J. App. Phy., vol. 103, no. 6, Apr. 2008, Art. no. 064302.

[41] A. Crépieux and P. Bruno, "Theory of the anomalous hall effect from the Kubo formula and the dirac equation," Phys. Rev. B, vol. 64, no. 1, Jun. 2001, Art. no. 014416.

[42] K. Niu, P. Li, Z. Huang, L. Jiang and H. Bagci, "Numerical Methods for Electromagnetic Modeling of Graphene: A Review", *IEEE Journal on Multiscale and Multiphysics Computational Techniques*, vol. 5, pp. 44-58, 2020. Available: 10.1109/jmmct.2020.2983336.

[43] X. Huang, Z. Hu and P. Liu, "Graphene based tunable fractal Hilbert curve array broadband radar absorbing screen for radar cross section reduction", *AIP Advances*, vol. 4, no. 11, p. 117103, 2014. Available: 10.1063/1.4901187.

[44] M. Tamagnone, J. Gómez-Díaz, J. Mosig and J. Perruisseau-Carrier, "Reconfigurable terahertz plasmonic antenna concept using a graphene stack", *Applied Physics Letters*, vol. 101, no. 21, p. 214102, 2012. Available: 10.1063/1.4767338.

[45] D. Correas-Serrano, J. Gomez-Diaz, J. Perruisseau-Carrier and A. Alvarez-Melcon, "Graphene-Based Plasmonic Tunable Low-Pass Filters in the Terahertz Band", *IEEE Transactions on Nanotechnology*, vol. 13, no. 6, pp. 1145-1153, 2014. Available: 10.1109/tnano.2014.2344973.

[46] B. Wu, Y. Hu, Y. Zhao, W. Lu and W. Zhang, "Large angle beam steering THz antenna using active frequency selective surface based on hybrid graphene-gold structure", *Optics Express*, vol. 26, no. 12, p. 15353, 2018. Available: 10.1364/oe.26.015353.]

[47] P. Blake et al., “Graphene-based liquid crystal device,” Nano Lett., vol. 8, no. 6, pp. 1704–1708, Apr. 2008.

[48] K. S. Novoselov et al., “Room-temperature quantum Hall effect in graphene,” Science, vol. 315, no. 5817, pp. 1379–1379, Mar. 2007.

[49] F. Bonaccorso, Z. Sun, T. Hasan, and A. Ferrari, “Graphene photonics and optoelectronics,” Nature Photon., vol. 4, no. 9, pp. 611–622, Aug. 2010.

[50] J. Lee, H. Ahn, J. Yoon and J. Jang, "Three-dimensional nano-foam of few-layer graphene grown by CVD for DSSC", *Physical Chemistry Chemical Physics*, vol. 14, no. 22, p. 7938, 2012. Available: 10.1039/c2cp40810d.

[51] B. Wu, H.M. Tuncer, A. Katsounaros, W. Wu, M.T. Cole, K. Ying, L. Zhang, W.I. Milne, Y. Hao, Microwave absorption and radiation from large-area multilayer CVD graphene, Carbon N. Y. 77 (2014) 814–822.

[52] X. Li et al., "Large-Area Synthesis of High-Quality and Uniform Graphene Films on Copper Foils", *Science*, vol. 324, no. 5932, pp. 1312-1314, 2009. Available: 10.1126/science.1171245.

[53] K. Kim et al., "Large-scale pattern growth of graphene films for stretchable transparent electrodes", *Nature*, vol. 457, no. 7230, pp. 706-710, 2009. Available: 10.1038/nature07719..

[54] A. Reina et al., "Large Area, Few-Layer Graphene Films on Arbitrary Substrates by Chemical Vapor Deposition", *Nano Letters*, vol. 9, no. 1, pp. 30-35, 2009. Available: 10.1021/nl801827v.

[55] P. Avouris and F. Xia, "Graphene applications in electronics and photonics", *MRS Bulletin*, vol. 37, no. 12, pp. 1225-1234, 2012. Available: 10.1557/mrs.2012.206.

[56] T. Leng et al., "Screen-Printed Graphite Nanoplate Conductive Ink for Machine Learning Enabled Wireless Radiofrequency-Identification Sensors", *ACS Applied Nano Materials*, vol. 2, no. 10, pp. 6197-6208, 2019. Available: 10.1021/acsanm.9b01034.

[57] S. Biccai et al., "Exfoliation of 2D materials by high shear mixing", *2D Materials*, vol. 6, no. 1, p. 015008, 2018. Available: 10.1088/2053-1583/aae7e3.

[58] K. Kouroupis-Agalou et al., "Fragmentation and exfoliation of 2-dimensional materials: a statistical approach", *Nanoscale*, vol. 6, no. 11, pp. 5926-5933, 2014. Available: 10.1039/c3nr06919b.

[59] K. Paton et al., "Scalable production of large quantities of defect-free few-layer graphene by shear exfoliation in liquids", *Nature Materials*, vol. 13, no. 6, pp. 624-630, 2014. Available: 10.1038/nmat3944.

[60] C. Backes et al., "Production and processing of graphene and related materials. ", *2D Mater., 2020,* 7, 022001.

[61] D. Nuvoli et al., "High concentration few-layer graphene sheets obtained by liquid phase exfoliation of graphite in ionic liquid", *J. Mater. Chem.*, vol. 21, no. 10, pp. 3428-3431, 2011. Available: 10.1039/c0jm02461a.

[62] U. Khan, A. O'Neill, M. Lotya, S. De and J. Coleman, "High-Concentration Solvent Exfoliation of Graphene", *Small*, vol. 6, no. 7, pp. 864-871, 2010. Available: 10.1002/smll.200902066.

[63] C. Huo, Z. Yan, X. Song and H. Zeng, "2D materials via liquid exfoliation: a review on fabrication and applications", *Science Bulletin*, vol. 60, no. 23, pp. 1994-2008, 2015. Available: 10.1007/s11434-015-0936-3.

[64] P. Turner, M. Hodnett, R. Dorey and J. Carey, "Controlled Sonication as a Route to in-situ Graphene Flake Size Control", *Scientific Reports*, vol. 9, no. 1, 2019. Available: 10.1038/s41598-019-45059-5.

[65] T. Hansen et al., "Resolution enhancement of scanning four-point-probe measurements on two-dimensional systems", *Review of Scientific Instruments*, vol. 74, no. 8, pp. 3701-3708, 2003. Available: 10.1063/1.1589161.

[66] S. Saeed, C. Balanis and C. Birtcher, "Inkjet-Printed Flexible Reconfigurable Antenna for Conformal WLAN/WiMAX Wireless Devices", *IEEE Antennas and Wireless Propagation Letters*, vol. 15, pp. 1979-1982, 2016. Available: 10.1109/lawp.2016.2547338.

[67] M. Tyona, "A comprehensive study of spin coating as a thin film deposition technique and spin coating equipment", *Advances in materials Research*, vol. 2, no. 4, pp. 181-193, 2013. Available: 10.12989/amr.2013.2.4.181.

[68] A. Kamyshny and S. Magdassi, "Conductive Nanomaterials for Printed Electronics", *Small*, vol. 10, no. 17, pp. 3515-3535, 2014. Available: 10.1002/smll.201303000.

[69] X. Huang, T. Leng, T. Georgiou, J. Abraham, R. Nair, K. S. Novoselov, and Z. Hu, “Graphene oxide dielectric permittivity at GHz and its applications for wireless humidity sensing,” Scientific reports, vol. 8, no. 1, p. 43, 2018.

[70] Y. Seekaew, S. Lokavee, D. Phokharatkul, A. Wisitsoraat, T. Kerdcharoen and C. Wongchoosuk, "Low-cost and flexible printed graphene–PEDOT:PSS gas sensor for ammonia detection", *Organic Electronics*, vol. 15, no. 11, pp. 2971-2981, 2014. Available: 10.1016/j.orgel.2014.08.044.

[71] A. Kaye and D. George, "Transmission of Multiplexed PAM Signals Over Multiple Channel and Diversity Systems", *IEEE Transactions on Communications*, vol. 18, no. 5, pp. 520-526, 1970. Available: 10.1109/tcom.1970.1090417.

[72] "Arogyaswami Paulraj – Marconi Society". *marconisociety.org (in American English)*. Retrieved 2017-01-21.

[73] L. Malviya, R. Panigrahi and M. Kartikeyan, "MIMO antennas with diversity

and mutual coupling reduction techniques: a review", *International Journal of Microwave and Wireless Technologies*, vol. 9, no. 8, pp. 1763-1780, 2017. Available: 10.1017/s1759078717000538.

[74] G. Jeong, S. Choi, K. Lee and W. Kim, "Low-Profile Dual-Wideband MIMO Antenna with Low ECC for LTE and Wi-Fi Applications", *International Journal of Antennas and Propagation*, vol. 2014, pp. 1-6, 2014. Available: 10.1155/2014/158028.

[75] W. Lee and Yu Yeh, "Polarization Diversity System for Mobile Radio", *IEEE Transactions on Communications*, vol. 20, no. 5, pp. 912-923, 1972. Available: 10.1109/tcom.1972.1091263.

[76] J. Oh and K. Sarabandi, "Compact, Low Profile, Common Aperture Polarization, and Pattern Diversity Antennas", *IEEE Transactions on Antennas and Propagation*, vol. 62, no. 2, pp. 569-576, 2014. Available: 10.1109/tap.2013.2291901.

[77] J. Costa, E. Lima, C. Medeiros and C. Fernandes, "Evaluation of a New Wideband Slot Array for MIMO Performance Enhancement in Indoor WLANs", *IEEE Transactions on Antennas and Propagation*, vol. 59, no. 4, pp. 1200-1206, 2011. Available: 10.1109/tap.2011.2109685.

[78] G. Adamiuk, S. Beer, W. Wiesbeck and T. Zwick, "Dual-Orthogonal Polarized Antenna for UWB-IR Technology", *IEEE Antennas and Wireless Propagation Letters*, vol. 8, pp. 981-984, 2009. Available: 10.1109/lawp.2009.2029880.

[79] C. Wu, G. Zhou, Y. Wu and T. Ma, "Stub-Loaded Reactive Decoupling Network for Two-Element Array Using Even–Odd Analysis", *IEEE Antennas and Wireless Propagation Letters*, vol. 12, pp. 452-455, 2013. Available: 10.1109/lawp.2013.2255255.

[80] F. Yang and Y. Rahmat-Samii, "Microstrip antennas integrated with electromagnetic band-gap (EBG) structures: A low mutual coupling design for array applications", *IEEE Transactions on Antennas and Propagation*, vol. 51, no. 10, pp. 2936-2946, 2003. Available: 10.1109/tap.2003.817983.

[81] M. Ahmad, W. Mohyuddin, H. Choi and K. Kim, "4 × 4 MIMO antenna design with folded ground plane for 2.4 GHz WLAN applications", *Microwave and Optical Technology Letters*, vol. 60, no. 2, pp. 395-399, 2018. Available: 10.1002/mop.30969.

[82] J. Thaysen and K. Jakobsen, "Envelope correlation in (N,N) MIMO antenna array from scattering parameters", *Microwave and Optical Technology Letters*, vol. 48, no. 5, pp. 832-834, 2006. Available: 10.1002/mop.21490.

[83] S. Tripathi, A. Mohan and S. Yadav, "A Compact Koch Fractal UWB MIMO Antenna With WLAN Band-Rejection", *IEEE Antennas and Wireless Propagation Letters*, vol. 14, pp. 1565-1568, 2015. Available: 10.1109/lawp.2015.2412659.

[84] A Paulraj RN, Gore D: *Introduction to Space-time Wireless Communications*. Cambridge University Press, USA; 2005.

[85] Q. He, Z. Wang, J. Hu and R. Blum, "Performance Gains From Cooperative MIMO Radar and MIMO Communication Systems", *IEEE Signal Processing Letters*, vol. 26, no. 1, pp. 194-198, 2019. Available: 10.1109/lsp.2018.2880836.

[86] L. Yang, S. Yan and T. Li, "COMPACT PRINTED FOUR-ELEMENT MIMO ANTENNA SYSTEM FOR LTE/ISM OPERATIONS", *Progress In Electromagnetics Research Letters*, vol. 54, pp. 47-53, 2015. Available: 10.2528/pierl15060801.

[87] T. Qaradaghi and D. Hussein, "Evaluation of different 4x4 Coded MIMO System", *Journal of Zankoy Sulaimani - Part A*, vol. 17, no. 2, pp. 71-84, 2015. Available: 10.17656/jzs.10382.

[88] A. D., "MIMO based Channel Selection Technique for Automation Broadband Networks with IoT Applications", *International Journal of Psychosocial Rehabilitation*, vol. 23, no. 3, pp. 1002-1011, 2019. Available: 10.37200/ijpr/v23i3/pr190500.

[89] B. Wang and Y. Lo, "Microstrip antennas for dual-frequency operation", *IEEE Transactions on Antennas and Propagation*, vol. 32, no. 9, pp. 938-943, 1984. Available: 10.1109/tap.1984.1143459.

[90] J. Yu, Y. Sun, H. Fang and F. Li, "A novel stacked patch antenna with dual band and diverse pattern characteristics", *Microwave and Optical Technology Letters*, vol. 62, no. 1, pp. 453-465, 2019. Available: 10.1002/mop.32036.

[91] A. Manouare, S. Ibnyaich, A. Idrissi, A. Ghammaz and N. Touhami, "A Compact Dual-Band CPW-Fed Planar Monopole Antenna for 2.62–2.73 GHz Frequency Band, WiMAX and WLAN Applications", *Journal of Microwaves, Optoelectronics and Electromagnetic Applications*, vol. 16, no. 2, pp. 564-576, 2017. Available: 10.1590/2179-10742017v16i2911.

[92] S. Heydari, K. Pedram, Z. Ahmed and F. Zarrabi, "Dual band monopole antenna based on metamaterial structure with narrowband and UWB resonances with reconfigurable quality", *AEU - International Journal of Electronics and Communications*, vol. 81, pp. 92-98, 2017. Available: 10.1016/j.aeue.2017.07.015.

[93] S. Menon, "Microstrip Patch Antenna Assisted Compact Dual Band Planar Crossover", *Electronics*, vol. 6, no. 4, p. 74, 2017. Available: 10.3390/electronics6040074.

[94] D. Naji, "Design of Compact Dual-band and Tri-band Microstrip Patch Antennas", *Article.sapub.org*, 2018. [Online]. Available: http://article.sapub.org/10.5923.j.ijea.20180801.02.html. [Accessed: 22- Aug- 2021].

[95] H. Friis, "A Note on a Simple Transmission Formula", *Proceedings of the IRE*, vol. 34, no. 5, pp. 254-256, 1946. Available: 10.1109/jrproc.1946.234568.

Chapter 2 Background Theory and Literature Review

This chapter is dedicated to presenting the background knowledge acquired during the research, including review of recently proposed flexible and conformal antennas and more specifically graphene-printed soft electronics along with their fabrication methodology, graphene modeling method, also includes the design and measurement of multiple types of planar antennas, and how they relate to the broader fields of study. Thereby demonstrating a clear observation of further research interests based on market needs.

2.1 Flexible Antennas

2.1.1 Review of recent flexible antenna designs and related applications

The field of flexible electronics has bloomed and brought a new era to wireless communications. Huge application fields have been generated by the vast development of flexible printed electronics, for instance, bendable displays, thin film transistors, portable energy-harvesting devices, sensors, electronic skin, and transparent electrode [1-4, 70]. These inventions could significantly benefit body centric network, military and police security system, health monitoring systems, and modern mobile networks, to most people's top concern at the moment.

As conventional antennas which consist of solid metal and rigid substrate are incapable of bending and deforming, wearable soft sensors are clearly needed to

provide the required flexibility for a large range of applications. Hence, to enhance the integration and incorporation with the systems and to meet future requirements, developing lightweight, environmentally friendly and low-cost antennas (which can be twisted, bended, deformed and easily reshaped) will be the primary goal for researchers to address.

In pursuit of developing flexible and bendable antennas, different approaches have been proposed in recent years, such as electroplating thin metal foils on dielectric elastomer[5], inkjet-printing on a flexible polyethylene terephthalate substrate [6], printing metallic nanoparticles on various substrates[7], embedding silver nanowires(AgNWs) on elastomers[8], using conductive acrylonitrile butadiene styrene (ABS) materials in the fabrication of flexible three-dimensional (3D) antennas [9], etc.

Ingrid et al. from the University of Cambridge has proposed some reversibly stretchable electronics in [10], 50 nm thick gold was thermally evaporated on microstructured PDMS substrate as the radiating conductor. A shadow mask was used for defining the shape of the conductor. Acceptable stability and electrical continuity were proved, however when further stretched, both lateral and transversal cracks have been observed which severely increased the resistance. The fabrication procedure of this approach is time-consuming, inefficient and of

high cost, contributing to its incapability for mass industrial production in low-cost wireless portable applications.

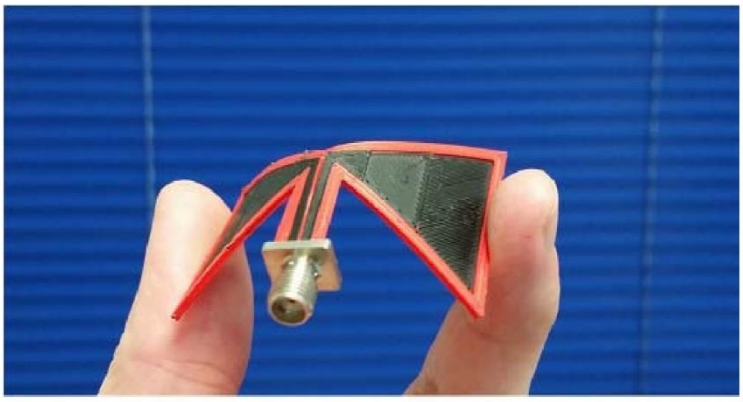

Fig. 2-1. 3D printed bowtie antenna structure [9].

In [9], an additive manufacturing method (Makerbot® dual 3D printer) was used to design and fabricate a flexible three-dimensional antenna made of acrylonitrile butadiene styrene (ABS) materials (conductive structure) and flexible polylactic acid (dielectric substrate). Fig. 2-1 shows the proposed antenna, where the red material (PLA plastic) represents the substrate and the black one (conductive ABS) indicates the conductive radiating part. This antenna features light-weight, small in size and good flexibility, however, this technique is both chemically and thermally unstable.

Aside from the instability of conductive polymer, its conductivity is still too low for RF signal transmission and radiation, although it can yield acceptable performance when used in sensors and solar cells.

Carbon nanotubes (CNTs) were once considered as an alternative to metallic nanoparticles. However, the exceptionally high junction resistance between them leads to low surface conductivity, which substantially hinders their application [11-13].

AgNWs and CuNWs based antennas can be fabricated by embedding nanowires in silicones and plastics, however, a sample thickness of 3 mm AgNWs can only achieve a sheet resistance of 5 Ω/sq [14], which would introduce huge loss while signal transmission.

Printing silver and gold nanoparticle ink on flexible substrate [15, 16] could achieve the highest conductivity among them all. In [17], researchers successfully achieved a conformal silver nanoparticle printed antenna on paper substrate using direct-write printing process for 10 passes, which does not

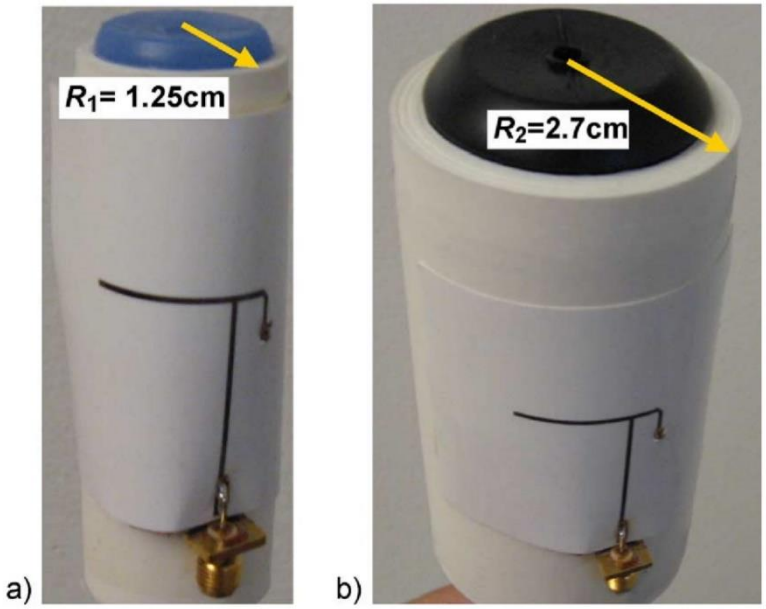

Fig. 2-2. Antenna bending condition around different radius (a) R=1.25 cm, (b)R=2.7 cm

produce metallic or chemical waste like milling and chemical etching techniques, however complex designs cannot be supported by direct-writing, the precision would be much lower than expected. In Fig. 2-2, the antenna was bent around cylindrical structures with different radius: (a) R=1.25 cm, (b)R=2.7 cm. By

using this method, cracks could be easily introduced to the conductive radiating part of the antenna during multiple bending procedures, contributing to discontinuities of surface current, limiting the repeatability usage of the antenna.

To enhance the robustness of the antenna and prevent discontinuities during

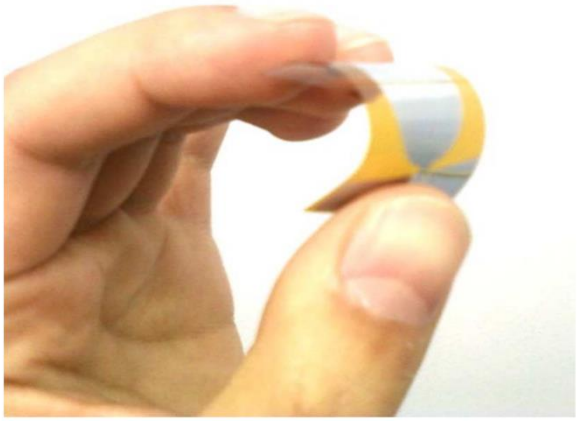

Fig. 2-3. The polyimide-based flexible low-profile UWB antenna proposed in [18].

high-level deformation, Haider has proposed a solution in [18], inkjet-printing three layers of ink based on silver nanoparticles to maintain the pattern's continuity and robustness. A soft Kapton polyimide was used as the substrate. This ultra-wide band antenna in Fig. 2-3 realize1.7 dBi gain at 2.45 GHz and a stable gain variation from 3.1-10.6 GHz. After taking the flexibility tests, the antenna was proved nearly immune to performance degradation caused by deformation.

Although the conductivity and effectiveness of printable silver nanoparticle inks can be proved, yet the high cost of silver strictly limits its large-scale production. Other metallic inks, such as copper and aluminum, are much cheaper in comparison with gold and silver, but they tend to be oxidized very quickly (within 100 picoseconds for aluminum) [19], degrading the conductivity of the ink.

Oxidation can be prevented by an additional sintering process, but such a high-temperature process is not applicable to heat-sensitive substrates. Considering the search for lightweight, low-cost, flexible, and bendable antennas, however, researchers have turned their attention to unusual substrates, for example, paper, plastics, and textiles, which are all heat-sensitive materials.

2.1.2 Graphene printed antennas

The mechanical characteristics of conventional rigid, expensive and not environmental-friendly materials which are being broadly used in electronics have limited the development of portable wearable electronics to a great extent. Printed electronics, especially electronics with flexible substrates has therefore drawn great attention and motivation for the enhancement of user comfort and space utilization.

As we could observe during the literature exploration of previous flexible electronics, various conductive inks have been used to print desired patterns, giving lightweight, flexibility as well as manufacture convenience. However, the use of metallic ink cannot reduce manufacture expenses or fit in large scale industrial manufacturing and would easily introduce cracks while bending.

With high electrical conductivity, high strength, excellent electron transfer rate and low cost, graphene has been considered as a very promising substitution of metal for better integration into systems that require flexibility since 2004, when it was first isolated from High Ordered Pyrolytic Graphite (HOPG) [20]. Taking advantage of its excellent properties, printed graphene antennas have been

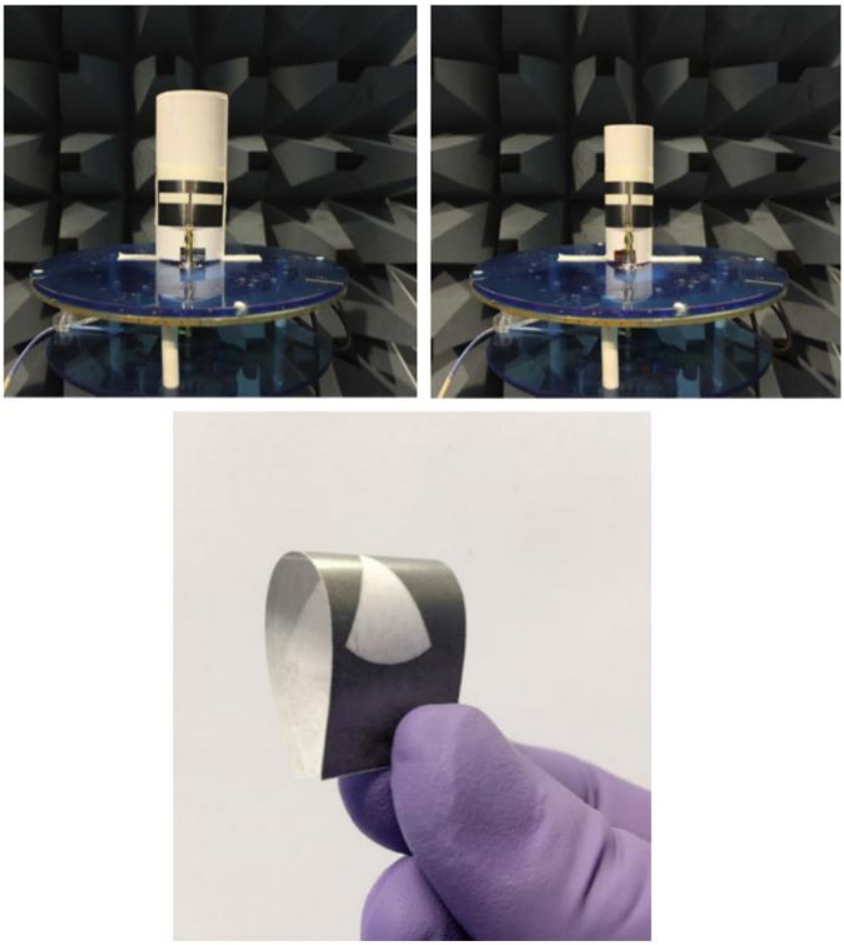

Fig. 2-4, Flexible printed graphene antennas [22, 25].

extensively studied [21-30], the research is mostly aimed at simple dipole [24, 26 30] and RFID tag antennas [21, 25, 28-29]. The advantages of printed antennas lie on their printability, flexibility, conformability, disposability plus low cost for mass production. The realized gain of printed graphene antennas shows the effectiveness of RF radiation, and it is greatly depends on the conductivity and preparation of

the conductive ink, where the ink evolution will be elaborated in Chapter 2.3.

Table 2-1 shows a comparison of performance of some typical graphene-based antennas. The major challenges in producing printed graphene antennas are:

1) Remain flexibility
2) Remain low-cost properties of the material, proceed with easily accessible fabrication process suitable for large scale sustainable manufacturing.

In [31], although graphene-based antenna is integrated with 5G high speed multiple input and multiple output (MIMO) signal transmission and shows excellent performance, the graphene-assembled film reported in this work requires a very high temperature (2850℃) annealing of graphitization. Such film behaves just like any metal film. Furthermore, the antenna has taken advantage of metallic ground plane, discarding the intrinsic flexibility of graphene material.

3) Improve the design of the antennas to obtain better performance

A performance comparison of printed graphene antennas including dipoles, monopoles, and the first graphene printed MIMO antenna presented in Chapter 3 is shown below [22, 24, 30, 33] in Table 2-1, wide bandwidths can be found in most of the work due to the use of graphene material, acceptable gains can be observed.

In [30], obtaining -0.6 dBi maximum gain is good enough for low-cost RFID and sensing applications, however, to overcome power dissipation in graphene, it is much anticipated for researchers to design structure so that the radiation path has lower dissipation loss and higher gain at desired frequencies and thereby enabling boarder applications of printed graphene antennas in wireless communication field

where reliable and timely response is expected.

Table 2-1 Performance comparison of conformal printed graphene antennas

Refs	*Operating range (GHz)*	*Bandwidth (%)*	*Measured Peak Gain*	*ECC*	*Fabrication process and cost*
[22]	1.73-3.77	74	0.2 dBi	/	Simple, low cost
[33]	1.7-5	98	0.6 dBi	/	Simple, require 350℃ thermal annealing
[30]	0.89-1.02	3.4	-0.6 dBi		Simple, low cost
[24]	0.98-1.05	6.7	-4 dBi	/	Simple, low cost
This work (Chapter 3)	2.22-3.85	54	0.92 dBi	0.2×10^{-6}	Simple, low cost

*Not mentioned

/ Not applicable

With all the effort and development made in this field by researchers, it could now be recognized as a common cognitive that flexible graphene printed electronic products have tremendous potential and important practical significance in biological monitoring applications, energy storage systems, and even paper-based electronics. The high demand for electronic devices with flexible and compact structures will not subside in decades, especially for bendable, environment-friendly, low-cost, compact antennas for large-scale adoption in IoT applications in the fifth generation (5G) wireless communication bands.

2.2 Graphene Modeling

Graphene, a honeycomb crystal structure of sp2 hybridized carbon atoms exfoliated from graphite, is the essential building block of graphite, carbon nanotubes and fullerenes [34]. It looks like a plane made of a hexagonal grid, with

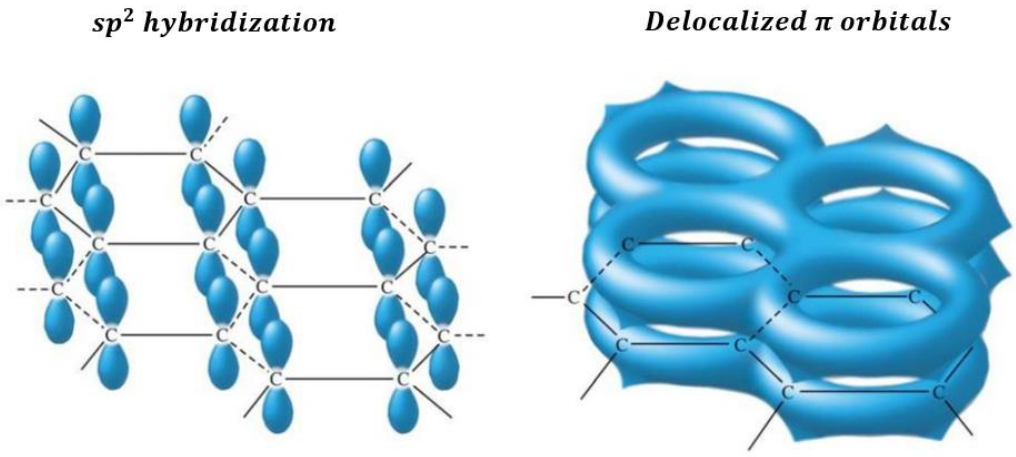

Fig. 2-5. The sp^2 hybridization of graphene. The unhybridized p orbitals overlap to form a sheet of delocalized π electrons [35].

extremely stable structure and pliable connections between carbon atoms, as shown in Fig. 2-5. This special hybridization and interatomic forces can make each carbon atom contribute the remaining p-orbital electron (4 outer shell electrons of carbon atom are connected to 3 other carbon atoms on the same plane, leaving one free electron in the third dimension, which is called a π electron) to forming a strong π bond, π electrons can then move freely, granting graphene superior electrical conductivity and immune to interference. In graphene, electrons are less prone to scattering during transportation, and can achieve a 2×10^5 $cm^2/(V \cdot s)$

electron mobility, 140 times of the mobility in Si [36]. The sheet resistance of graphene is 31 Ω/sq, it is regarded as the best conductive material under room temperature. The electrical conductivity of graphene can be chemically controlled by means of modification, and simultaneously obtain various graphene-based derivatives [37]. In 2004 [20], Novoselov and Geim discovered that graphene supports strong bi-polar electric field effects and exhibits semi-metallic properties. It was also revealed that graphene-based transistor can be tuned by voltage and that its properties are similar to those of a semiconductor except for the zero band gap. In the presence of an external electric field, the stability of the carrier density renders graphene a promising candidate for tunable components.

Meanwhile, graphene also possesses excellent mechanical and thermal properties. It is the strongest and hardest crystalline structure of any known materials, with about 100 times the strength of regular steel, and can be applied as a typical two-dimensional reinforcing phase in the field of composite materials [37]. The thermal conductivity of graphene is 5×10^3 W/m · K, 10 times of that of copper under room temperature, with a theoretical specific surface area of 2630 m^2/g [38]. Microsensors that are made of graphene can sense individual atoms or molecules. When gas molecules are attached to or detached from the graphene surface, the attached ones will change the local carrier concentration of graphene, resulting in a step change in resistance. This property can be used to make gas sensors.

In order to carry out design and investigation of graphene and graphene-based devices, numerical modeling and simulation of graphene sheets is an imperative and crucial part of the research. Graphene can be modeled as a thin-layer conductor with a surface conductivity σ_d, which is denoted by Kubo

formula, a function of wavelength, temperature and chemical potential [39-41].

$$\sigma_d = \frac{je^2(\omega - j2\Gamma)}{\pi h^2}\left[-\int_0^\infty \varepsilon \frac{f_d(-\varepsilon)}{(\omega - j2\Gamma)^2 - 4\left(\frac{\varepsilon}{h}\right)^2} d\varepsilon + \frac{1}{(\omega - j2\Gamma)^2}\right] \int_0^\infty \varepsilon \left(\frac{\partial f_d(\varepsilon)}{\partial \varepsilon} - \frac{\partial f_d(-\varepsilon)}{\partial \varepsilon}\right) d\varepsilon \quad (2.1)$$

where Γ is the electron scattering rate ($\tau = \frac{1}{2\Gamma}$), τ is the electron scattering time, ω is the radian frequency, e is the electron charge, h is the reduced Plank constant, and ε is the energy state. f_d is the Fermi-Dirac distribution, related to temperature T, Boltzmann constant k_B, and chemical potential μ_c as $f_d = (e^{\frac{\varepsilon - |\mu_c|}{k_B T}} + 1)^{-1}$. This equation is the sum of the intra-band (2.2) and inter-band (2.3) contributions.

$$\sigma_{d,intra} = \frac{je^2 k_B T}{\pi h^2(\omega - j2\Gamma)}\left(\frac{\mu_c}{k_B T} + 2\ln\left(e^{\frac{-|\mu_c|}{k_B T}} + 1\right)\right) \quad (2.2)$$

$$\sigma_{d,inter} = \frac{-je^2}{4\pi h}\ln\left(\frac{2|\mu_c| - (\omega - j2\Gamma)h}{2|\mu_c| + (\omega - j2\Gamma)h}\right) \quad (2.3)$$

At frequencies in microwave region (i.e., below THz), interband transition is extremely weak that it can be neglected, the impedance of graphene can be simply considered as the inverse of $\sigma_{d,intra}$, and the behavior of it is just like a conductive film, which can be simply described by the Drude model [42]. Early research on graphene physics explicitly pointed out that the conductivity of monolayer graphene exhibits a slight sublinear dependence on the electron density. Whereas, in contrast, the electrical conductivity of bilayer graphene and multilayer graphene consistently shows a strong linear dependence on the electron density.

In Fig. 2-6, the surface conductivity of graphene at T = 300 K, τ = 0.2 ps, has been analyzed with different μ_c, ranging from microwave to infrared band [43]. Below 100 GHz, the imaginary part of the conductivity is extremely small that an almost constant conductivity, reluctant to the change in μ_c, can be observed. This has also been proved by the works [22, 32-33] in similar frequency ranges.

In other word, in microwave region, graphene is considered frequency independent, while in THz region, the tunability of graphene's conductivity is useful in absorber field.

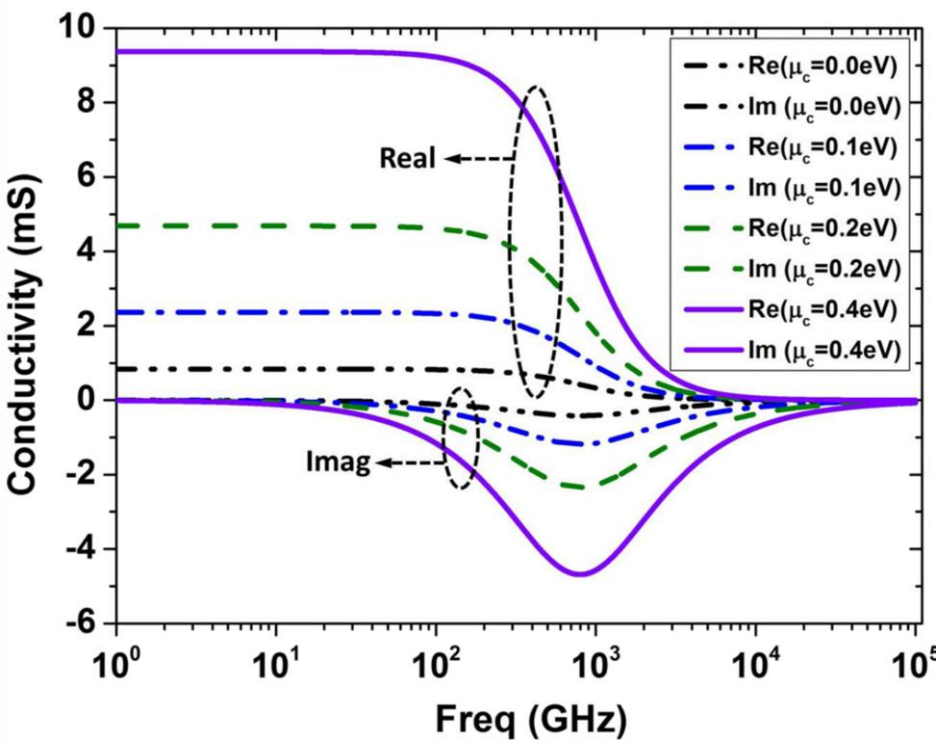

Fig. 2-6. The tunability of graphene's surface conductivity from microwave to THz frequency bands [43]

As it is too expensive to exfoliate monolayer graphene, the cheaply printed graphene which is now being heavily researched and applied in the flexible electronics industry are multilayer graphene or few-layer graphene. The printed

graphene laminates made of these materials can be directly simulated as ohmic sheets, since the skin depth is much larger than the thickness of the printed graphene layer in microwave region [22].

2.3 Graphene Ink Fabrication and Patterning

The successful synthesis of large-area graphene sheets has enabled its applications in the field of electronic and information. Advanced graphene synthesis methods, such as chemical vapor deposition (CVD) and liquid phase exfoliation (LPE), has enabled the fabrication of graphene samples with relatively large areas, thereby boosting the interest in research on electronic devices. Graphene integrated metamaterials, high-speed transistors, organic light-emitting diodes (OLEDs), plasmonics, batteries, antennas, and solar cells are among the top recognized applications [44-49]. In contrast with CVD, which needs to slowly grow large area graphene on metal surfaces and transfer to other substrates [50-53], LPE is simple, low cost, scalable, and its suitability for chemical functionalization allows the feasibility of high-volume production. Thin films acquired from liquid suspensions of graphene sheets are likely to overcome other methods' limitations [54-55] and would allow for extensive use in large batches.

The size of graphene flakes is extremely important for the electrical

conductivity of the printed graphene, as larger graphene flakes can have smaller number of interfaces with each other, contributing to better current flow, yet they may introduce voids when printed on substrates; smaller flakes can have better stacking, however, the huge numbers of interfaces eventually increase the resistance [25]. Hence, the appropriate size of the flakes is decisive for best conductivity and printing quality, avoiding performance degradation in applications. Usually, the lateral accurate dimension distributions were determined by the analysis of scanning electron microscopy (SEM), electron transfer microscopy (TEM) and atomic force microscopy (AFM) images.

Shear mixing exfoliation treatment was demonstrated in [58, 60-61, 64]. Tt has been proved that sheer mixing process can quickly reduce the flake size to avoid resource consumption produced by long hours of ultrasonication. In [58-59, 60-63], it has been emphasized that one decisive parameter to control the size of graphene nanoflakes and other related 2D material ones is the ultrasonic time, which can directly affect the conductivity. The systematical study on process optimization on the graphene conductivity has been reported in [25, 56]. In [25], it has displayed a sheet resistance comparison of Cyrene and NMP inks under the same bath ultrasonication treatment. It takes 20 hours for the sheet resistance of graphene laminate to decrease to the lowest point under ultrasonic exfoliation for NMP solvent, while the sheet resistance of graphene laminate processed with Cyrene solvent instantly drops in 8 hours. Also, temperature increase during sonication can result in inconsistent exfoliation [57, 60], i.e., deteriorating the properties of the material and lowering the dispersed concentrations, thus the ultrasonic process should be controlled at room temperature.

The conductivity of graphene is relevant to the in-house developed ink as well as the printing operation. Adding binders can increase adhesion, however, the insulating feature of binders greatly reduces the conductivity of the inks. Thus, high temperature thermal annealing needs to be processed to increase conductivity, which is not compatible with heat-sensitive substrates, such as normal A4 paper. By using a binder-free technique with NMP solvent suitable for industrial scale screen printing [30], a flexible dipole antenna on paper substrate was illustrated. Using binder-free NMP solvent can be regarded as a simple way to achieve high conductivity at high yields for printed flexible electronics without the use of high temperature annealing, however, the toxicity of the solvent hinders its broad application.

The conductivity reported without thermal annealing can be as high as 7.13×10^4 S m^{-1} with the use of Cyrene solvent [25]. However, Cyrene is very expensive comparing to NMP. To enable the industrial scale of this approach, Chapter 7 introduces a sustainable method using recycled Cyrene for cheap and highly efficient graphene ink production.

Different fabrication approaches have been intensively researched for printing graphene-based flexible electronic devices over the years, such as reactive sputtering [65], ink-jet printing [66], spin coating [67], thermal evaporation [68] and screen printing [22, 69]. Whereas sputtering and spin coating does not support patterns with high-resolution, and thermal evaporation requires very high temperature which makes it incompatible with heat sensitive substrates. Thus, more investigations have been carried out on using ink-jet printing and screen printing.

2.4 Antenna Designs

2.4.1 MIMO Antennas

MIMO technology was firstly proposed to overcome deep fading in wireless communication early in 1970s [71], however, the actual tremendous influence was accomplished by Arogyaswami and Thomas in 1990s [72]. With the arrival of the fifth-generation communication networks, additional functions and high requirements of antenna bandwidth, channel capacity, system efficiency and reliability are being expected to be generated and integrated in mobile terminals. As the number and bandwidth of the existing non-overlapping channels have been limited and strictly regulated, the basic principle of this approach is to convert unused space to a kind of resource which could be used for enhancing transmission performance and enlarging the coverage area of wireless systems, so that increasing data handling capacity and transmission distance, also reducing bit error rate at the same time. More precisely, by using multiple antennas transmission, the paths that signals can be transmitted are significantly increased. It is unlikely that all propagations experience deep fading at the same time, therefore, the system reliability can be guaranteed by either selecting or combining of the received signals.

It can be clearly seen that, MIMO technology is indispensable for the pervasive deployment of IoT smart applications to attain additional functions and requirements, and face massive data throughput for low latency, system reliability and real-time information exchange [73] based on the high-speed data transmission enabled.

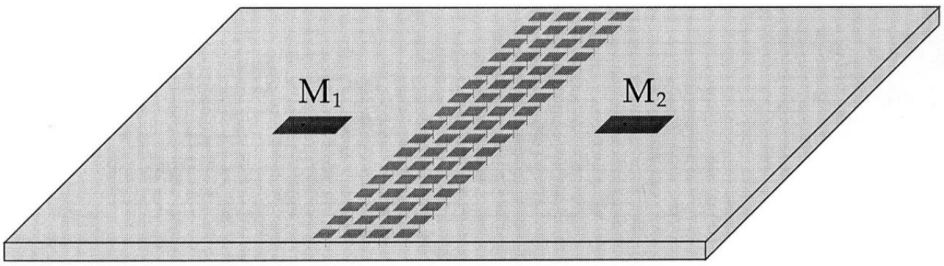

Fig. 2-7. EBG structure proposed in [80] designed for mutual coupling reduction.

However, it is important to note that installing multiple antenna elements on the small space available in portable devices will inevitably cause severe mutual coupling and significantly degrade the diversity performance. To deal with this, some approaches have been presented, for instance, space diversity [74], polarization diversity [75], pattern diversity [76], introducing slots on antenna structures or putting additional decoupling structure between antennas [77], orthogonal placement of antennas [78], stub extension from the ground for better control of current flow [79], electromagnetic band gap [80] and so on.

In Fig. 2-7 [80], low mutual coupling was achieved by using periodic multi-layered electromagnetic band gap structures between two patch antennas. The EBG structure has successfully suppressed surface wave and obtained 30dB improvement of isolation at the operating frequency. However, it also causes bandwidth reduction due to antenna mismatch affection, and failure of space distance compression.

Another study suitable for WLAN applications has been proposed in [81], as shown in Fig. 2-8, consisting of radiating patches, parasitic patches, and folded ground planes around the substrate and coaxial feed applied to the antennas individually. The mutual coupling between the antennas is improved, yet the

antenna construction could be cumbersome when applied to portable devices.

Different decoupling methods generate a diverse of performances in different systems. A well-behaved isolation may partially lead to antenna mismatch and the complexity of the whole antenna system. Therefore, it is vital to select a proper

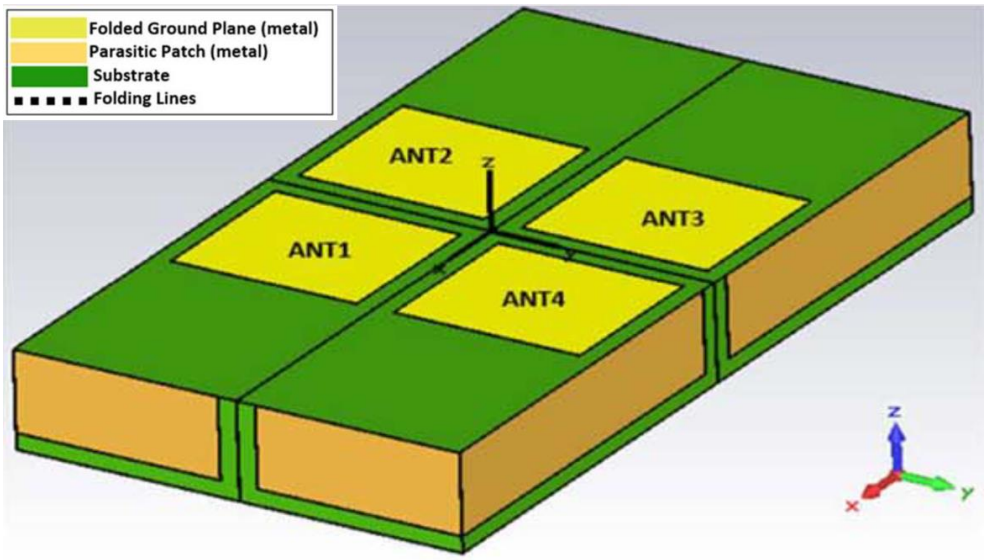

Fig. 2-8. Folded ground MIMO antenna for 2.4 GHz WLAN applications [81]

approach to attain desired characteristics.

ECC (envelope correlation coefficient) is the parameter evaluating the performance of uncorrelated channels. It involves scattering parameters of the system, estimating the mutual coupling between any of the two ports. The lower the ECC, the lesser correlation could be generated during communications in the MIMO antennas. For mobile applications, it is required that ECC value must be lower than 0.5 to achieve good diversity. The ECC value [82] could be expressed as equation (2.4),

$$|\rho_e(i,j,N)| = \frac{\left|\sum_{n=1}^{N} S_{i,n}^{*} S_{n,j}\right|^2}{\prod_{k(=i,j)}\left[1-\sum_{n=1}^{N} S_{k,n}^{*} S_{n,k}\right]} \tag{2.4}$$

where N is the number of antennas, i=1 to n, j=1 to n

The channel capacity loss (CCL) between two antenna elements is estimated by (2.5), (2.6) and (2.7) [83]

$$CCL = -\log_2 \det(\psi^R) \tag{2.5}$$

$$\psi^R = \begin{bmatrix} \rho_{11} & \rho_{12} \\ \rho_{21} & \rho_{22} \end{bmatrix} \tag{2.6}$$

$$\text{where} \quad \rho_{ii} = 1 - \left(|S_{ii}|^2 + \left|S_{ij}\right|^2 \right) \text{ and}$$
$$\rho_{ij} = -\left(S_{ii}^* S_{ij} + S_{ji}^* S_{jj} \right) \qquad \text{for i, j = 1 or 2.} \tag{2.7}$$

The standard CCL for a 4×4 MIMO antenna is below 0.4 bits/s/Hz, where the channel capacity of a MIMO communication system varies with the number of antennas responsible for transmitting and receiving signals, the signal-to-noise ratio, the state of the channel, and the covariance matrix of the vector of transmitted signals [84].

There has been a huge amount of literature discussing on the theory and performance of MIMO systems [85-88], which covers a wide range of content. However, since the wireless mobile communication is a time-varying and non-stationary system, there are still many problems to be studied. In this study, we will only focus on MIMO antenna designs

2.4.2 Dual/Multi-band Antennas

A dual-band or multi-band antenna can transmit or receive RF signals at two or more distinct frequency ranges. It was first reported in 1984 by Wang and Lo, inserting shorting pins in normal rectangular patches [89]. The use of dual-band or multi-frequency antennas has historically been proven to remarkably improve the stability of wireless connections. Using non-overlapping uncrowded channels can reduce interference that degrades transmission speeds, moreover, enable backward

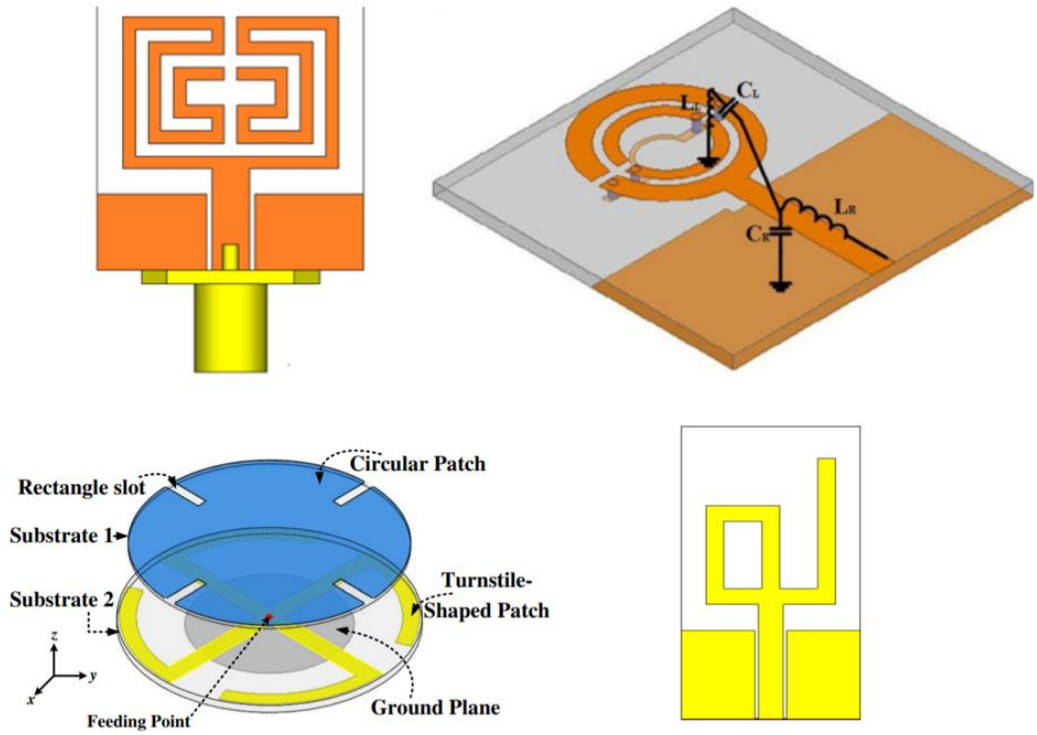

Fig. 2-9. Typical designs of dual/multiband antennas [90-92, 94].

compatibility, using either frequency for accessing earlier versions of WiFi or mobile networks, it can also double the bandwidth using two bands for different purposes.

Depending on their configuration designs, these multi-band antennas have the

ability to use any of these frequencies individually or simultaneously. 2.4 GHz and 5 GHz bands are often seen as pairs of dual-band antennas, as they are commonly used in WiFi networks. A well-designed multi-band antenna should be optimized to be matched at all desired frequencies so that good VSWR can be achieved in all bands. In terms of the design level, these antennas are typically constructed by adopting more than two monopole or dipole elements. Each of the integrated antenna units resonates at one of the target frequencies. The length of each antenna element needs to be adjusted according to the wavelength of the different target frequencies to guarantee good sensitivity at each frequency. Typical designs are shown in Fig. 2-9, involve etching slot or notch in the patch, adding parasitic structures, using U and T shapes, stacking different dielectric substrates, and applying meandered lines [90-94].

2.5 Antenna Gain Measurement

To evaluate an antenna's far field characteristics, the ideal condition is to illuminate the test antenna using planes waves with uniform amplitude and phase. It has been demonstrated that at a separation distance of $2D^2/\lambda$, which is defined as the inner boarder of far-field, the incident field generated by an ideal uniform plane wave gives a maximum phase error of 22.5°.

The peak gain of an antenna can be measured by applying the Friis Transmission Equation (2.8) and a standard test antenna with known performance

[95]:

$$P_R = \frac{P_T G_T G_R \lambda^2}{(4\pi R)^2} \tag{2.8}$$

where P_R is the received power from the receiver antenna, P_T is the transmitted power from the source antenna, G_T is the gain of the transmitting antenna and G_R is the gain of the receiving antenna, R is the separation distance of the two antennas, relating the path loss in free space, wavelength, and antenna gains to the received and transmitted powers.

To express Friis Transmission Equation in terms of S21 in dB:

$$S21_{dB} = P_L + G_T + G_R \tag{2.9}$$

where the path loss in dB is:

$$P_L = 20Log\left(\frac{\lambda}{4\pi d}\right) \tag{2.10}$$

The most widely used standard test antennas are thin half-wave dipole antennas and horn antennas, which typically offer peak gains of 2.15 dBi and 15-25 dBi respectively. This is called the standard antenna method.

The three-antenna method (For instance antenna A, B, C) uses the same equations with three unknowns, with its measurement pairs established as [A, B], [B, C] and [A,C]:

$$S21_{AB} = P_L + G_A + G_B \tag{2.11}$$

$$S21_{BC} = P_L + G_B + G_C \tag{2.12}$$

$$S21_{AC} = P_L + G_A + G_C \tag{2.13}$$

Then the gain (dB) can be derived from

$$G_A = \frac{S21_{AB} + S21_{AC} - S21_{BC} - P_L}{2} \tag{2.14}$$

$$G_B = G_A + S21_{BC} - S21_{AC} \tag{2.15}$$

$$G_C = S21_{BC} - P_L - G_B \tag{2.16}$$

2.6 Sheet Resistance Measurement

Sheet resistance of thin electroconductive films can be determined by a four-point probe measurement method and a semiconductor characterization system [65]. The sheet resistance can be expressed as

$$\mathrm{R}_s = \frac{\rho}{t} \tag{2.17}$$

where ρ is the resistivity and t is the thickness of the measured conductive film.

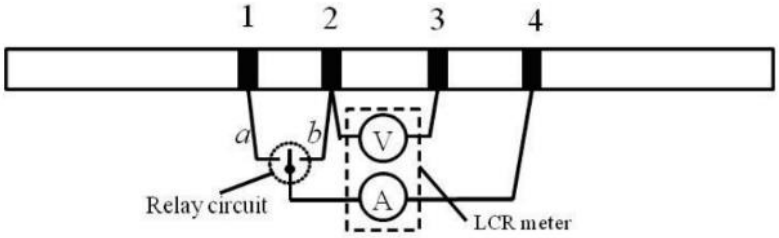

Fig. 2-10. The four-probe measurement method [96].

As illustrated in Fig. 2-10, in the four-probe measurement system, electrodes 1 and 4 are used to apply electric current, while electrode 2 and 3 testing the voltage change as the relay circuit switches to “a”. Since the current flow in the voltammeter can be neglected, with the fixed distance between the probes, the electrical contact sheet resistance can therefore be measured accurately and independently by using this four-probe method.

References

[1] D. Anagnostou, A. Gheethan, A. Amert and K. Whites, "A Direct-Write Printed Antenna on Paper-Based Organic Substrate for Flexible Displays and WLAN Applications", *Journal of Display Technology*, vol. 6, no. 11, pp. 558-564, 2010. Available: 10.1109/jdt.2010.2045474.

[2] F. Aieta, P. Genevet, M. Kats and F. Capasso, "Aberrations of flat lenses and aplanatic metasurfaces", *Optics Express*, vol. 21, no. 25, p. 31530, 2013. Available: 10.1364/oe.21.031530.

[3] S. Zhao and R. Zhu, "Electronic Skin: Electronic Skin with Multifunction Sensors Based on Thermosensation (Adv. Mater. 15/2017)", *Advanced Materials*, vol. 29, no. 15, 2017. Available: 10.1002/adma.201770099.

[4] A. Ono, M. Takishita, M. Sumiyoshi and V. Mizeikis, "Laser Induced Photoreduction for Metal Based Flexible Transparent Electrode", *Proceedings of the International Display Workshops*, p. 939, 2020. Available: 10.36463/idw.2020.0939.

[5] N. Ooi, H. Aoki, D. Watanabe, J. Jeong, C. Kimura and T. Sugino, "Cu Electroplating Process with Magnetic Field for Flexible Device", *Japanese Journal of Applied Physics*, vol. 48, no. 4, p. 046504, 2009. Available: 10.1143/jjap.48.046504.

[6] W. Whittow et al., "Inkjet-Printed Microstrip Patch Antennas Realized on Textile for Wearable Applications", *IEEE Antennas and Wireless Propagation Letters*, vol. 13, pp. 71-74, 2014. Available: 10.1109/lawp.2013.2295942.

[7] M. Saleh, C. Hu and R. Panat, "Three-dimensional microarchitected materials and devices using nanoparticle assembly by pointwise spatial printing", *Science Advances*, vol. 3, no. 3, 2017. Available: 10.1126/sciadv.1601986.

[8] L. Song, A. Myers, J. Adams and Y. Zhu, "Stretchable and Reversibly Deformable Radio Frequency Antennas Based on Silver Nanowires", *ACS Applied Materials & Interfaces*, vol. 6, no. 6, pp. 4248-4253, 2014. Available: 10.1021/am405972e.

[9] M. Mirzaee, S. Noghanian, L. Wiest and I. Chang, "Developing flexible 3D printed antenna using conductive ABS materials," *2015 IEEE International Symposium on Antennas and Propagation & USNC/URSI National Radio Science Meeting*, 2015, pp. 1308-1309, doi: 10.1109/APS.2015.7305043.

[10] I. M. Graz, D. P. J. Cotton, and S. P. Lacour, "Extended cyclic uniaxial loading of stretchable gold thin-films on elastomeric substrates",*Applied Physics Letters,* Vol. 94, No. 7, Feb. 2009.

[11] Hu L, Hecht DS, Gruner G. Carbon nanotube thin films: fabrication, properties, and applications. Chem Rev 2010;110:5790–844.

[12] K. Lu, R. Lago, Y. Chen, M. Green, P. Harris and S. Tsang, "Mechanical damage of carbon nanotubes by ultrasound", *Carbon*, vol. 34, no. 6, pp. 814-816, 1996. Available: 10.1016/0008-6223(96)89470-x.

[13] S. Azoubel and S. Magdassi, "The formation of carbon nanotube dispersions by high pressure homogenization and their rapid characterization by analytical centrifuge", *Carbon*, vol. 48, no. 12, pp. 3346-3352, 2010. Available: 10.1016/j.carbon.2010.05.024.

[14] T. Rai, P. Dantes, B. Bahreyni and W. Kim, "A Stretchable RF Antenna With Silver Nanowires", *IEEE Electron Device Letters*, vol. 34, no. 4, pp. 544-546, 2013. Available: 10.1109/led.2013.2245626.

[15] A. Rathmell and B. Wiley, "The Synthesis and Coating of Long, Thin Copper Nanowires to Make Flexible, Transparent Conducting Films on Plastic Substrates", *Advanced Materials*, vol. 23, no. 41, pp. 4798-4803, 2011. Available: 10.1002/adma.201102284.

[16] H. Shirakawa, E. Louis, A. MacDiarmid, C. Chiang and A. Heeger, "Synthesis of electrically conducting organic polymers: halogen derivatives of polyacetylene, (CH) x", *Journal of the Chemical Society, Chemical Communications*, no. 16, p. 578, 1977. Available: 10.1039/c39770000578.

[17] R. J. Vyas, A. Rida, L. Yang, and M. M. Tentzeris, “Design and development of the first entirely paper-based wireless sensor module,” in IEEE Antennas Propag Soc. Int. Symp., Jul. 5–11, 2008, pp. 1–4.

[18] K. Namiki, X. Cheng and H. Takahashi, "Indirectly Reactive Sputtering Coater for High Quality Optical Coatings", *IEICE Transactions on Electronics*, vol. 91-, no. 10, pp. 1673-1674, 2008. Available: 10.1093/ietele/e91-c.10.1673.

[19] T. Campbell, R. Kalia, A. Nakano, P. Vashishta, S. Ogata and S. Rodgers, "Dynamics of Oxidation of Aluminum Nanoclusters using Variable Charge Molecular-Dynamics Simulations on Parallel Computers", *Physical Review Letters*, vol. 82, no. 24, pp. 4866-4869, 1999. Available: 10.1103/physrevlett.82.4866.

[20] K. Novoselov et al., "Electric Field Effect in Atomically Thin Carbon Films", *Science*, vol. 306, no. 5696, pp. 666-669, 2004. Available: 10.1126/science.1102896.

[21] X. Huang, T. Leng, T. Georgiou, J. Abraham, R. Nair, K. S. Novoselov, and Z. Hu, “Graphene oxide dielectric permittivity at GHz and its applications for wireless humidity sensing,” *Scientific reports*, vol. 8, no. 1, p. 43, 2018.

[22] X. Huang et al., "Highly Flexible and Conductive Printed Graphene for Wireless Wearable Communications Applications", *Scientific Reports*, vol. 5, no. 1, 2015. Available: 10.1038/srep18298.

[23] T. Leng et al., "Printed graphene/WS2 battery-free wireless photosensor on papers", *2D Materials*, vol. 7, no. 2, p. 024004, 2020. Available:

10.1088/2053-1583/ab602f.

[24] T. Leng, X. Huang, K. Chang, J. Chen, M. Abdalla and Z. Hu, "Graphene Nanoflakes Printed Flexible Meandered-Line Dipole Antenna on Paper Substrate for Low-Cost RFID and Sensing Applications", *IEEE Antennas and Wireless Propagation Letters*, vol. 15, pp. 1565-1568, 2016. Available: 10.1109/lawp.2016.2518746.

[25] K. Pan et al., "Sustainable production of highly conductive multilayer graphene ink for wireless connectivity and IoT applications", *Nature Communications*, vol. 9, no. 1, 2018. Available: 10.1038/s41467-018-07632-w.

[26] A. Lamminen et al., "Graphene-Flakes Printed Wideband Elliptical Dipole Antenna for Low-Cost Wireless Communications Applications", *IEEE Antennas and Wireless Propagation Letters*, vol. 16, pp. 1883-1886, 2017. Available: 10.1109/lawp.2017.2684907.

[27] K. Arapov et al., "Graphene screen-printed radio-frequency identification devices on flexible substrates", physica status solidi (RRL) - *Rapid Research Letters*, vol. 10, no. 11, pp. 812-818, 2016. Available: 10.1002/pssr.201600330.

[28] K. Jaakkola, H. Sandberg, M. Lahti and V. Ermolov, "Near-Field UHF RFID Transponder With a Screen-Printed Graphene Antenna", *IEEE Transactions on Components*, Packaging and Manufacturing Technology, vol. 9, no. 4, pp. 616-623, 2019. Available: 10.1109/tcpmt.2019.2902322.

[29] X. Huang, T. Leng, K. Chang, J. Chen, K. Novoselov and Z. Hu, "Graphene radio frequency and microwave passive components for low cost wearable electronics", *2D Materials*, vol. 3, no. 2, p. 025021, 2016. Available: 10.1088/2053-1583/3/2/025021.

[30] X. Huang et al., "Binder-free highly conductive graphene laminate for low cost printed radio frequency applications", *Applied Physics Letters*, vol. 106, no. 20, p. 203105, 2015. Available: 10.1063/1.4919935.

[31] R. Song et al., "A Graphene-Assembled Film Based MIMO Antenna Array with High Isolation for 5G Wireless Communication", *Applied Sciences*, vol. 11, no. 5, p. 2382, 2021. Available: 10.3390/app11052382.

[32] O.M. Slobodian, P.M. Lytvyn, A.S. Nikolenko, V.M. Naseka, O.Y. Khyzhun, A. V Vasin, S. V Sevostianov, A.N. Nazarov, Low-Temperature Reduction of Graphene Oxide: Electrical Conductance and Scanning Kelvin Probe Force Microscopy, *Nanoscale Res. Lett*. 13 (2018) 139.

[33] A. Lamminen et al., "Graphene-Flakes Printed Wideband Elliptical Dipole Antenna for Low-Cost Wireless Communications Applications", *IEEE Antennas and Wireless Propagation Letters*, vol. 16, pp. 1883-1886, 2017. Available: 10.1109/lawp.2017.2684907.

[34] A. Geim and K. Novoselov, "The rise of graphene", *Nature Materials*, vol. 6, no. 3, pp. 183-191, 2007. Available: 10.1038/nmat1849.

[35] L. Berry, " Liquids and Solids Chapter 10.," Slideplayer, 2019.

[36] H. Abutarboush and A. Shamim, "Paper-Based Inkjet-Printed Tri-Band U-Slot Monopole Antenna for Wireless Applications", *IEEE Antennas and Wireless Propagation Letters*, vol. 11, pp. 1234-1237, 2012. Available: 10.1109/lawp.2012.2223751.

[37] H. Zhu, Z. Xu, D. Xie and Y. Fang, *Graphene*. London: Academic Press, an imprint of Elsevier, 2018.

[38] K. Novoselov, "Beyond the wonder material", *Physics World*, vol. 22, no. 08, pp. 27-30, 2009. Available: 10.1088/2058-7058/22/08/33.

[39] V. Gusynin, S. Sharapov, and J. Carbotte, “Magneto-optical conductivity in graphene,” J. Phys.: Condens. Matter, vol. 19, no. 2, Dec. 2006, Art. no. 026222.

[40] G. W. Hanson, “Dyadic Green’s functions and guided surface waves for a surface conductivity model of graphene,” J. App. Phy., vol. 103, no. 6, Apr. 2008, Art. no. 064302.

[41] A. Crépieux and P. Bruno, “Theory of the anomalous hall effect from the Kubo formula and the dirac equation,” Phys. Rev. B, vol. 64, no. 1, Jun. 2001, Art. no. 014416.

[42] K. Niu, P. Li, Z. Huang, L. Jiang and H. Bagci, "Numerical Methods for Electromagnetic Modeling of Graphene: A Review", *IEEE Journal on Multiscale and Multiphysics Computational Techniques*, vol. 5, pp. 44-58, 2020. Available: 10.1109/jmmct.2020.2983336.

[43] X. Huang, Z. Hu and P. Liu, "Graphene based tunable fractal Hilbert curve array broadband radar absorbing screen for radar cross section reduction", *AIP Advances*, vol. 4, no. 11, p. 117103, 2014. Available: 10.1063/1.4901187.

[44] M. Tamagnone, J. Gómez-Díaz, J. Mosig and J. Perruisseau-Carrier, "Reconfigurable terahertz plasmonic antenna concept using a graphene stack", *Applied Physics Letters*, vol. 101, no. 21, p. 214102, 2012. Available: 10.1063/1.4767338.

[45] D. Correas-Serrano, J. Gomez-Diaz, J. Perruisseau-Carrier and A. Alvarez-Melcon, "Graphene-Based Plasmonic Tunable Low-Pass Filters in the Terahertz Band", *IEEE Transactions on Nanotechnology*, vol. 13, no. 6, pp. 1145-1153, 2014. Available: 10.1109/tnano.2014.2344973.

[46] B. Wu, Y. Hu, Y. Zhao, W. Lu and W. Zhang, "Large angle beam steering THz antenna using active frequency selective surface based on hybrid graphene-gold structure", *Optics Express*, vol. 26, no. 12, p. 15353, 2018. Available: 10.1364/oe.26.015353.]

[47] P. Blake et al., “Graphene-based liquid crystal device,” Nano Lett., vol. 8, no. 6, pp. 1704–1708, Apr. 2008.

[48] K. S. Novoselov et al., “Room-temperature quantum Hall effect in graphene,” Science, vol. 315, no. 5817, pp. 1379–1379, Mar. 2007.

[49] F. Bonaccorso, Z. Sun, T. Hasan, and A. Ferrari, “Graphene photonics and optoelectronics,” Nature Photon., vol. 4, no. 9, pp. 611–622, Aug. 2010.

[50] J. Lee, H. Ahn, J. Yoon and J. Jang, "Three-dimensional nano-foam of few-layer graphene grown by CVD for DSSC", *Physical Chemistry Chemical Physics*, vol. 14, no. 22, p. 7938, 2012. Available: 10.1039/c2cp40810d.

[51] B. Wu, H.M. Tuncer, A. Katsounaros, W. Wu, M.T. Cole, K. Ying, L. Zhang, W.I. Milne, Y. Hao, Microwave absorption and radiation from

large-area multilayer CVD graphene, Carbon N. Y. 77 (2014) 814–822.

[52] X. Li et al., "Large-Area Synthesis of High-Quality and Uniform Graphene Films on Copper Foils", *Science*, vol. 324, no. 5932, pp. 1312-1314, 2009. Available: 10.1126/science.1171245.

[53] K. Kim et al., "Large-scale pattern growth of graphene films for stretchable transparent electrodes", *Nature*, vol. 457, no. 7230, pp. 706-710, 2009. Available: 10.1038/nature07719..

[54] A. Reina et al., "Large Area, Few-Layer Graphene Films on Arbitrary Substrates by Chemical Vapor Deposition", *Nano Letters*, vol. 9, no. 1, pp. 30-35, 2009. Available: 10.1021/nl801827v.

[55] P. Avouris and F. Xia, "Graphene applications in electronics and photonics", *MRS Bulletin*, vol. 37, no. 12, pp. 1225-1234, 2012. Available: 10.1557/mrs.2012.206.

[56] T. Leng et al., "Screen-Printed Graphite Nanoplate Conductive Ink for Machine Learning Enabled Wireless Radiofrequency-Identification Sensors", *ACS Applied Nano Materials*, vol. 2, no. 10, pp. 6197-6208, 2019. Available: 10.1021/acsanm.9b01034.

[57] S. Biccai et al., "Exfoliation of 2D materials by high shear mixing", *2D Materials*, vol. 6, no. 1, p. 015008, 2018. Available: 10.1088/2053-1583/aae7e3.

[58] K. Kouroupis-Agalou et al., "Fragmentation and exfoliation of 2-dimensional materials: a statistical approach", *Nanoscale*, vol. 6, no. 11, pp. 5926-5933, 2014. Available: 10.1039/c3nr06919b.

[59] K. Paton et al., "Scalable production of large quantities of defect-free few-layer graphene by shear exfoliation in liquids", *Nature Materials*, vol. 13, no. 6, pp. 624-630, 2014. Available: 10.1038/nmat3944.

[60] C. Backes et al., "Production and processing of graphene and related materials. ", *2D Mater., 2020,* 7, 022001.

[61] D. Nuvoli et al., "High concentration few-layer graphene sheets obtained by liquid phase exfoliation of graphite in ionic liquid", *J. Mater. Chem.*, vol. 21, no. 10, pp. 3428-3431, 2011. Available: 10.1039/c0jm02461a.

[62] U. Khan, A. O'Neill, M. Lotya, S. De and J. Coleman, "High-Concentration Solvent Exfoliation of Graphene", *Small*, vol. 6, no. 7, pp. 864-871, 2010. Available: 10.1002/smll.200902066.

[63] C. Huo, Z. Yan, X. Song and H. Zeng, "2D materials via liquid exfoliation: a review on fabrication and applications", *Science Bulletin*, vol. 60, no. 23, pp. 1994-2008, 2015. Available: 10.1007/s11434-015-0936-3.

[64] P. Turner, M. Hodnett, R. Dorey and J. Carey, "Controlled Sonication as a Route to in-situ Graphene Flake Size Control", *Scientific Reports*, vol. 9, no. 1, 2019. Available: 10.1038/s41598-019-45059-5.

[65] T. Hansen et al., "Resolution enhancement of scanning four-point-probe measurements on two-dimensional systems", *Review of Scientific Instruments*, vol. 74, no. 8, pp. 3701-3708, 2003. Available: 10.1063/1.1589161.

[66] S. Saeed, C. Balanis and C. Birtcher, "Inkjet-Printed Flexible Reconfigurable Antenna for Conformal WLAN/WiMAX Wireless Devices", *IEEE Antennas and Wireless Propagation Letters*, vol. 15, pp. 1979-1982, 2016. Available: 10.1109/lawp.2016.2547338.

[67] M. Tyona, "A comprehensive study of spin coating as a thin film deposition technique and spin coating equipment", *Advances in materials Research*, vol. 2, no. 4, pp. 181-193, 2013. Available: 10.12989/amr.2013.2.4.181.

[68] A. Kamyshny and S. Magdassi, "Conductive Nanomaterials for Printed Electronics", *Small*, vol. 10, no. 17, pp. 3515-3535, 2014. Available: 10.1002/smll.201303000.

[69] X. Huang, T. Leng, T. Georgiou, J. Abraham, R. Nair, K. S. Novoselov, and Z. Hu, “Graphene oxide dielectric permittivity at GHz and its applications for wireless humidity sensing,” Scientific reports, vol. 8, no. 1, p. 43, 2018.

[70] Y. Seekaew, S. Lokavee, D. Phokharatkul, A. Wisitsoraat, T. Kerdcharoen and C. Wongchoosuk, "Low-cost and flexible printed graphene–PEDOT:PSS gas sensor for ammonia detection", *Organic Electronics*, vol. 15, no. 11, pp. 2971-2981, 2014. Available: 10.1016/j.orgel.2014.08.044.

[71] A. Kaye and D. George, "Transmission of Multiplexed PAM Signals Over Multiple Channel and Diversity Systems", *IEEE Transactions on Communications*, vol. 18, no. 5, pp. 520-526, 1970. Available: 10.1109/tcom.1970.1090417.

[72] *"Arogyaswami Paulraj – Marconi Society". marconisociety.org (in American English)*. Retrieved 2017-01-21.

[73] L. Malviya, R. Panigrahi and M. Kartikeyan, "MIMO antennas with diversity and mutual coupling reduction techniques: a review", *International Journal of Microwave and Wireless Technologies*, vol. 9, no. 8, pp. 1763-1780, 2017. Available: 10.1017/s1759078717000538.

[74] G. Jeong, S. Choi, K. Lee and W. Kim, "Low-Profile Dual-Wideband MIMO Antenna with Low ECC for LTE and Wi-Fi Applications", *International Journal of Antennas and Propagation*, vol. 2014, pp. 1-6, 2014. Available: 10.1155/2014/158028.

[75] W. Lee and Yu Yeh, "Polarization Diversity System for Mobile Radio", *IEEE Transactions on Communications*, vol. 20, no. 5, pp. 912-923, 1972. Available: 10.1109/tcom.1972.1091263.

[76]J. Oh and K. Sarabandi, "Compact, Low Profile, Common Aperture Polarization, and Pattern Diversity Antennas", *IEEE Transactions on*

Antennas and Propagation, vol. 62, no. 2, pp. 569-576, 2014. Available: 10.1109/tap.2013.2291901.

[77]J. Costa, E. Lima, C. Medeiros and C. Fernandes, "Evaluation of a New Wideband Slot Array for MIMO Performance Enhancement in Indoor WLANs", *IEEE Transactions on Antennas and Propagation*, vol. 59, no. 4, pp. 1200-1206, 2011. Available: 10.1109/tap.2011.2109685.

[78] G. Adamiuk, S. Beer, W. Wiesbeck and T. Zwick, "Dual-Orthogonal Polarized Antenna for UWB-IR Technology", *IEEE Antennas and Wireless Propagation Letters*, vol. 8, pp. 981-984, 2009. Available: 10.1109/lawp.2009.2029880.

[79]C. Wu, G. Zhou, Y. Wu and T. Ma, "Stub-Loaded Reactive Decoupling Network for Two-Element Array Using Even–Odd Analysis", *IEEE Antennas and Wireless Propagation Letters*, vol. 12, pp. 452-455, 2013. Available: 10.1109/lawp.2013.2255255.

[80]F. Yang and Y. Rahmat-Samii, "Microstrip antennas integrated with electromagnetic band-gap (EBG) structures: A low mutual coupling design for array applications", *IEEE Transactions on Antennas and Propagation*, vol. 51, no. 10, pp. 2936-2946, 2003. Available: 10.1109/tap.2003.817983.

[81]M. Ahmad, W. Mohyuddin, H. Choi and K. Kim, "4 × 4 MIMO antenna design with folded ground plane for 2.4 GHz WLAN applications", *Microwave and Optical Technology Letters*, vol. 60, no. 2, pp. 395-399, 2018. Available: 10.1002/mop.30969.

[82]J. Thaysen and K. Jakobsen, "Envelope correlation in (N,N) MIMO antenna array from scattering parameters", *Microwave and Optical Technology Letters*, vol. 48, no. 5, pp. 832-834, 2006. Available: 10.1002/mop.21490.

[83]S. Tripathi, A. Mohan and S. Yadav, "A Compact Koch Fractal UWB MIMO Antenna With WLAN Band-Rejection", *IEEE Antennas and*

Wireless Propagation Letters, vol. 14, pp. 1565-1568, 2015. Available: 10.1109/lawp.2015.2412659.

[84] A Paulraj RN, Gore D: *Introduction to Space-time Wireless Communications*. Cambridge University Press, USA; 2005.

[85] Q. He, Z. Wang, J. Hu and R. Blum, "Performance Gains From Cooperative MIMO Radar and MIMO Communication Systems", *IEEE Signal Processing Letters*, vol. 26, no. 1, pp. 194-198, 2019. Available: 10.1109/lsp.2018.2880836.

[86] L. Yang, S. Yan and T. Li, "COMPACT PRINTED FOUR-ELEMENT MIMO ANTENNA SYSTEM FOR LTE/ISM OPERATIONS", *Progress In Electromagnetics Research Letters*, vol. 54, pp. 47-53, 2015. Available: 10.2528/pierl15060801.

[87] T. Qaradaghi and D. Hussein, "Evaluation of different 4x4 Coded MIMO System", *Journal of Zankoy Sulaimani - Part A*, vol. 17, no. 2, pp. 71-84, 2015. Available: 10.17656/jzs.10382.

[88] A. D., "MIMO based Channel Selection Technique for Automation Broadband Networks with IoT Applications", *International Journal of Psychosocial Rehabilitation*, vol. 23, no. 3, pp. 1002-1011, 2019. Available: 10.37200/ijpr/v23i3/pr190500.

[89] B. Wang and Y. Lo, "Microstrip antennas for dual-frequency operation", *IEEE Transactions on Antennas and Propagation*, vol. 32, no. 9, pp. 938-943, 1984. Available: 10.1109/tap.1984.1143459.

[90] J. Yu, Y. Sun, H. Fang and F. Li, "A novel stacked patch antenna with dual band and diverse pattern characteristics", *Microwave and Optical Technology Letters*, vol. 62, no. 1, pp. 453-465, 2019. Available: 10.1002/mop.32036.

[91] A. Manouare, S. Ibnyaich, A. Idrissi, A. Ghammaz and N. Touhami, "A Compact Dual-Band CPW-Fed Planar Monopole Antenna for 2.62–2.73 GHz Frequency Band, WiMAX and WLAN Applications", *Journal of*

Microwaves, Optoelectronics and Electromagnetic Applications, vol. 16, no. 2, pp. 564-576, 2017. Available: 10.1590/2179-10742017v16i2911.

[92] S. Heydari, K. Pedram, Z. Ahmed and F. Zarrabi, "Dual band monopole antenna based on metamaterial structure with narrowband and UWB resonances with reconfigurable quality", *AEU - International Journal of Electronics and Communications*, vol. 81, pp. 92-98, 2017. Available: 10.1016/j.aeue.2017.07.015.

[93] S. Menon, "Microstrip Patch Antenna Assisted Compact Dual Band Planar Crossover", *Electronics*, vol. 6, no. 4, p. 74, 2017. Available: 10.3390/electronics6040074.

[94] D. Naji, "Design of Compact Dual-band and Tri-band Microstrip Patch Antennas", *Article.sapub.org*, 2018. [Online]. Available: http://article.sapub.org/10.5923.j.ijea.20180801.02.html. [Accessed: 22- Aug- 2021].

[95] H. Friis, "A Note on a Simple Transmission Formula", *Proceedings of the IRE*, vol. 34, no. 5, pp. 254-256, 1946. Available: 10.1109/jrproc.1946.234568.

Chapter 3 Conformal Screen Printed Graphene 4×4 Wideband MIMO Antenna On Flexible Substrate For 5G Communication and IoT Applications

Xinyao Zhou, Ting Leng, Kewen Pan, Mahmoud Abdalla, Kostya S. Novoselov and Zhirun Hu

2D Materials, vol. 8, no. 4, p. 045021, 2021.

My contributions:

I have prepared the graphene ink, designed and fabricated the proposed device, performed all the measurement, calculated and analysed all the data, and drew all the graphs.

Abstract

The work was aimed for integrating MIMO technology with low-cost, biodegradable printed graphene technique to conquer the most concerned surge in electronic waste caused by the mass production of antennas spurred by the significant deployment of IoT applications, while at the same time fully supporting 5G wireless communication mass data throughput and high performance IoT applications, guaranteeing high-speed data transmission and system reliability.

The major novelties in our work are: 1) flexibility brought by printing graphene technology, 2) low-cost and easily accessible fabrication process suitable for large scale sustainable manufacturing, and 3) the design of wideband flexible MIMO antenna with very low mutual coupling. The work is a novel aggregation of screen-printed graphene and MIMO technology, enabling easy integration of low-cost, flexible and green MIMO antennas for massive IoT applications.

Screen-printed graphene is integrated with MIMO technology to conquer the most concerned surge in electronic waste caused by the mass deployment of IoT applications. A flexible MIMO antenna is implemented with simple fabrication process suitable for large-scale production by screen printing graphene highly conductive ink on paper substrate, ensuring high-speed 5G mass data wireless transmission without damaging the ecological environment. This environmental-friendly, low-cost, flexible and conformal MIMO antenna with orthogonal polarization diversity employs co-planar waveguide (CPW) feed and planar pattern for achieving high space utilization and better integration in most scenarios, for instance, body centric networks and monitoring systems. Excellent performance has been achieved due to the high conductivity of the graphene: the fabricated antenna exhibits an average sheet resistance of $\mathbf{1.9\ \Omega/sq}$. The bandwidth of the antenna ranges from $\mathbf{2.22\ GHz\ to\ 3.85\ GHz}$ (53.71% fractional bandwidth), covering $\mathbf{4G}$ LTE, sub 6 GHz $\mathbf{5G}$ mobile communication networks, 2.5 and 3.5 GHz WiMAX, and 2.4 and 3.6 GHz WLAN. Within this range, the antenna exhibits effective radiation, also its envelope correlation coefficient (ECC) remains below $\mathbf{0.2 \times 10^{-6}}$, manifesting outstanding signal transmission quality in a variety of wireless networks. This work illustrates a novel aggregation of MIMO technology and graphene printing electronics, enabling cheap accessible and green MIMO antennas to be massively integrated in IoT applications.

3.1 Introduction

Spurred by the arrival of the 5G revolution, the implementation of Internet of Things (IoT) and its extended concept, Internet of Everything (IoE), have greatly increased the yield requirement of conformal wireless printed electronics as well as the quality of communication networks. Intense efforts have been put in developing nanomaterials with excellent properties and simpler fabrication process with lower cost and higher feasibility. Among all the 2D materials, graphene has been the most extensively investigated for its prominent properties given by its two-dimensional crystal structure [1], such as its high carrier mobility, conductivity, and high strength.

To produce graphene at high yields, liquid-phase exfoliation of graphite flakes [2] surpasses other approaches such as micromechanical cleavage, dispersion and exfoliation of graphene oxide (GO), growth on metal substrates or annealing on SiC substrates for its high production efficiency and preserve of graphene's electronic structure. This method is also attainable for other 2D materials such as transition metal dichalcogenides (TMDs), black phosphorus (BP) and hexagonal-Boron Nitride (h-BN) with a variety of solvents [3]. The efficiency of exfoliation is closely related to the ratios of the surface tension component of the solvent and that of the 2D material. These dispersions can then be used to produce ink and deposit flakes on desirable substrates by simple printing methods, realizing mass scalable and fully printable 2D material applications including energy storage, conductive inks, sensors and optical devices [4].

Different printing techniques of 2D materials have been developed on substrates such as polymers, glass and paper [5], exhibiting multi functionalities and

promising potentials. However, mass manufacturing of electronic equipments brings mass disposal. Waste disposition of electronics has been an insurmountable obstacle that drawn the most concerns. To keep large-scale industrial production compatible with sustainable development, at the same time in pursuit of low cost and flexiblility, a large amount of work has been devoted to fabricating 2D materials on flexible substrate, such as paper, to ensure the biological degradability of electronic devices [6-9, 26, 38]. By taking good advantage of the porosity of paper, printing formulated ink on paper allows fast absorption, enhancing the resolution of pattern and avoiding unwanted diffusion. Graphene, making a good substitution of conventional metal for its high conductivity and strength, environmental amity, and extremely low cost, has been reported fully compatible with paper substrate using simple printing techniques [6-9, 38], which even enhances the robustness of flexible devices including electrodes, transistors, antennas and interconnecting transmission lines, and prevents discontinuities during high-level deformation [10], suitable for large scale manufacture and disposable use.

Sub-6 GHz based 5G achitecture has brought IoT applications into the spotlight as they establish interconnection between people and machines and between machines and machines, make information exchange swift, convenient and precise in people's everyday life. The occurrence of multiple-input multiple-output (MIMO) technology is regarded as a significant breakthrough that breaks the data throughput limit exists in conventional single-input single-output (SISO) systems, provides full use of space resource and multiplies channel capacity, spectral efficiency and data handling capacity without actual extension of frequency usage or any antenna transmitting power increase [11-12]. The use of MIMO technology

is indispensable for the pervasive deployment of IoT smart applications to attain additional functions and requirements, and face massive data throughput for the achievement of low latency, reliability and real-time information exchange [13]. A number of MIMO antennas with large bandwidth designed for 5G cellular networks and IoT platform have been investigated in [14-16], designed with rigid metal and conventional substrates. However, to meet the rapid development of IoT, flexibility of electronic devices is particularly necessary to enhance adaptability and user comfort, yet few efforts have been made using flexible substrate [17-18]. For instance, MIMO antennas implemented on textiles [17] require large soldering area on the plate, weakening its reconfigurability and sustainability. To attach antenna patterns to substrates, planar conformal antennas, such as printed flexible antennas would be the best choice, thanks to the advances in the modern printed electronic technology. Ink-jet printing silver nanoparticle ink on polyethylene terephthalate (PET) substrate can also be a way [18], yet it significantly rises the cost of manufacturing and introduces cracks during heavy deformation.

To fabricate graphene antennas with high pattern accuracy, most work have been focused on using ink-jet printing and screen printing techniques [6-9, 19]. With its extremely low cost and easy process, screen printing transcends ink-jet printing from the perspective of mass production [20]. Screen printed graphene antennas have been reported [6-9, 20, 28-31, 38], the research is mostly aimed at simple dipole [9, 28, 38] and RFID tag antennas [6, 20, 29-30]. These screen printed graphene antennas exhibit outstanding performances including electrical conductivity, mechanical stability and environmental sustainability, revealing screen printing graphene antennas as a promising candidate for wireless communication and sensing applications, where flexibility, massive production

and low cost are especially required, promoting the incorporation of graphene in flexible printed electronics. MIMO technology is essential for 5G wireless communications and high performance IoT applications, guaranteeing high-speed data transmission and system reliability. However, due to the complicated structures induced by MIMO antenna design such as lowering the mutual coupling between antennas, needs of high conductivity and environmentally friendly ink, lack of scalable and affordable fabrication process, screen printed graphene MIMO has yet to be reported.

Here, we present the novel aggregation of two technologies, screen printing MIMO antenna with home-made highly conductive graphene ink [7, 20] on paper substrate, with the aim of integrating low-cost disposable flexible antennas with the 5G IoT applications and increasing the data throughput. A graphene printed, co-planar waveguide (CPW) fed, highly isolated, wideband 4 × 4 MIMO antenna was designed and fabricated by first developing a graphene ink (50 mg mL^{-1}) with a high conductivity of 3.68×10^4 S/m using N-methyl-2-pyrrolidone (NMP) and viscous Ethylene Glycol (EG) solvents for screen printing, then depositing the dispersion of graphene flakes on paper substrate with a resolution of 0.4 mm to achieve our designed pattern. The SMA feeds were then connected to the antennas using conductive epoxy, supporting multiple data transmission links. The MIMO consists of four identical antennas orthogonal to each other and the ground extension stubs altering the current flow. The SEM cross-sectional view, Raman and XPS spectra of the printed graphene antenna were investigated. To assess the flexibility of the graphene printed conformal antenna and evaluate its working performance, tests under different bending conditions have been carried out.

This paper is organized as follows. First, the fabrication process and electrical properties of the printed graphene MIMO antenna are elaborated in Section II, involving graphene ink preparation and screen-printing technology. The designs and modeling of the MIMO antenna are then illusrated with effects of parameter alteration, explaining polarization diversity and other mutual coupling reduction techniques. After that, antenna performances with and without bending applied are observed and evaluated. Finally, the work is concluded with some final remarks

.

3.2 Material Preparation and Electrical Properties

The production process of printed graphene can be briefly introduced as 1) shear mixing in chosen dispersant to reduce the physical size of graphite flakes which increase the exfoliation efficiency for the following steps, 2) high power ultrasonication treatment to produce few-layer graphene. 3) initial filtration for the removing of large particles, and tuning the ink to appropriate viscosity, 4) printing and 5) compression. To be specific, the graphene conductive ink was prepared from pristine graphite flakes (Alfa Aesar, 325 mesh, purity: 99.8%). The dried graphite flakes were mixed with NMP (Sigma, anhydrous, purity: 99.5%) at a concentration of 20 mg mL^{-1} [8], followed by 2-hour sheer mixing at 8000 rpm (Silverson L4R mixer) where the temperature was controlled around 20 ℃ (Constant temperature was maintained by circulating water cooling system to prevent overheating). During this process, the graphite flakes were initially

exfoliated. For ultrasonication treatment, NMP solvent was used for graphene exfoliation as it can achieve low residual and excellent stability [2]. It is crucial to properly control sonication parameters, such as sonication time. The sonication time can directly affect the ink conductivity [20]. To maximize the conductivity of printed graphene, 24-hour sonication process was applied to the mixture in glass bottle with ultrasonic bath (SHESTO, UT8061-EUK). The temperature was controlled as well. After that, filtration took place by first using 300-mesh stainless steel screen to filter out unexfoliated large graphite particles, then employing Whatman qualitative filter paper (Grade 5) on a glass funnel (140 mL Aldrich Buchner) for vacuum suction filtration to remove the remained NMP solvent. The collected solute from the filter paper was then dispersed in EG (Alfa Aesar, anhydrous, purity: 99%) and filtered by the same process to further remove the NMP. The remained solute was again dissolved in EG and centrifuged at low speed (500 RPM) to remove relatively large, unexfoliated graphite flakes. The process was repeated three times. Finally, we collected the graphene nanoflakes dispersion and tuned it to the right concentration for screen printing by vacuum evaporation. The final conductive ink for screen printing was made with a concentration of 50 mg mL^{-1}, ensuring both the smooth deposition of the ink during printing process and the viscosity of the ink.

Screen printing operation was carried out on a semiautomatic screen printer with the assist of a slant squeegee with the angle of inclination of 70° moving at a chosen constant speed (50-100 mm s^{-1}) for sufficient ink depositing. A 24T mesh printing screen with negatively patterned antenna shape was fabricated by exposing capillary film (ULANO, EZ50-Orange) in an exposure machine with the application of vacuum pressure regulating valve to lock the location of the screen

and achieve good resolution. The mesh of the screen was chosen according to the desired pattern accuracy and adequate amount of ink deposition. Higher resolution can be achieved by finer mesh, however, it impedes ink from transferring to substrate.

(a)

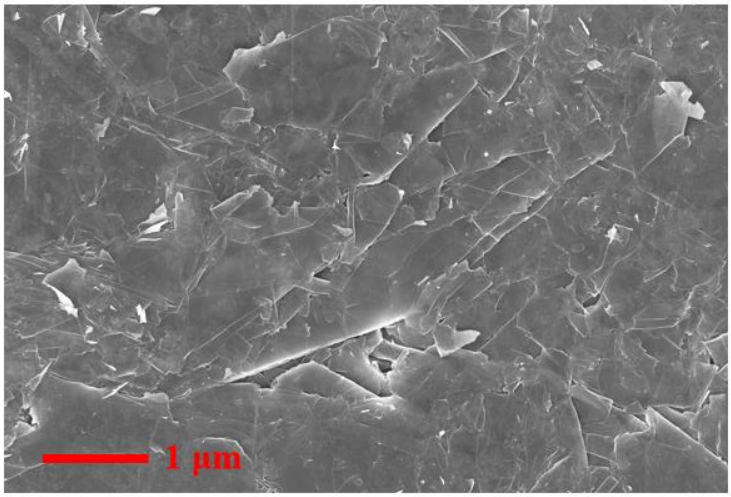
1 µm

(b)

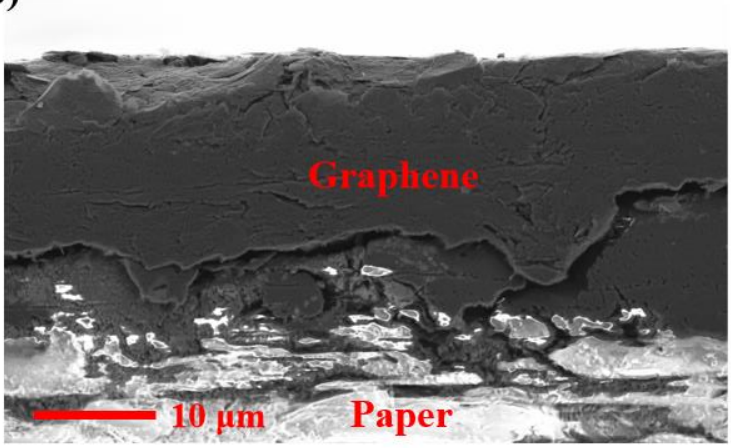
Graphene
10 µm
Paper

(c)

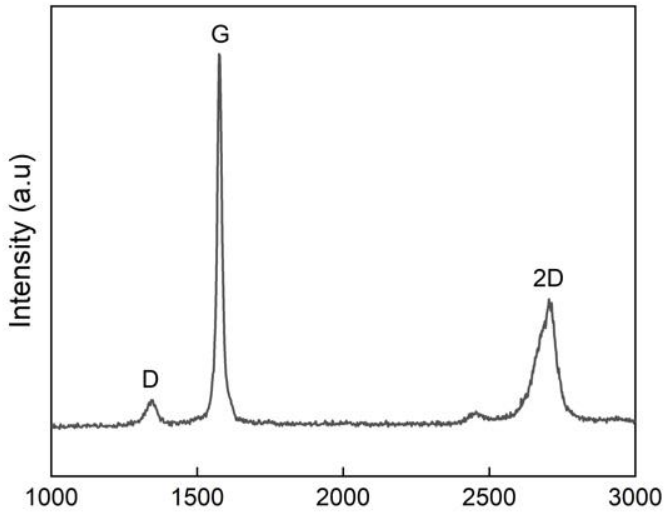
G
2D
D
Intensity (a.u)
1000
1500
2000
2500
3000

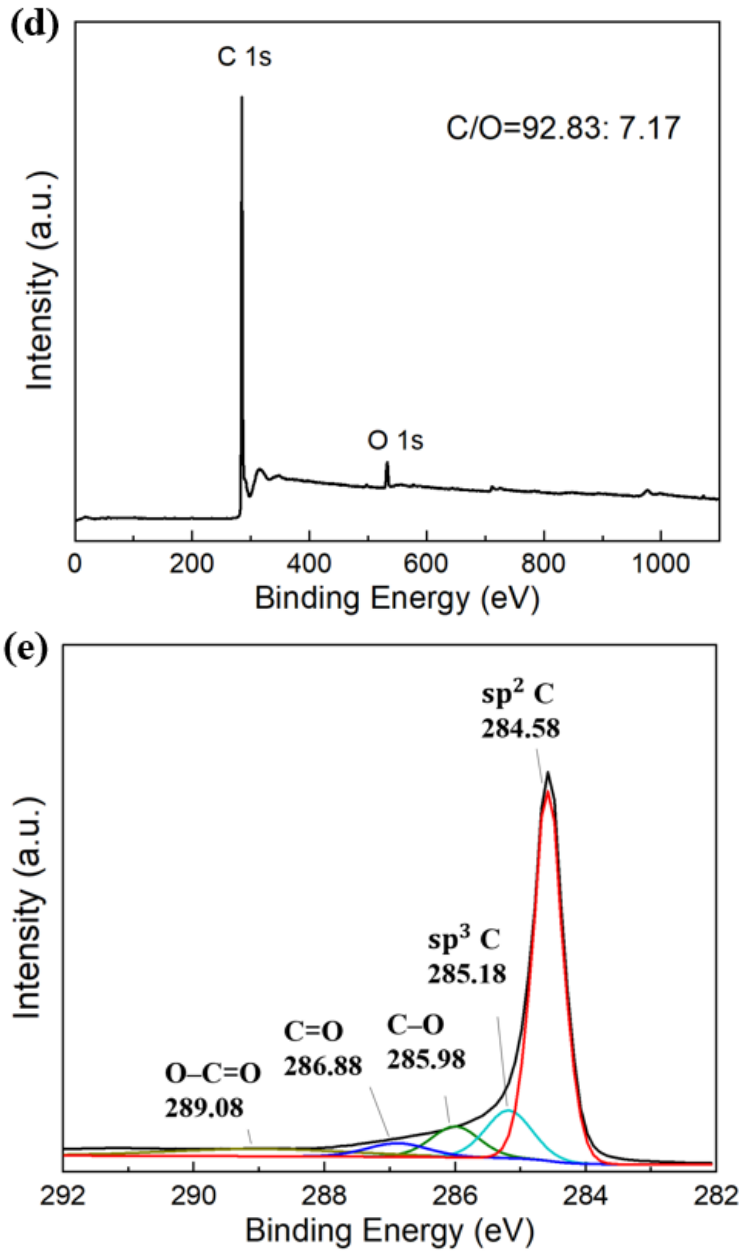

Fig. 3-1. (a) 10k× magnified SEM top view of the screen-printed graphene surface with $1\ \mu m$ scaled bar. (b) 500× magnified SEM cross-sectional view of the antenna with $10\ \mu m$ scaled bar, the average thickness of the graphene laminate is $19.4\ \mu m$. (c) Raman spectra of printed graphene, (d) wide-scan XPS spectra and (e) deconvolution of C 1s XPS spectra of the printed graphene

After printing the designed antenna pattern on paper substrate (Xerox Performer

A4 Paper 80 gsm), the antenna prototype is heated at 100 °C for 4h for volatilizing the dispersant and at the same time prevent the substrate from overheating. A further rolling compression is applied to enhance the printed film conductivity, as printed graphene layer is porous and has high sheet resistance. Rolling compression was operated by a rolling machine (Agile F130 Manual Mill). The compression can reduce the sheet resistance to its tenths, greatly increasing the conductivity [38]. By compression, the surface of printed graphene was visibly smoothened, forming well-aligned laminated structure, allowing better flow of surface current and higher conductivity. Fig. 3-1(a) exhibits the top view of the compressed graphene layer with 10k times magnification.

Sheet resistance characterisation with the four-point probe measurement method were performed on 10 different positions of the resultant films, 1.9 Ω/sq average sheet resistance was achieved**.**

Good adhesion can be manifested by investigation of the SEM image cross-section in Fig. 3-1 (b), ambiguous boundary was found between the graphene and paper substrate. The average thickness of the screen-printed graphene layer after rolling compression is measured as 19.4 μm. The conductivity can be calculated as 3.68×10^4 S/m using (1), which is close to a reported work [27], but without the use of high temperature annealing (350℃).

$$\sigma = \frac{1}{R_s t} \tag{3.1}$$

where R_s is the sheet resistance. Raman spectroscopy of printed graphene is shown in Fig. 3-1 (c). The sample is excited from a 532 nm laser source which causes phonon energy shift by Horiba Raman Spectrometer. Three main peaks can be

spotted at D-band (1347 cm^{-1}), associated with the ring breathing mode of sp^2 carbon atoms and typically weak in graphene of high quality, G-band (1575 cm^{-1}), revealing the in-plane vibrational mode of graphite lattice, and relatively wide 2D-band (2704 cm^{-1}), representing an overtone of the D band, resulting from a 2-phonon lattice vibration [20, 33-34]. In Fig. 3-1 (c), low I_D/I_G ratio can be observed, indicating very few structural defects on graphene flakes, contributing to highly effective electron flow. To further analyse the surface composition of the graphene, Fig. 3-1 (d) shows the wide-scan XPS spectra of the printed graphene sample, exhibiting the presence of carbon and oxygen with a ratio of 92.83:7.17. The high ratio of C 1s peak and O 1s peak indicates that only a small quantity of defects exists in the form of oxides, which were possibly inserted during fabrication process [35-37]. Fig. 3-1 (e) displays the deconvoluted C 1s XPS spectra of the printed graphene sample with an extremely significant peak at 284.6 eV and a lower peak at 285.2 eV, representing the sp^2 and sp^3 hybridized carbon respectively. The three much weaker carbon–oxygen peaks are attributed to C–O (286.0 eV), C=O (286.9 eV) and O–C=O (289.1 eV) bonds.

3.3 Antenna Design and Simulation

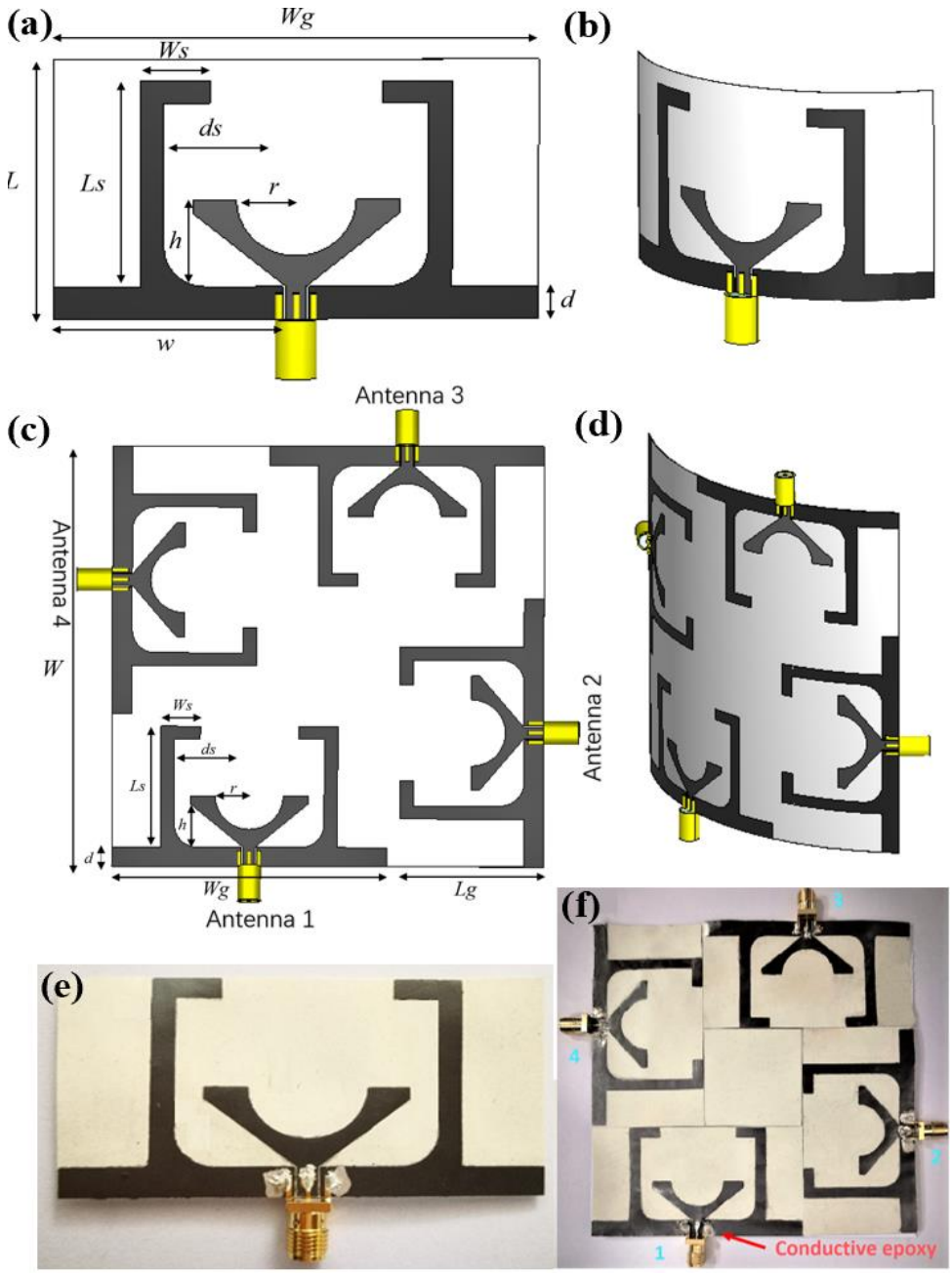

Fig. 3-2. Proposed flexible graphene printed antennas. (a) Designed single antenna model and related parameters. (b) Conformal antenna. (c) Designed MIMO antenna model and related parameters. (d) Conformal MIMO antenna. (e) Screen-printed antenna prototype. (f) Screen-printed MIMO antenna with four identical elements orthogonal to each other.

A CST model with labelled parameters of the proposed graphene screen-printed MIMO antenna is displayed in Fig. 3-2 (a) [21]. Paper substrate has been used in this work for its flexibility, low cost and environmental protection. For impeding the conductive ink from double-sided permeation on paper substrate, we've deployed CPW feeding so as to place the ground on the same side as the antenna.

Also, planar structures ensure compactness of the structure and allowance of better space resource usage. The paper substrate in the simulation has a dielectric constant of 2.3, permeability of 1 and a thickness of 0.1 mm. The loss tangent of 80 gsm paper at room temperature is set to 0.02 according to [32]. The printed graphene layer was modelled as ohmic sheet as its skin depth is much larger than its thickness [7]. The resistance of the modelled graphene sheet was set to 1.9 Ω/sq as measured on ten different points each on five printed samples using a four-point probe station (Jandel, RM3000) and semiconductor characterization system (Keithley, 4200C). To improve simulation accuracy, four SMA connectors were modelled at the end of each feeding line, fixing the port impedance at 50 Ω (Fig. 3-2 (a)).

The design of the conformal graphene printed MIMO antenna was first started with the individual antenna structure, as presented in Fig. 3-2(a) and (b). The round outline of the graphene helps broadening the bandwidth of the antenna. The performances of three configurations for single antenna design evolution are exhibited in Fig. 3-3 to estimate the effects of the stub extensions of different shapes. Antenna I features two inverted L-shaped stubs extended from the ground, whereas Antenna II only consists of bare ground and Antenna III contains I-shaped extensions (all the rest parameters are the same).

Table 3-1 Dimensions of the proposed graphene-printed antennas

Parameters	*mm*	*Parameters*	*mm*
Single antenna			
Substrate Length, L	40	Circle radius, r	8.67
Stub Length, Ls	31.68	Substrate width, Wg	70
Feeding length, d	5	Height of patch, h	13.3
Distance of stub, ds (from the edge of the ground)	17.2	Width of stub, Ws	10
Ground width, w	33.1		
MIMO antenna			
Length of MIMO, W	110	Distance of stub, ds	17.2
Width of element, Wg	70	Circle radius, r	8.67
Length of element, Lg	36.68	Height of patch, h	13.3
Stub length, Ls	31.68	Width of stub, Ws	10
Feeding length, d	5		

As shown in Fig. 3-3 (b) and (c), which compares the surface current and return loss of the three patterns, Antenna II does not resonate at 2.4 GHz as Antenna I and III do and stronger surface current in Antenna II at 2.4 GHz is gathered at the feeding line instead of radiating parts. To compensate this, Wg needs to be increased by more than 20 mm, severely degrading the compactness of the antenna. Furthermore, from the plots depicted in Fig. 3-3 (d) and (e), with the occurrence of the I-shaped stubs, a significant rise in gain and efficiency at 2.2-3 GHz can be observed. This is because the extension stubs not only improve the matching of the

antenna at lower frequency without enlarging structural size, but also enhance the radiation orthogonal to the antenna plane [22]. The bar of the inverted L-shape further improves the gain at lower frequency as seen from the surface current of Antenna I. The extension stubs radiate sufficient power as the main radiating element at 2.4 GHz with enhanced efficiency. Therefore, Antenna I is selected as a desirable compact antenna with reasonable bandwidth, efficiency, and gain.

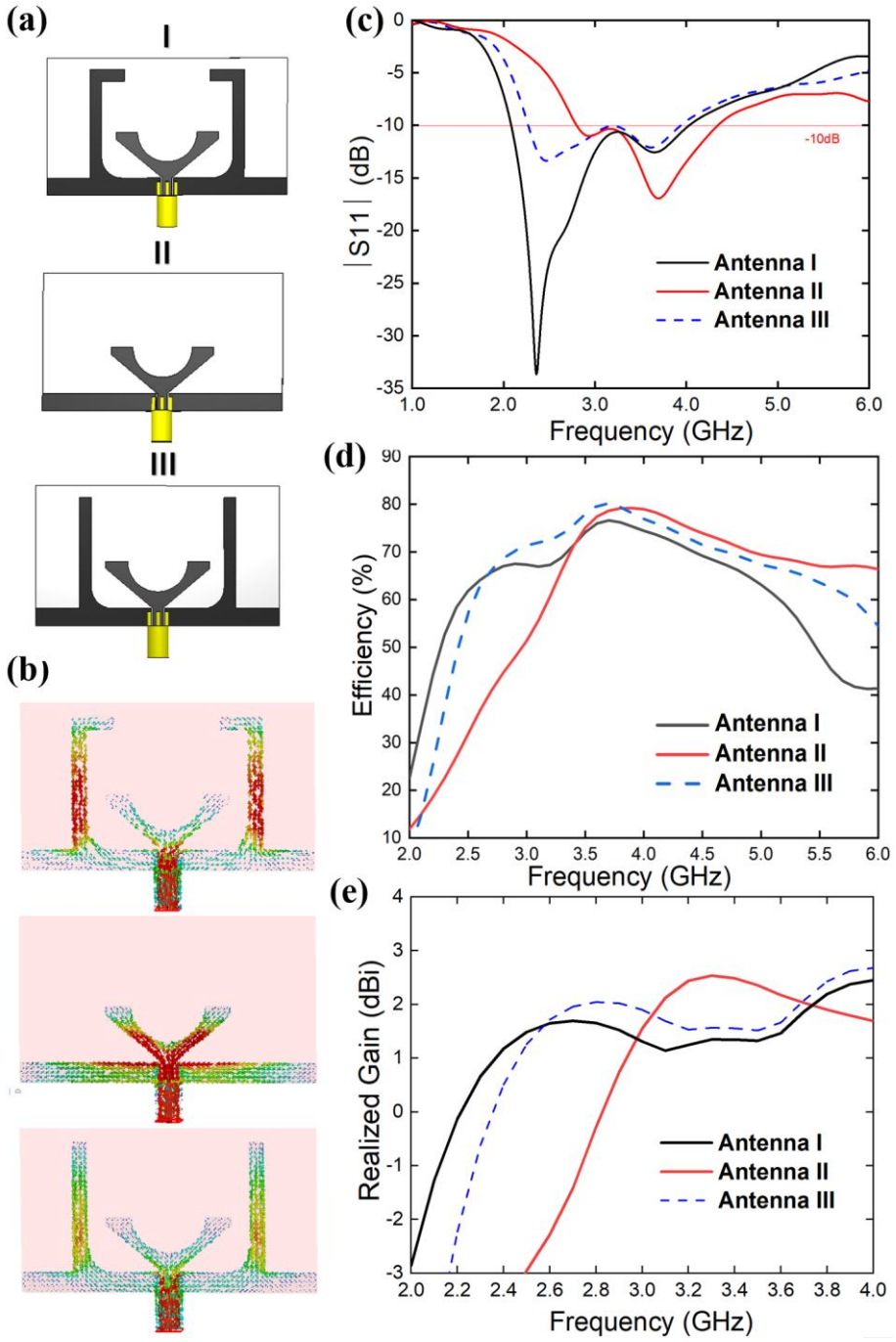

Fig. 3-3. Simulated results for three configurations of stub extensions. (a) Three configurations. (b) Surface current of three configurations at 2.4 GHz. (c) S11 of three antennas. (d) Efficiencies of the antennas. (e) Realized gain plots of the antennas.

Parametric study of the antenna is crucial to achieve desirable characteristics. Effects of graphene sheet resistance on antenna performance are shown in Fig. 3-4 (a) and (b), revealing that while the return loss is not very sensitive to the change of the sheet resistance, 1 Ω /sq reduction in sheet resistance can bring the realized gain down by about 1 dB. Parameters listed in Table 3-1, such as feeding line length d and ground width Wg of the antenna have been studied and optimized, presented in Fig. 3-4 (c) and (d), so that full excitation of the antenna for signal transmission at its operating frequency bands is guaranteed and unnecessary power dissipation in the feeding line can be avoided.

By comparing the S11 plots in Fig. 3-4 (d) and (e), it is proved that the distance of the stubs on the sides alters the resonant frequency of the antenna instead of the ground width Wg, and by adjusting the length Ls of the stubs, the realized gain can be optimized within the operating frequency band as shown in Fig. 3-4 (f).

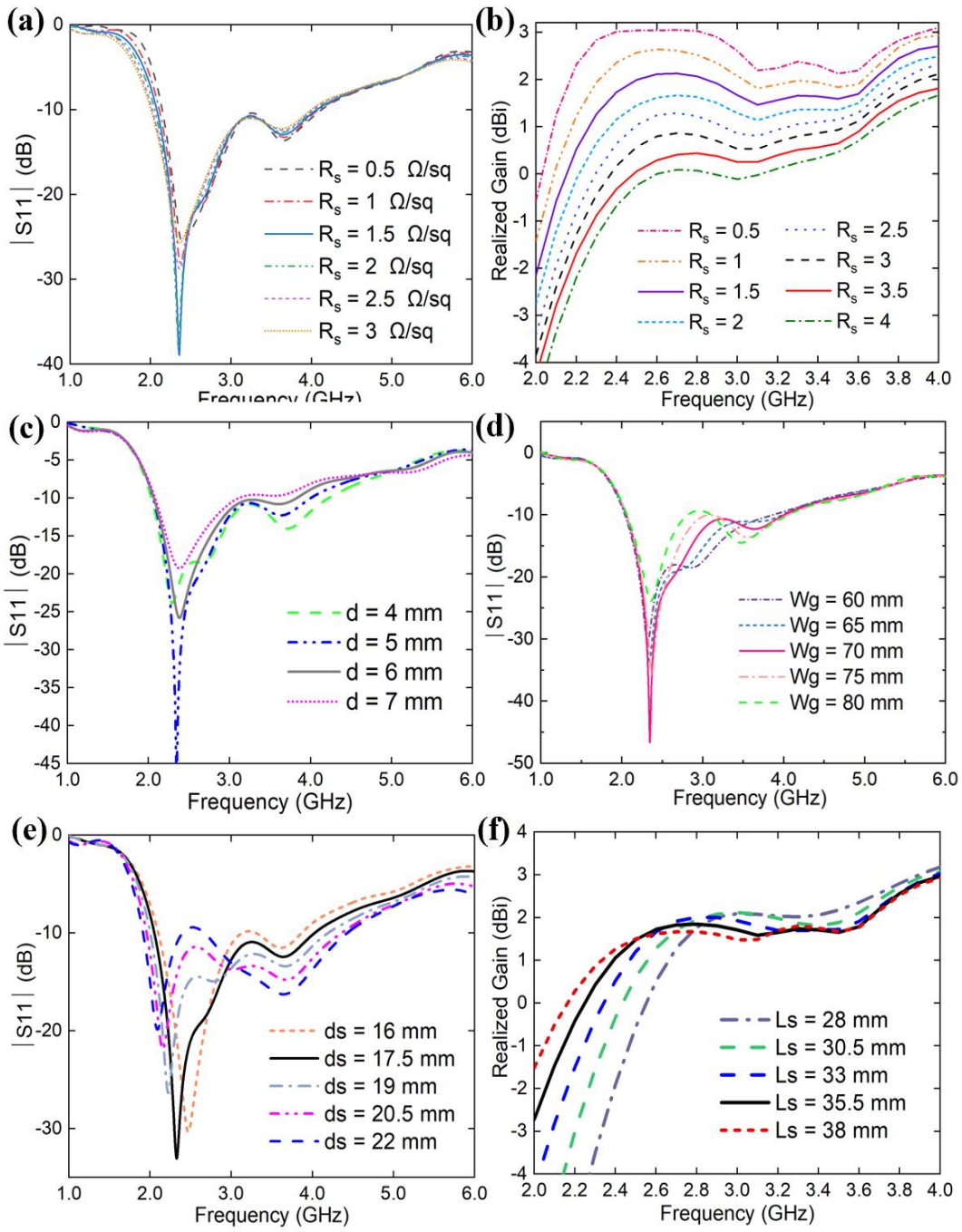

Fig. 3-4. Simulated results for parametric analysis. The influence of sheet resistance R_s (Ω/sq) on (a) S11 and (b) gain of the proposed antenna. The impact of (c) feeding length d, (d) width Wg and (e) distance of the stub ds on magnitude of S11, (f) stub length Ls on gain.

Moreover, the function of the inverted L-shape stub in MIMO antenna performance (Antenna I) is not only limited to gain enhancement and size reduction, it also reduces the mutual coupling between the antenna elements as it suppresses the surface current on the antenna plane. The simulation results for return loss (S_{11}) and isolation (S_{12} and S_{13}) of MIMO antenna I and II are displayed in Fig. 3-5(a) and (b). As seen from the comparison, for frequency higher than 2.7 GHz, more than 10 dB decrease in S_{13} and 3 dB in S_{12} are achieved with the insertion of ground extension stubs, indicating higher isolation in both directions and higher gain at desired frequency. When $R_s = 4\ \Omega/sq$, in Fig. 3-5(b), a 2 dB drop in gain occurs comparing with the gain curve of $R_s = 1.9\ \Omega/sq$, conforming to the observation from Fig. 3-4(b) that gain decreases with the increase of R_s.

Another desirable feature which should also be highlighted is the orthogonal placement of the four single antennas. Four single identical antennas are positioned perpendicularly to each other, with the intention of mitigating correlation with orthogonal polarization diversity, which can void spatial correlation and decrease structure size. Thus, interference between adjacent antennas, when two or more ports are activated, is lowered to a great extent, achieving good isolation with less spatial resource.

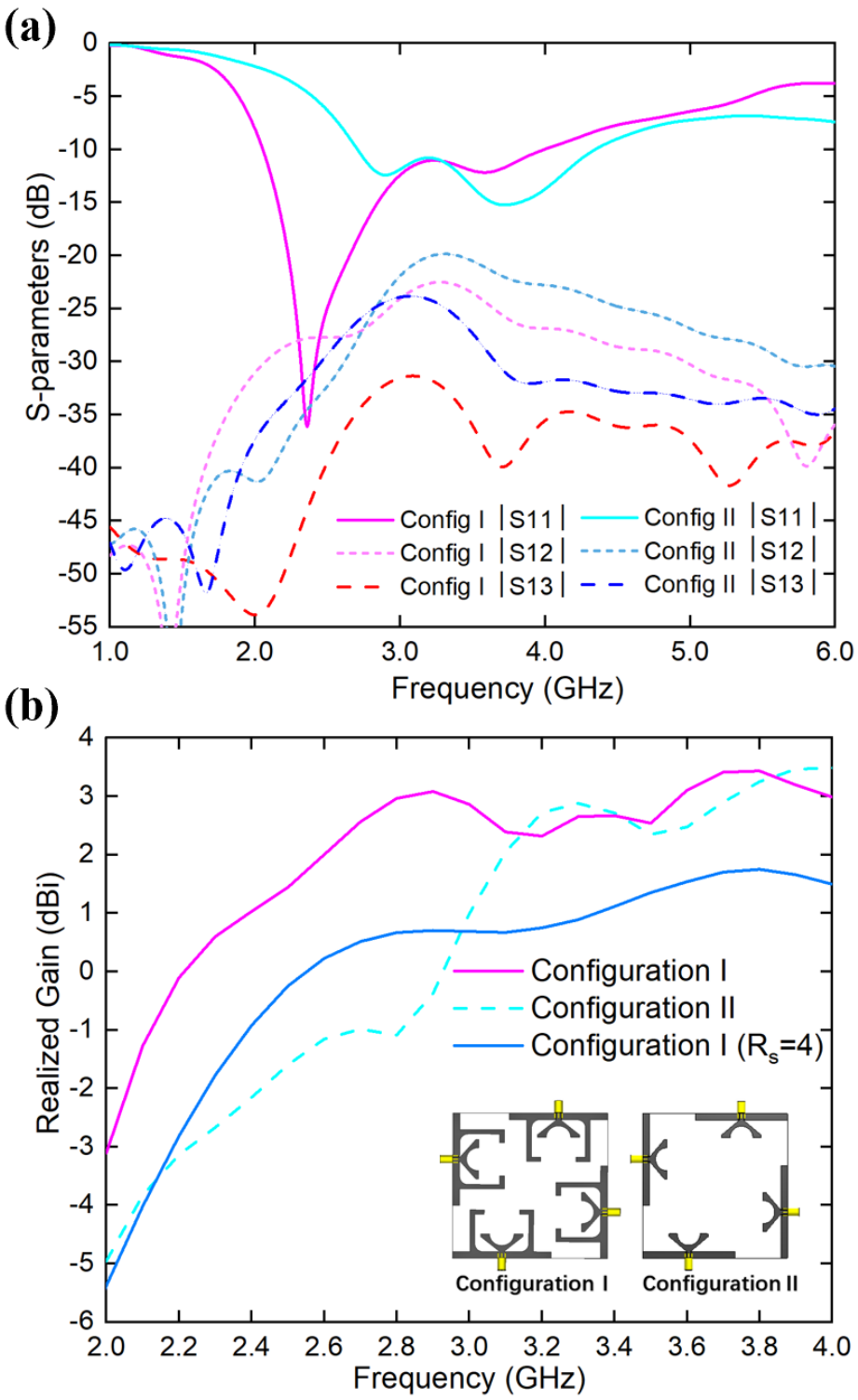

Fig. 3-5. Comparison of simulated results for (a) S-parameters and (b) realized gain of two different configurations (with and without ground extension stubs).

3.4 Measurement Results and Discussions

Fig. 3-2(f) shows the fabricated conformal screen-printed graphene MIMO antenna on paper substrate. Four 50 Ω SMA connectors were connected to four CPW feeding point by using conductive epoxy. A Vector Network Analyzer (VNA Agilent E5071B) was used to determine the scattering parameters of the printed graphene MIMO antenna. A horn antenna was employed in an anechoic chamber for two-antenna method with its known performance, measuring the radiation pattern and gain of the fabricated antenna. The setup of experiment apparatus is illustrated in Fig. 3-6, where the distance between the horn antenna and the printed graphene antenna was fixed to 0.8 m.

For the ease of measurement, the antenna was supported by a flexible screen made of Polypropylene with relative permittivity of 2.27, loss tangent of 0.002 at 1 GHz and permeability of 1 [23]. By comparison, the use of flexible screen leads to a tiny shift (about 50 MHz) to lower frequency, which should have minimal effect on antenna performance according to the simulation results in Fig. 3-7(a) and gain in Fig. 3-7(b). Due to the unique design of the structure, identical performance can be observed for antennas 1 and 3, likewise for antennas 2 and 4. Thus, for a clearer display of the scattering parameters of the MIMO antenna, only S_{11}, S_{12} and S_{13} are shown in Fig. 3-7 (a).

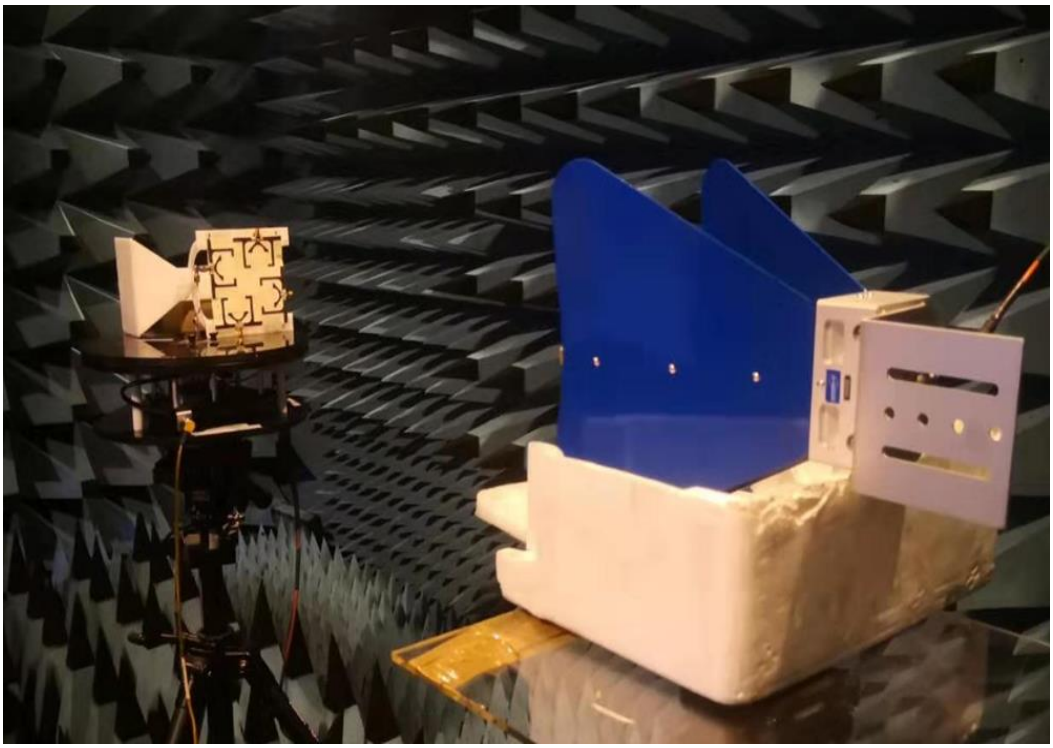

Fig. 3-6. Antenna measurement set up with a horn antenna in anechoic chamber, the distance between the horn antenna and the MIMO antenna under test is 0.8 m.

A good agreement between the simulated and measured S-parameters can be observed. The 10 dB bandwidth of the antenna is 2.22-3.85 GHz from the measurement and 2.05-3.89 GHz from the simulation. The discrepancy may be caused by the material parameter variations due to screen printing and after-printing processes, such as compression tolerance, e.g., the uneven surface caused by manual control of compression (hence causing conductivity variation), the difference in the dielectric constant of paper substrate from the simulation or less perfect contact between the conductive epoxy and the feeding. It is important to note that, the licensed global 5G spectrum in mid band range is entirely covered by this wide bandwidth of the antenna in the test.

From measured S_{12} and S_{13} in Fig. 3-7 (a) we can see that the isolation between two orthogonally placed antennas is below -30 dB, realizing excellent mutual coupling reduction within the desired frequency band. This is achieved by altering the orientation of the adjacent antennas and stubs. Even lower mutual coupling can be found between opposite antennas, as it can be seen that the value of S_{13} is about 10 dB lower than S_{12} in both simulated and measured results. Fig.3-7 (b) compares the simulated realized gain to the measured gain of the MIMO antenna with the support of flexible screen, obtained with a horn antenna by two-antenna method. Apart from an average 2 dB fall in magnitude, which most likely to be caused by higher sheet resistance than expected sheet resistance (1.9 Ω/sq was used in the simulation) as verified in Fig. 3-4 (b) (the impact of sheet resistance on gain reduction), the shape of the measured gain is in good agreement to the simulated within the operating frequency band. The measured gain features 0.4 dBi at 2.4 GHz and 0.56 dBi at 3.5 GHz, reaches its peak value 0.92 dBi at 2.6 GHz, acceptable for low-cost disposable use for 4G LTE, WiMAX and 5G mid-band applications. Simulated and measured radiation patterns in both E- and H-plane at 2.4 GHz and 3.5 GHz are plotted in Fig. 3-8 respectively.

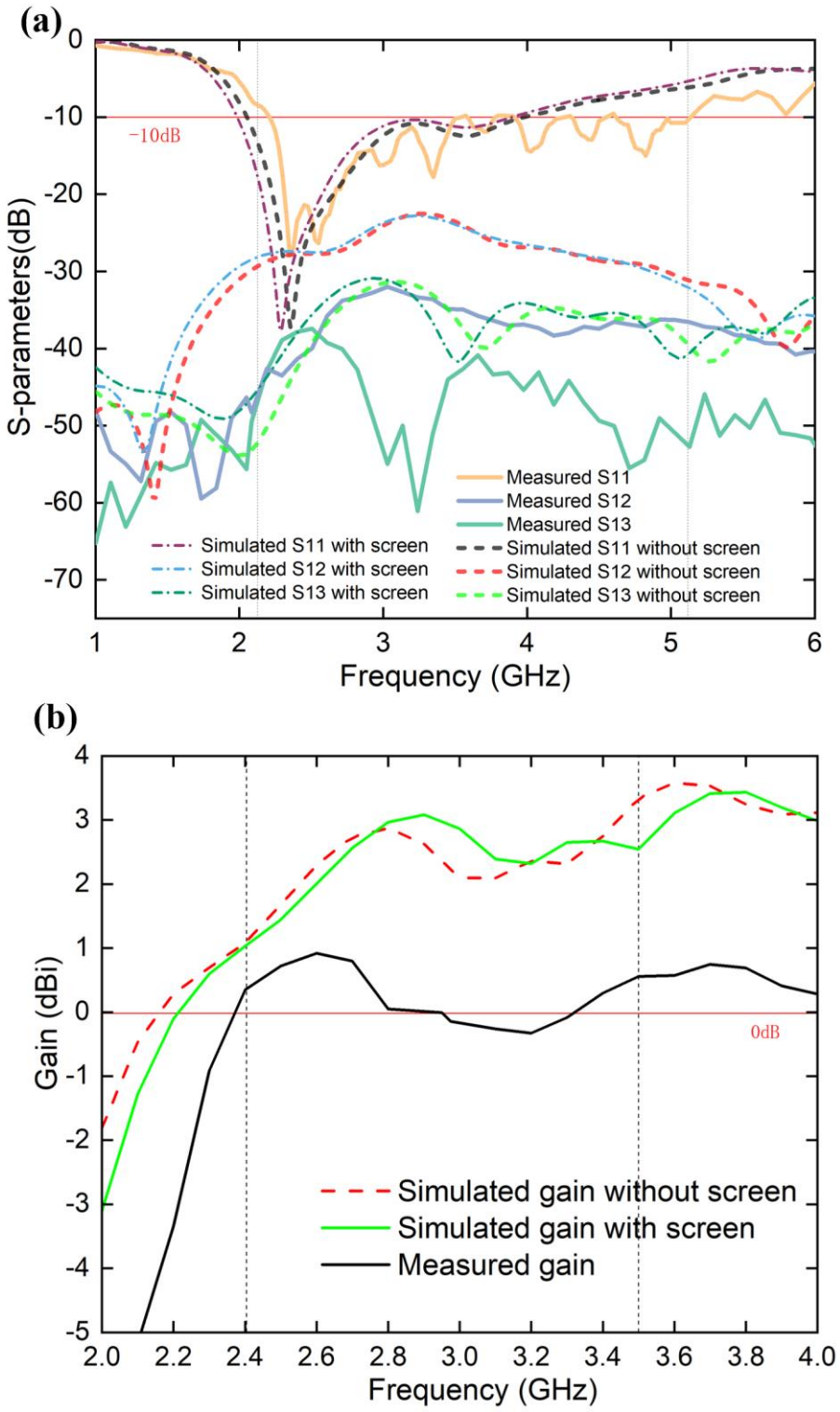

Fig. 3-7. (a) Measured and simulated S-parameters with and without flexible screen, (b) simulated gain with and without screen with different resistances, and measured gain using a standard horn antenna.

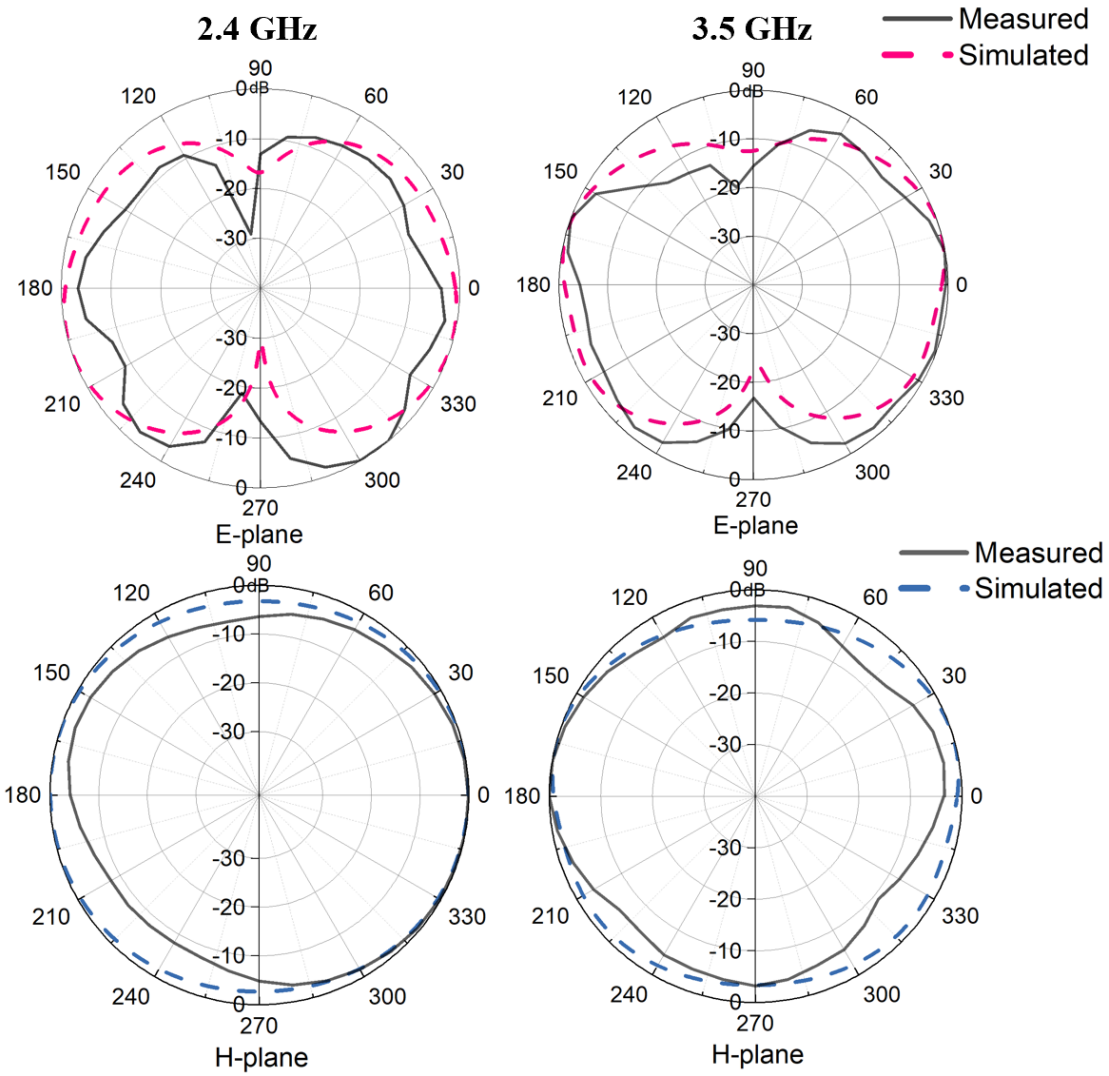

Fig. 3-8. Normalized simulated and measured radiation patterns on E-plane and H-plane at 2.4 GHz and 3.5 GHz.

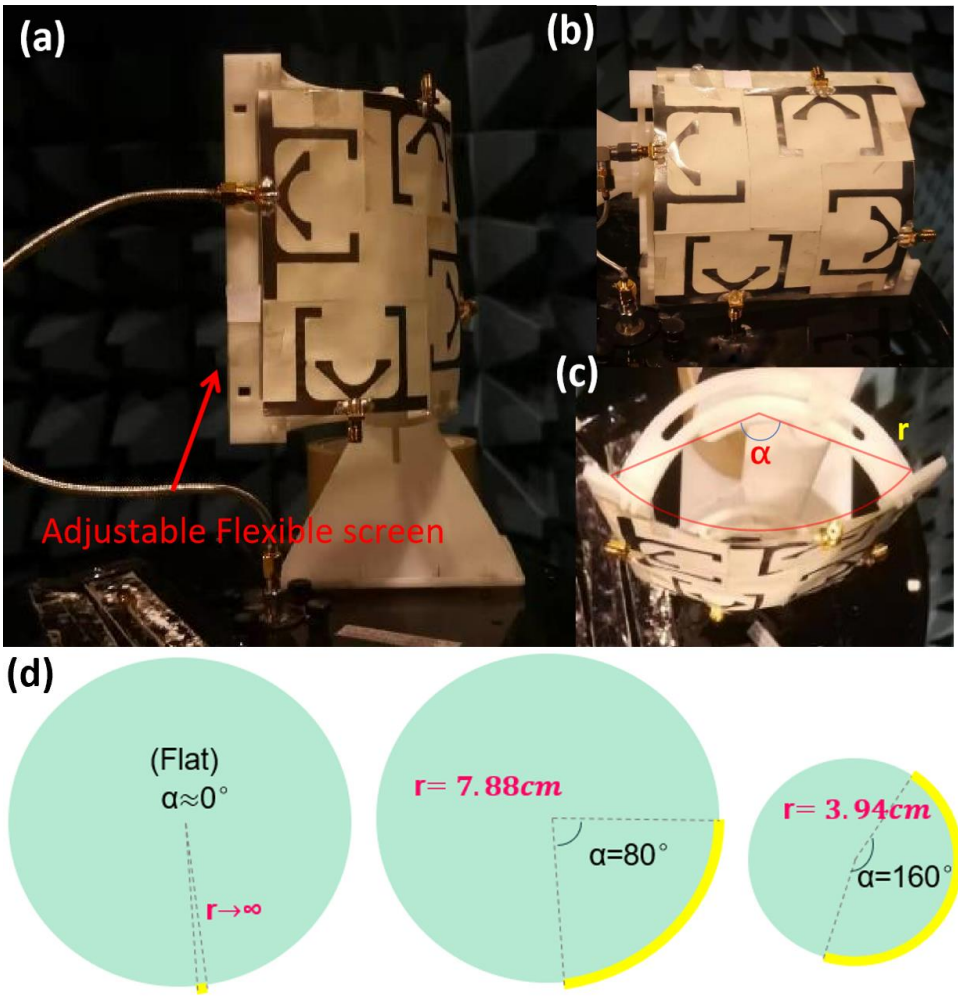

Fig. 3-9. (a) Front view of the screen-printed graphene MIMO antenna being vertically bent by α= 160° on a scaled adjustable flexible screen with one of its ports connected to the Vector Network Analyzer, and (b) horizontally bent by 120°, (c) top view of the antenna when fixed on the flexible screen with r=5.3cm and α=120°. (d) Bending with α=0°, 80° and 160°. The yellow arc represents the curved side length of the antenna (W=110mm).

The directivity is maximized on the orthogonal plane of the antenna plane, i.e., 0° and 180°. As can be observed, the measured patterns are in acceptable agreement with simulated ones.

For a more precise illustration of the achieved isolation, the envelope correlation coefficients (ECC) of both opposite and adjacent antennas are calculated using (3.2) [24]

$$|\rho_e(i,j,N)| = \frac{\left|\sum_{n=1}^{N} S_{i,n}^{*} S_{n,j}\right|^2}{\prod_{k(=i,j)}\left[1-\sum_{n=1}^{N} S_{k,n}^{*} S_{n,k}\right]} \tag{3.2}$$

where N is the number of antennas, i=1 to n, j=1 to n.

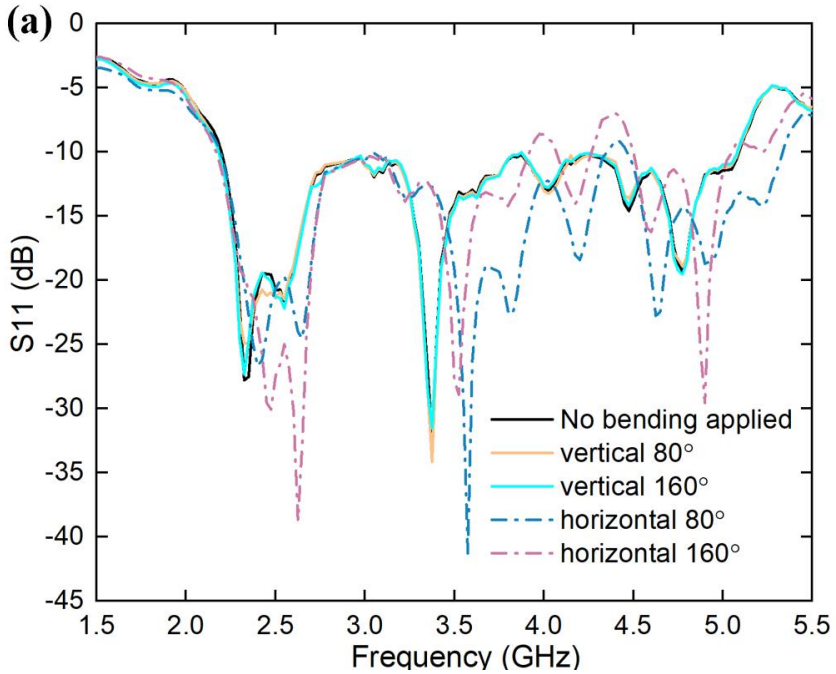

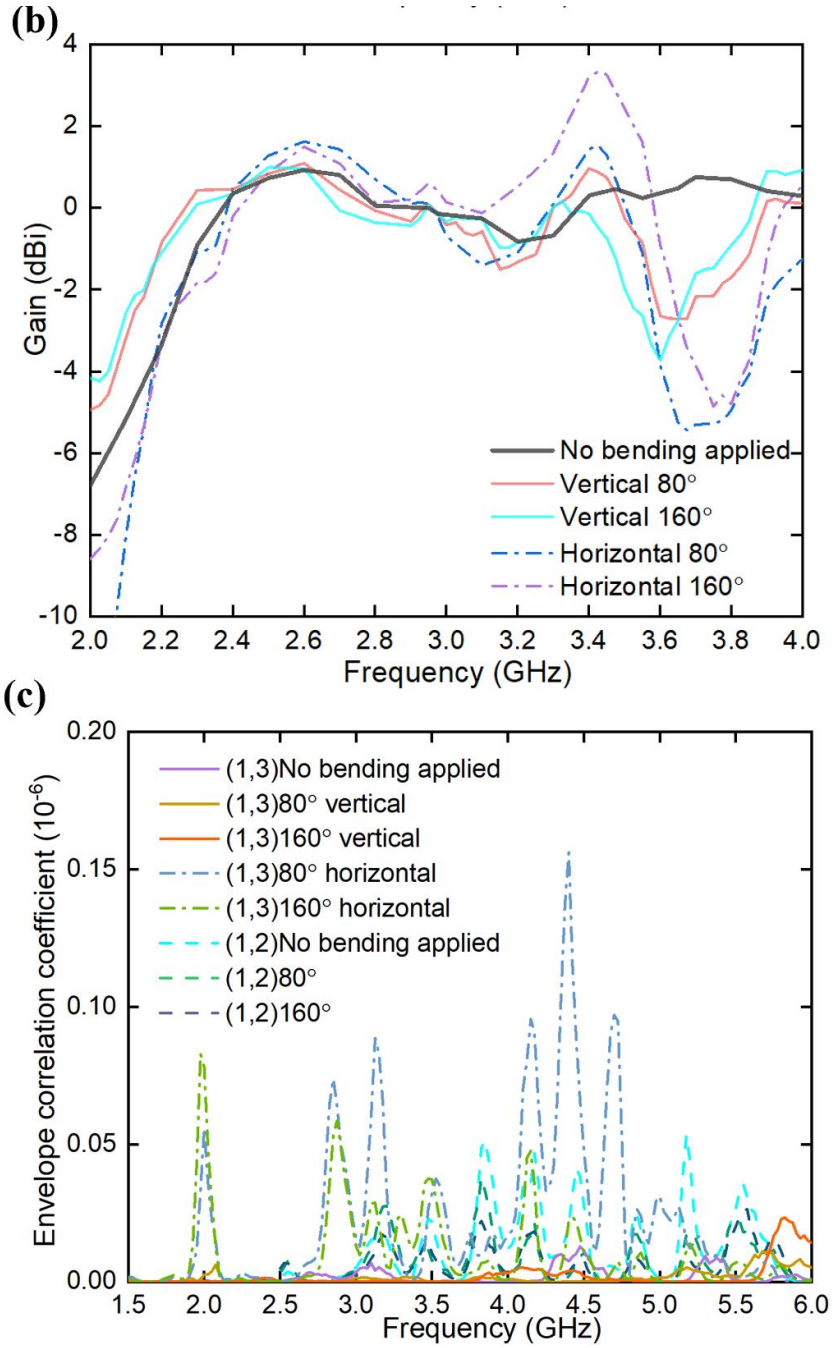

Fig. 3-10. (a) Measured S11 variation with increasing bending with α=0° (when no bending is applied), 80° and 160° vertically and horizontally respectively, (b) Measured antenna gain with vertical and horizontal bending alteration, (c) Envelope correlation coefficient (ECC) between antenna 1 and 2, and antenna 1 and 3 calculated from measured scattering parameters.

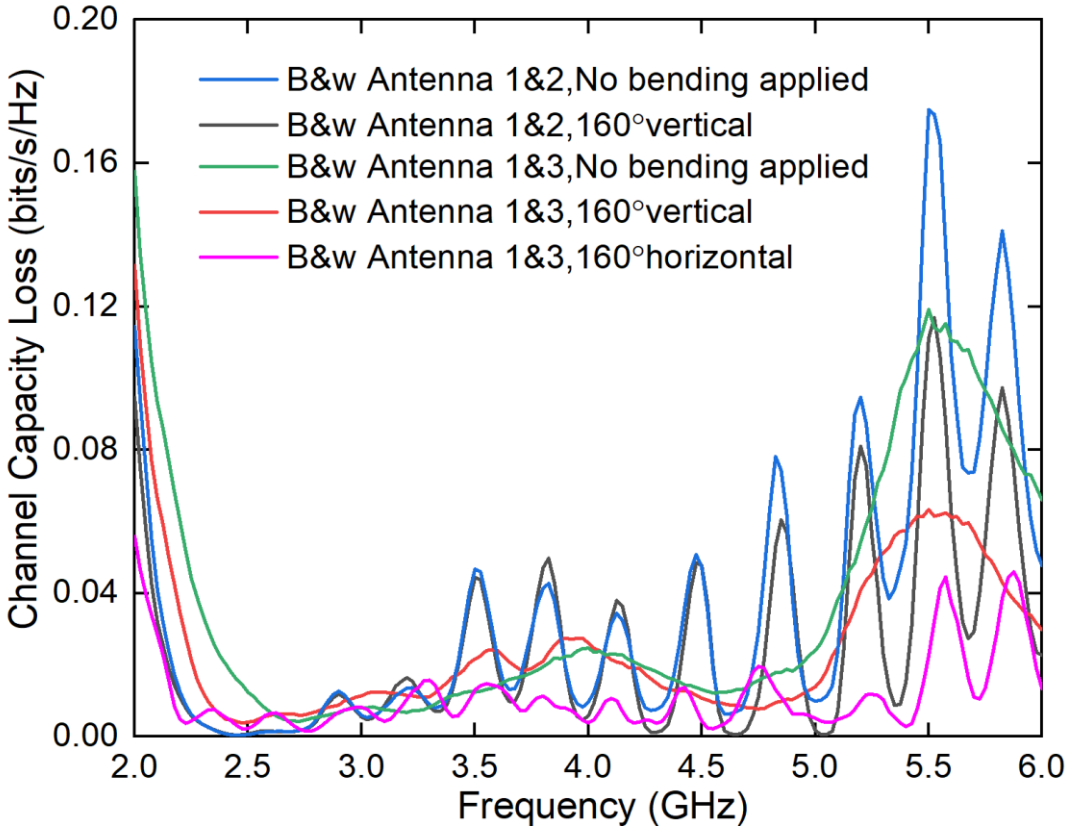

Fig. 3-11. Channel capacity loss between antennas with and without being bent calculated from measured scattering parameters.

From 2-6 GHz, the ECC values between both of the adjacent antennas and opposite antennas, as seen in Fig. 3-10 (c), indicating negligible correlation (ECC$<0.2\times10^{-6}$ for the whole desired frequency range), fully testifies the transmission quality of each antenna in the structure.

To accomplish the 5G network revolution blueprint and bring high-quality IoT to everyday life, it is crucial not only to deal with massive data throughput, conformability of electronic elements is also an essential factor to attain better adaptability, usability, and sustainability in applications, such as user-interactive

health monitoring systems, virtual reality gaming systems, vehicle to vehicle communications, robotics and autonomous systems. By being attached to human bodies who take part in physical activity monitoring systems, conformal antennas provide better user comfort than the ones which consist of rigid metals. To bend the antenna to a desired angle, a scaled adjustable and flexible screen was designed and fabricated, shown in Fig. 3-9 (a). The bending of the screen can be adjusted by altering the arc. During the conformability tests, the MIMO antenna was supported by this flexible screen in an anechoic chamber.

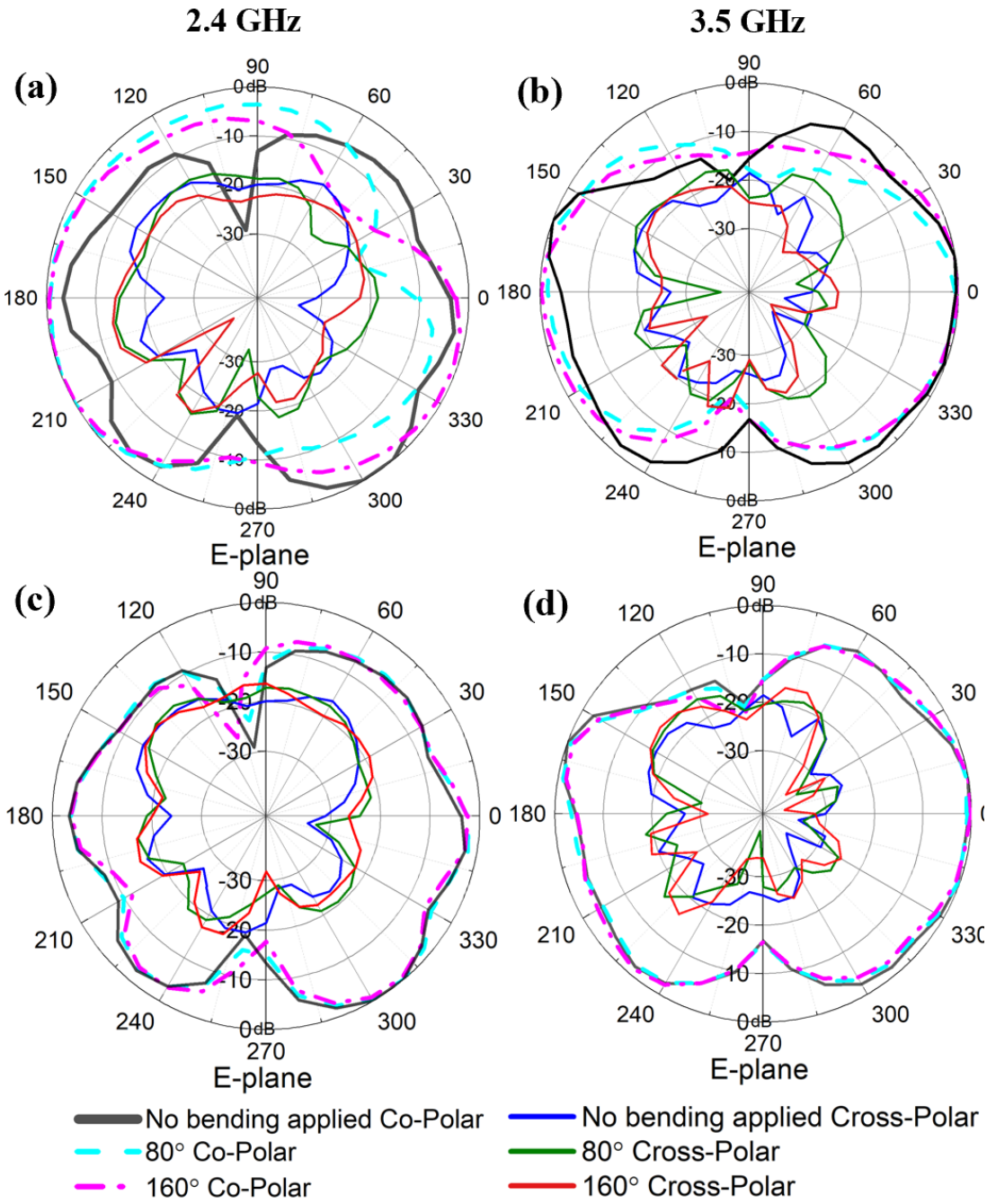

Fig. 3-12. Normalized MIMO antenna radiation pattern on H-plane at (a) 2.4 GHz with vertical bending, (b) 3.5 GHz with vertical bending, (c) 2.4 GHz with horizontal bending and (d) 3.5 GHz with horizontal bending with α=0°, 80° and 160°.

Both vertical and horizontal bending, shown in Fig. 3-9 (a) and (b), were conducted separately to inspect the performance of the antenna with increasing bending stress. As tested, the bending limit for the antenna to remain at its working condition is at α=160°, where α refers to the angle between the two radii that form the arc, as shown in Fig. 3-9 (c). Imagining the flexible screen as a cylinder, the antenna is attached to this cylinder with an adjustable radius r. By adjusting the supporting arc behind the flexible screen, bending conditions with α = 80° and 160° are realized for conducting S-parameters and ECC tests. The corresponding radii for α= 80° and 160° are r = 7.88 and 3.94 cm respectively, as shown in Fig. 3-9 (d), where the length of the arc in yellow is fixed at W=110 mm, and α = 0° indicates infinite radius and flat surface. Fig. 3-9 (a) shows when the antenna is being vertically inflected with α = 160°.

S11 variations with vertical and horizontal bending can be observed in Fig. 3-10 (a). It can be seen that the resonant frequency does not move much during the bending tests but the reflection coefficient is distorted more when horizontal bending is applied. This is due to the ground extension stubs experience deformation to a greater extent in horizontal case. Fig. 3-10 (b) reveals that the gain changes more for horizontal bending than that for vertical bending; the peak gain goes up to 3.3 dBi for horizontal 160° bending and 1.3 dBi for 80° bending at about 3.5 GHz. The gain remains at 0.4 dBi with all bending cases around 2.4 GHz. There are dips occurring around 3.7 GHz for both bending cases, which could be caused by the deformation in radiating elements.

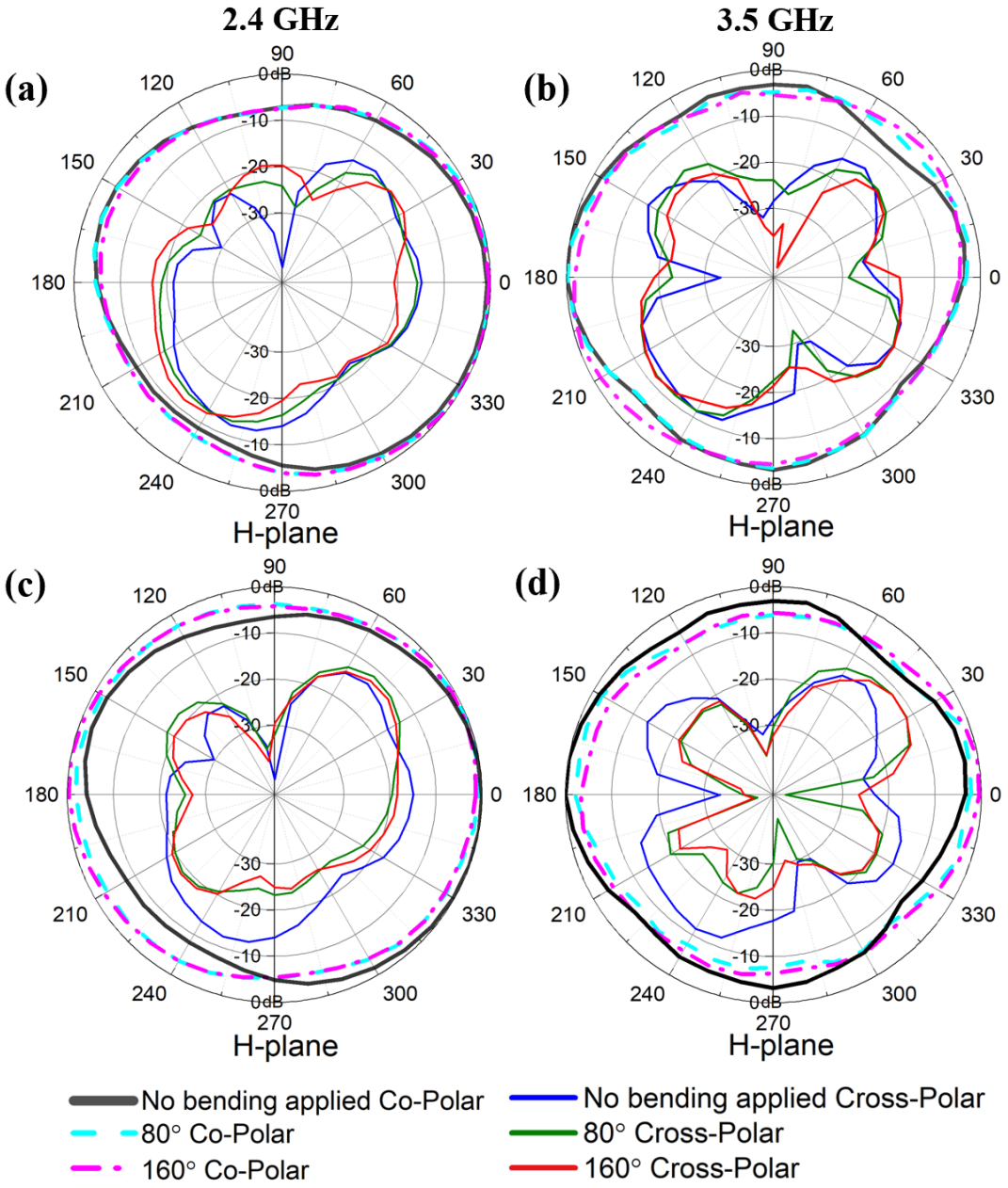

Fig. 3-13. Normalized MIMO antenna radiation pattern on H-plane at (a) 2.4 GHz with vertical bending, (b) 3.5 GHz with vertical bending, (c) 2.4 GHz with horizontal bending and (d) 3.5 GHz with horizontal bending with α=0°, 80° and 160°.

The ECC values for the bending cases can be simply derived from our measured scattering parameters using (2). Due to the special rotational symmetry of the

MIMO antenna, we consider ECC in terms of the relative positions of the elements for simplicity, that is, ECC(1,2) should behave like ECC(3,4) with same bending action applied, correspondingly, ECC(1,3) should behave the same as ECC(2,4). Hence, the adjoining antennas (1,2) and opposite antennas (1,3) with different curvatures are inspected in Fig. 3-10(c). Note that the orientation of bending makes no difference in ECC between adjoining antennas. From observation, ECC values for all conditions are below 0.2×10^{-6} for the entire operation frequency. At 2.4 GHz, the isolation even improves between adjacent antennas for horizontally bent opposite antennas since the bending alters the polarization and the relative position of the two antennas, reducing the interference along horizontal axis.

Also, the channel capacity loss (CCL) between two antenna elements in Fig. 3-11 is estimated by (3.3), (3.4) and (3.5) [25]

$$CCL = -\log_2 \det(\psi^R) \tag{3.3}$$

$$\psi^R = \begin{bmatrix} \rho_{11} & \rho_{12} \\ \rho_{21} & \rho_{22} \end{bmatrix} \tag{3.4}$$

$$\text{where} \quad \rho_{ii} = 1 - \left(|S_{ii}|^2 + |S_{ij}|^2\right) \text{ and}$$
$$\rho_{ij} = -\left(S_{ii}^* S_{ij} + S_{ji}^* S_{jj}\right) \qquad \text{for i, j = 1 or 2.} \tag{3.5}$$

Despite the compact arrangement of the antennas, the value of CCL remains below 0.2 bits/s/Hz from 2 to 6 GHz even with 160° bending applied, where the standard CCL for a 4×4 MIMO antenna is 0.4 bits/s/Hz [25]. The loss between adjacent antennas can be spotted a little higher than opposite polarized antennas due to the closer separation and polarization correlations.

Antenna radiation characteristics at 2.4 GHz and 3.5 GHz respectively with α = 0°, 80° and 160° can be examined from Fig. 3-12 and 13. In Fig. 3-12 (a), more offset of maximum directivity of the antenna in E-plane at 2.4 GHz can be seen with increasing vertical curvature than that of the case of horizontal curvature. This is because, when the MIMO antenna is being bent vertically, two side stubs are not co-planar anymore. At 2.4 GHz, the power is mainly radiated by the side stubs, as shown in Fig. 3-3 (b) (the surface current of Antenna I at 2.4 GHz), thus, changing the direction of the stubs causes the radiation distortion in E-field at 2.4 GHz. However, at 3.5 GHz, power is mostly radiated by the patch rather than the stubs, so that vertical bending does not break the radiation symmetry of element, as shown in Fig. 3-12 (b). Other than this, the antenna consistently remains at its normal working condition with horizontal bending.

Radiation patterns in magnetic field at both 2.4 GHz and 3.5 GHz can be observed in Fig. 3-13. Similarly, the field alters a little more when vertical bending applies than horizontal bending, however, this slight alteration in fields barely alters the transmission. In general, the antenna preserves its good radiation performance up to the bending angle of 160°, despite slight diversity change in electric field due to the break of symmetry, revealing good adhesion and stable power transfer performance of the antenna. Cross polarizations of the antenna under different bending conditions in E- and H-plane are measured and shown in Fig. 3-12 and 13. The results are normalized with respect to the maximum value of the co-polarization results. It can be observed that the cross-polarization results at broadside are about 30 dB and 20 dB down compared with the co-polarization levels in *E* and *H* -plane respectively at both 2.4 and 3.5 GHz under all bending conditions up to 160°, revealing good radiation performance. It can also be

observed that vertical bending affects more on cross-polarization orientation at 2.4 GHz due to the same reason as discussed on co-polarization variation by vertical bending at 2.4 GHz.

3.5 Conclusion

In this paper, a novel aggregation of graphene printing electronics and MIMO technology has been presented, enabling cheap accessible MIMO antennas to be massively deployed in various IoT applications. A conformal, well-isolated, environmental-friendly, screen-printed graphene MIMO antenna has been designed, fabricated and characterized, confirming the feasibility of using highly conductive printed graphene to promote the flexibility and biodegradability of high reliability and fast data transmission devices. Good isolation is evident with its extremely low ECC value below 0.2×10^{-6} for the entire desired frequency band with acceptable gain as a result of the ground extension stub and polarization diversity design. The conformability and usability of the antenna have been testified that it remains working for bending angle below 160°, suitable for most user case scenarios with good adhesion and stable power transmission. The bandwidth of the antenna covers a wide range of applications, including 4G Long Term Evolution (LTE) telecommunications networks, 2.45 GHz Industrial, Scientific, Medical (ISM), sub-6 GHz 5G mobile networks, WLAN and WiMAX applications. The low manufacturing cost and disposable features of this graphene printed MIMO antenna reveal its potential for massive production for 5G dense communication networks deployment. Furthermore, its compact size and flexibility directly lead to greater integration in flexible 5G front-ends, IoT systems,

as well as in next-generation wearable electronic devices.

References

[1]K. Novoselov, V. Fal′ko, L. Colombo, P. Gellert, M. Schwab and K. Kim, "A roadmap for graphene", *Nature*, vol. 490, no. 7419, pp. 192-200, 2012. Available: 10.1038/nature11458.

[2]Y. Hernandez, V. Nicolosi and M. Lotya, "High-yield production of graphene by liquid-phase exfoliation of graphite", *Nature Nanotech*, vol. 3, pp. 563–568, 2008.

[3]J. Shen et al., "Liquid Phase Exfoliation of Two-Dimensional Materials by Directly Probing and Matching Surface Tension Components", *Nano Letters*, vol. 15, no. 8, pp. 5449-5454, 2015. Available: 10.1021/acs.nanolett.5b01842.

[4]G.Hu et al., “Functional inks and printing of two-dimensional materials”, *Chemical Society Reviews*, 2018, doi: 10.17863/CAM.24846.

[5]L. Ng et al., *Printing of Graphene and Related 2D Materials*, 1st ed. Springer International Publishing, 2019, doi: 10.1007/978-3-319-91572-2.

[6]X. Huang, T. Leng, T. Georgiou, J. Abraham, R. Nair, K. S. Novoselov, and Z. Hu, “Graphene oxide dielectric permittivity at GHz and its applications for wireless humidity sensing,” *Scientific reports*, vol. 8, no. 1, p. 43, 2018.

[7]X. Huang et al., "Highly Flexible and Conductive Printed Graphene for Wireless Wearable Communications Applications", *Scientific Reports*, vol. 5, no. 1, 2015. Available: 10.1038/srep18298.

[8]T. Leng et al., "Printed graphene/WS2 battery-free wireless photosensor on papers", *2D Materials*, vol. 7, no. 2, p. 024004, 2020. Available: 10.1088/2053-1583/ab602f.

[9]T. Leng, X. Huang, K. Chang, J. Chen, M. Abdalla and Z. Hu, "Graphene Nanoflakes Printed Flexible Meandered-Line Dipole Antenna on Paper

Substrate for Low-Cost RFID and Sensing Applications", *IEEE Antennas and Wireless Propagation Letters*, vol. 15, pp. 1565-1568, 2016. Available: 10.1109/lawp.2016.2518746.

[10] T. Hertel, R. Walkup and P. Avouris, "Deformation of carbon nanotubes by surface van der Waals forces", *Physical Review B*, vol. 58, no. 20, pp. 13870-13873, 1998. Available: 10.1103/physrevb.58.13870.

[11] G. Psaltopoulos and A. Wittneben, "Nonlinear MIMO: affordable MIMO technology for wireless sensor networks", *IEEE Transactions on Wireless Communications*, vol. 9, no. 2, pp. 824-832, 2010. Available: 10.1109/twc.2010.02.090530.

[12] Y. Zhang and K. Letaief, "An Efficient Resource-Allocation Scheme for Spatial Multiuser Access in MIMO/OFDM Systems", *IEEE Transactions on Communications*, vol. 53, no. 1, pp. 107-116, 2005. Available: 10.1109/tcomm.2004.840666.

[13] A. Ijaz et al., "Enabling Massive IoT in 5G and Beyond Systems: PHY Radio Frame Design Considerations," in *IEEE Access*, vol. 4, pp. 3322-3339, 2016, doi: 10.1109/ACCESS.2016.2584178

[14] K. Jha, B. Bukhari, C. Singh, G. Mishra and S. Sharma, "Compact Planar Multistandard MIMO Antenna for IoT Applications", *IEEE Transactions on Antennas and Propagation*, vol. 66, no. 7, pp. 3327-3336, 2018. Available: 10.1109/tap.2018.2829533.

[15] L. Chang, Y. Yu, K. Wei and H. Wang, "Polarization-Orthogonal Co-frequency Dual Antenna Pair Suitable for 5G MIMO Smartphone With Metallic Bezels," in *IEEE Transactions on Antennas and Propagation*, vol. 67, no. 8, pp. 5212-5220, Aug. 2019, doi: 10.1109/TAP.2019.2913738.

[16] D. Samardzija et al., “Applications of MIMO Techniques to Sensing of Cardiopulmonary Activity”, Winlab.rutgers.edu, 2020. [Online]. Available: http://www.winlab.rutgers.edu/~samar/public/mimo_sensing_aces05.pdf. [Accessed: 12- May- 2020].

[17] H. Li, S. Sun, B. Wang and F. Wu, "Design of Compact Single-Layer Textile MIMO Antenna for Wearable Applications", *IEEE Transactions on Antennas and Propagation*, vol. 66, no. 6, pp. 3136-3141, 2018. Available: 10.1109/tap.2018.2811844.

[18] S. Jilani, A. Rahimian, Y. Alfadhl and A. Alomainy, "Low-profile flexible frequency-reconfigurable millimetre-wave antenna for 5G applications", *Flexible and Printed Electronics*, vol. 3, no. 3, p. 035003, 2018. Available: 10.1088/2058-8585/aad392.

[19] A. Capasso, A.E. Del Rio Castillo, H. Sun, A. Ansaldo, V. Pellegrini, F. Bonaccorso, “Ink-jet printing of graphene for flexible electronics: An environmentally-friendly approach”, *Solid State Communications*, Volume 224, 2015, Pages 53-63, ISSN 0038-1098, doi: 10.1016/j.ssc.2015.08.011.

[20] K. Pan et al., "Sustainable production of highly conductive multilayer graphene ink for wireless connectivity and IoT applications", *Nature Communications*, vol. 9, no. 1, 2018. Available: 10.1038/s41467-018-07632-w.

[21] Dassault Systèmes, 2019, CST Microwave Studios 2017 (Vélizy-Villacoublay: Dassault Systèmes)

[22] S. Jilani, M. Munoz, Q. Abbasi and A. Alomainy, "Millimeter-Wave Liquid Crystal Polymer Based Conformal Antenna Array for 5G Applications", *IEEE Antennas and Wireless Propagation Letters*, vol. 18, no. 1, pp. 84-88, 2019. Available: 10.1109/lawp.2018.2881303

[23] A. Bur, "Dielectric properties of polymers at microwave frequencies: a review", *Polymer*, vol. 26, no. 7, pp. 963-977, 1985. Available: 10.1016/0032-3861(85)90216-2.

[24] J. Thaysen and K. Jakobsen, "Envelope correlation in (N,N) MIMO antenna array from scattering parameters", *Microwave and Optical Technology Letters*, vol. 48, no. 5, pp. 832-834, 2006. Available: 10.1002/mop.21490.

[25] S. Tripathi, A. Mohan and S. Yadav, "A Compact Koch Fractal UWB MIMO Antenna With WLAN Band-Rejection", *IEEE Antennas and Wireless*

Propagation Letters, vol. 14, pp. 1565-1568, 2015. Available: 10.1109/lawp.2015.2412659.

[26] P. Pataniya and C. Sumesh, "WS2 Nanosheet/Graphene Heterostructures for Paper-Based Flexible Photodetectors", *ACS Applied Nano Materials*, vol. 3, no. 7, pp. 6935-6944, 2020. Available: 10.1021/acsanm.0c01276.

[27] E. Secor et al., "Enhanced Conductivity, Adhesion, and Environmental Stability of Printed Graphene Inks with Nitrocellulose", *Chemistry of Materials*, vol. 29, no. 5, pp. 2332-2340, 2017. Available: 10.1021/acs.chemmater.7b00029.

[28] A. Lamminen et al., "Graphene-Flakes Printed Wideband Elliptical Dipole Antenna for Low-Cost Wireless Communications Applications", *IEEE Antennas and Wireless Propagation Letters*, vol. 16, pp. 1883-1886, 2017. Available: 10.1109/lawp.2017.2684907.

[29] K. Arapov et al., "Graphene screen-printed radio-frequency identification devices on flexible substrates", physica status solidi (RRL) - *Rapid Research Letters*, vol. 10, no. 11, pp. 812-818, 2016. Available: 10.1002/pssr.201600330.

[30] K. Jaakkola, H. Sandberg, M. Lahti and V. Ermolov, "Near-Field UHF RFID Transponder With a Screen-Printed Graphene Antenna", *IEEE Transactions on Components*, Packaging and Manufacturing Technology, vol. 9, no. 4, pp. 616-623, 2019. Available: 10.1109/tcpmt.2019.2902322.

[31] X. Huang, T. Leng, K. Chang, J. Chen, K. Novoselov and Z. Hu, "Graphene radio frequency and microwave passive components for low cost wearable electronics", *2D Materials*, vol. 3, no. 2, p. 025021, 2016. Available: 10.1088/2053-1583/3/2/025021.

[32] V. Mandrić Radivojević, S. Rupčić, M. Srnović and G. Benšić, "Measuring the Dielectric Constant of Paper Using a Parallel Plate Capacitor", *International journal of electrical and computer engineering systems*, vol. 9, no. 1, pp. 1-10, 2018. Available: 10.32985/ijeces.9.1.1.

[33] F. Rashiddy Wong, A. Ahmed Ali, K. Yasui and A. Hashim, "Seed/Catalyst-

Free Growth of Gallium-Based Compound Materials on Graphene on Insulator by Electrochemical Deposition at Room Temperature", *Nanoscale Research Letters*, vol. 10, no. 1, 2015. Available: 10.1186/s11671-015-0943-y.

[34] T. Leng et al., "Screen-Printed Graphite Nanoplate Conductive Ink for Machine Learning Enabled Wireless Radiofrequency-Identification Sensors", *ACS Applied Nano Materials*, vol. 2, no. 10, pp. 6197-6208, 2019. Available: 10.1021/acsanm.9b01034.

[35] F. Johra, J. Lee and W. Jung, "Facile and safe graphene preparation on solution based platform", *Journal of Industrial and Engineering Chemistry*, vol. 20, no. 5, pp. 2883-2887, 2014. Available: 10.1016/j.jiec.2013.11.022.

[36] X. Chen, X. Wang and D. Fang, "A review on C1s XPS-spectra for some kinds of carbon materials", *Fullerenes, Nanotubes and Carbon Nanostructures*, vol. 28, no. 12, pp. 1048-1058, 2020. Available: 10.1080/1536383x.2020.1794851.

[37] U. Patil et al., "Effect of plasma treatment on multilayer graphene: X-ray photoelectron spectroscopy, surface morphology investigations and work function measurements", *RSC Advances*, vol. 6, no. 54, pp. 48843-48850, 2016. Available: 10.1039/c6ra03046g.

[38] X. Huang et al., "Binder-free highly conductive graphene laminate for low cost printed radio frequency applications", *Applied Physics Letters*, vol. 106, no. 20, p. 203105, 2015. Available: 10.1063/1.4919935.

Chapter 4 Graphene Printed Flexible and Conformal Array Antenna on Paper Substrate for 5.8 GHz Wireless Communications

---

Xinyao Zhou, Ting Leng, Kewen Pan, Mahmoud A. Abdalla, Zhirun Hu

2020 14th European Conference on Antennas and Propagation (EuCAP), 2020, pp. 1-4

My contributions:

I have prepared the graphene ink, designed, and fabricated the proposed device, performed all the measurement, calculated and analysed all the data, and drew all the graphs.

Abstract

In this paper, a printed graphene compact, low-cost, disposal, flexible and conformal, coplanar waveguide (CPW) fed, linear array antenna has been proposed. It was designed for 5.8 GHz radars, portable electronic devices, and commercial wireless LAN applications and manufactured by screen printing formulated highly conductive graphene ink on paper substrate. The array achieves 73% total radiation efficiency and a peak gain value of 4.5 dBi at 5.8 GHz, with its bandwidth ranges from 4.6 GHz to 7.9 GHz (52.8%). Over the operating frequency, the radiation of the antenna has been proved as a typical radiation pattern of a patch antenna array.

4.1 Introduction

Printed electronics has drawn extreme attention in modern communication field over the last decade [1]. This technology significantly enables the rapid development of a vast of soft electronic applications such as antennas [2], sensors [3-4], bendable displays [5], thin film transistors [6], electronic skin [7] and transparent electrodes [8] due to its tremendous influence on the enhancement of user comfort, space utilization and commercial manufacturing convenience. Among all the conductive inks that have been proposed so far, silver nanoparticle inks have been most often mentioned due to its high electric conductivity and chemical stability in free air [9]. However, the very

high cost of silver strictly limits its industrial manufacture. Other cheaper conductive inks based on common metallic nanoparticles such as copper and aluminum demand high thermal condition in the cause of oxidization prevention during fabrication [10], which narrows down the selection of substrates to a great extent.

Graphene-based ink has thus been regarded as a promising substitution of metallic conductive inks for its relatively high conductivity [11], excellent electron transfer rate [12], environmental amity and low cost, contributing to better integration into systems that require flexibility. Also, it enhances the robustness of devices and hence prevents discontinuities during high-level deformation unlike metal inks or carbon nanotubes [13]. Different fabrication approaches have been intensively researched for producing graphene-based flexible electronic devices over the years, such as reactive sputtering, ink-jet printing [14], spin coating [15], thermal evaporation [16] and screen printing [17]. Whereas sputtering and spin coating does not support patterns with high-resolution, and thermal evaporation requires very high temperature which makes it incompatible with heat sensitive substrates [18]. Thus, more investigations have been carried out on using ink-jet printing and screen printing due to the simplicity of the process, good surface conductivity [19], low temperature requirement and comparative effectiveness.

The key to graphene printed technology is to maintain a low sheet resistance and avoid introduction of cracks, at the same time get rid of the thermal annealing process for manufacture simplicity. A binder-free technique suitable for industrial scale screen printing has been proposed in [20], 4.3×10^4 S/m conductivity has been attained, validating the concept of the approach. Taking advantage of this technique, a flexible

dipole antenna on paper substrate was illustrated in [21], obtaining a −4 dBi maximum gain, and could be used for low-cost RFID and sensing applications with excellent sustainability and conformability. Nevertheless, for this structure, antenna bending could cause severe radiation pattern deformation and gain degradation, affecting signal transmission.

In this paper, a coplanar waveguide-fed flexible graphene-printed wide-band antenna array on paper substrate has been designed and then fabricated. 1.4 Ω/sq sheet resistance and 4.5 dBi gain at 5.8 GHz resonant frequency have been obtained, making it a good candidate for radars, health monitoring system, body centric networks and other commercial wireless LAN applications.

4.2 Antenna Design And fabrication

4.2.1 Antenna Design

The configuration and dimension of this proposed graphene printed antenna array has been shown in Fig. 4-1 (a). Coplanar waveguide feeding has been adopted for reducing the risk of ink permeation as the ground can thereby be addressed on the same side as the radiator. Further, planar structures ensure compact structure of devices and allow better usage of space resource. The conductive graphene sheet has been simulated with a 1.4 Ω/sq sheet resistance (fluctuates around 1.2-1.6 Ω/sq during four-point probe measurement). Paper substrate has been placed under the

graphene radiating pattern with a dielectric constant of 2.31 and a thickness of 0.1 mm. Parameters such as 0.52 mm spacing between antennas, 0.4mm coplanar waveguide

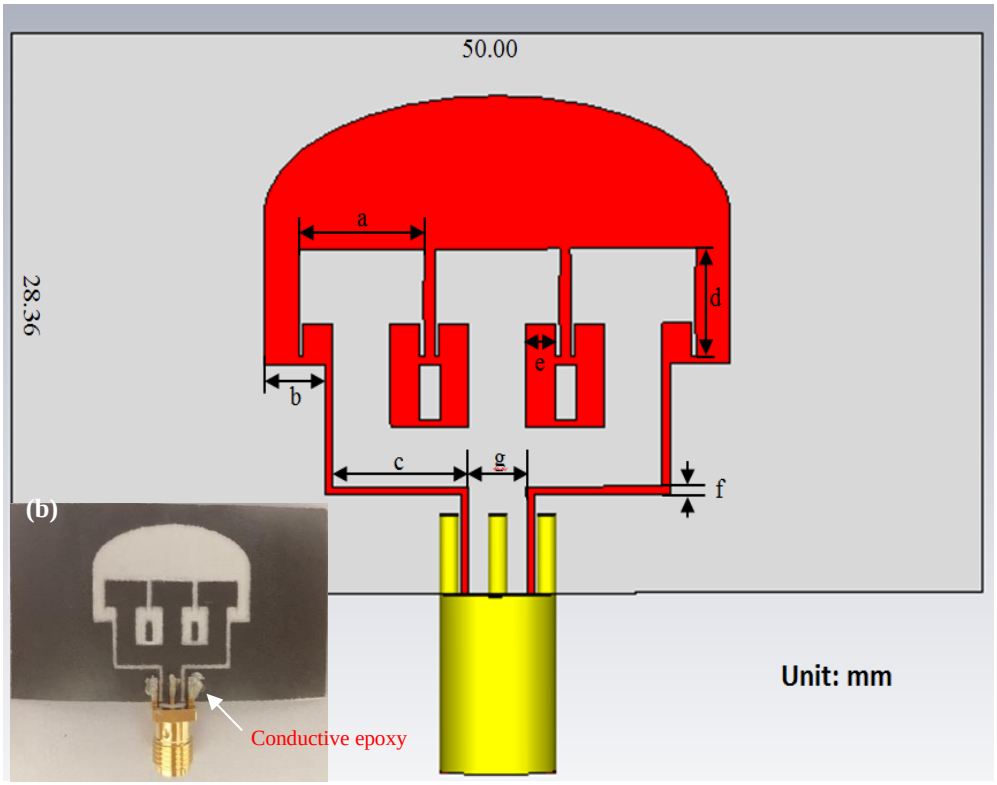

Fig. 4-1.(a) Geometry of graphene printed array antenna with an SMA connector attached for including mismatch during calculation. (a=6.48, b=3.10, c=7.00, d=5.45, e=1.50, f=0.4mm) (b)Fabricated graphene printed array antenna on paper substrate.

gap and 3mm feeding line width were analyzed and carefully selected for implementing antenna's best performance. Due the fact that the minimum separation current attainable screen printing technology can offer is 0.4 mm (the resolution of the screen-printed patterns), mismatch will be inevitably introduced between the antenna and the connector. In this case, an SMA connector has been placed at the end of the

feeding line, fixing the port impedance at 50 Ω in the simulation, thus including mismatch during the simulation calculation process. Rectangular structures have been

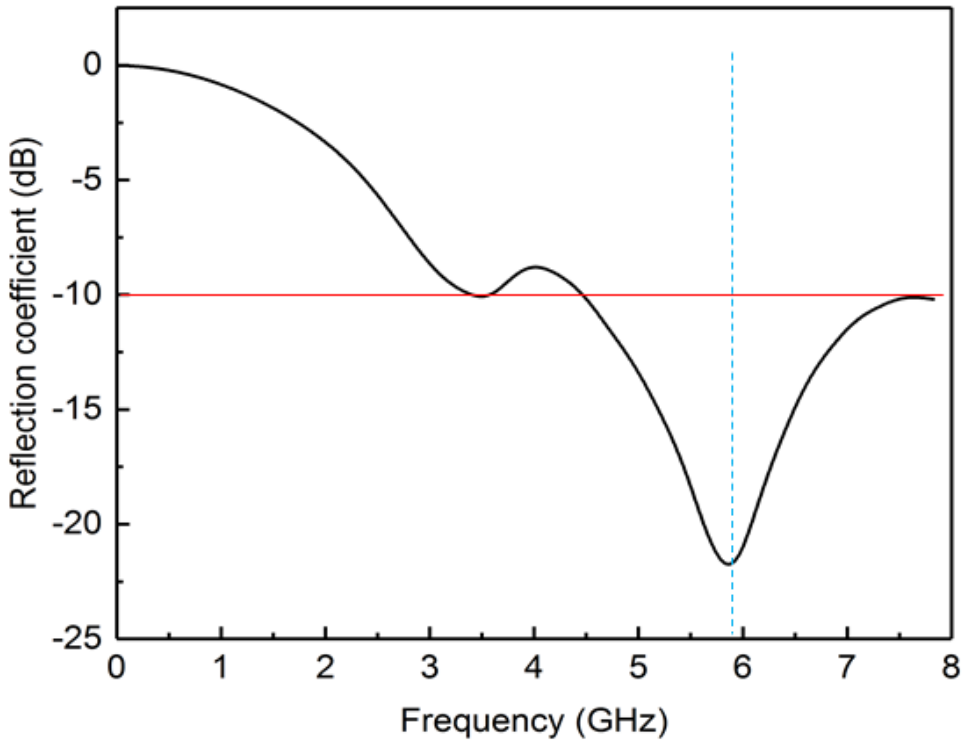

Fig. 4-2. Reflection coefficient of graphene nanoflakes printed cpw-fed antenna array over frequency, showing a 52.8% bandwidth. The -10dB line has been plotted in red and the resonant frequency in blue.

designed in between the array feeding lines to introduce coupling and diminish the loss, consequently enhance the transmission. The eclipse shape at the top helps widening the operating bandwidth and increasing gain value, aggregating high value gains in our desired frequency range 4.8-5 GHz for portable 5G networks and 5.8-6 GHz for Wi-MAX and WLAN. Distance between the antennas directly contributes to the influence on the reflectivity of the whole structure.

4.2.2 Antenna Fabrication

In this work, the conductive ink was made from first mixing graphene flakes with an organic solvent, N-methyl-2-pyrrolidone (NMP). Then, screen filtering and vacuum suction filtration were carried out to separate graphene with the solvent. The remained graphene was again dissolved in ethylene glycol, and tuned to the right concentration. Sonication has also been applied for a more even dissolution of the conductive graphene nanoflakes in ethylene glycol. After formulating the conductive ink, our desired pattern was printed on paper substrate using screen-printing technology. A 10-minute heating process (at 100 ◦C to protect substrate from over-heating) has been applied right after the printing to volatilize the dispersant. Then, rolling compression was operated for reducing the sheet resistance by about 1/10, increasing the contact area of conductive graphene nanoflakes, allowing better flow of surface current as well as higher conductivity of the radiator.

About 1.2-1.6 Ω/sq sheet resistance was measured for the fabricated antenna in Fig.4-1 (b) by four-point probe measurement method and semiconductor characterization system. The sheet resistance can be expressed as

$$\sigma = \frac{1}{R_s t} \tag{4.1}$$

where ρ is the resistivity and t is the thickness of the measured graphene conductive film.

Finally, a 50 Ω SMA connector has been connected to the structure by using

conductive epoxy with its one joint contacting to the radiator and the other two to the ground. The final fabricated graphene printed array antenna can be clearly observed in Fig. 4-1 (b). Fig. 4-2 shows the fabricated graphene printed array antenna on paper substrate.

4.3 Simulation results and discussion

The graphene printed array antenna shows a resonant frequency at 5.8 GHz, as seen in Fig. 4-2, S11 variation with frequency. The 52.8% bandwidth (-10 dB) of the array antenna ranges from 4.6 GHz to 7.9 GHz, covering a huge amount of applications such

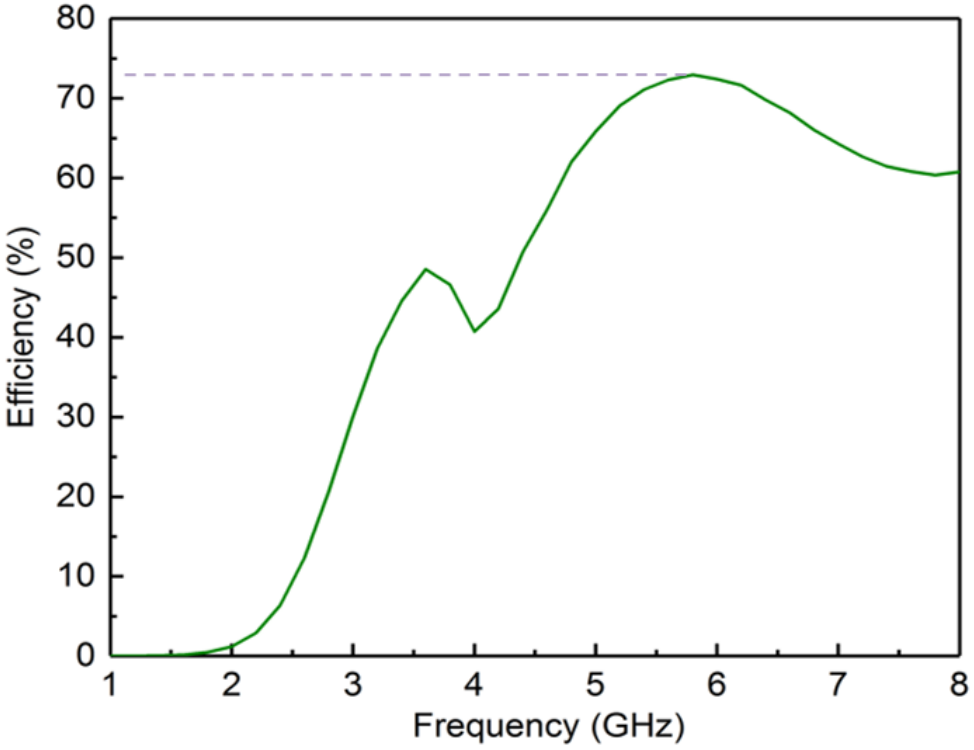

Fig. 4-3. Simulated total efficiency of the graphene nanoflakes printed cpw-fed array antenna on paper substrate.

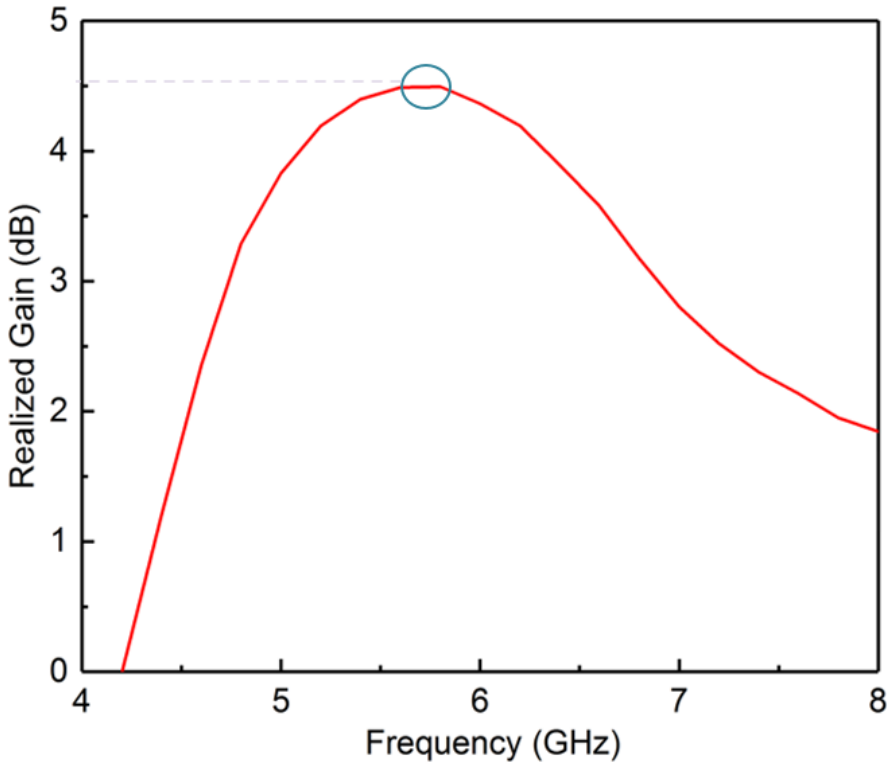

Fig. 4-4. Simulated realized gain of the graphene nanoflakes printed CPW-fed array antenna on paper substrate.

as x band satellite communication, portable devices allocated to 4.8-5 GHz 5G networks, EEE 802.16a 5.8 GHz Wi-MAX band and 5.8 GHz upper WLAN. In Fig. 4-3, the total efficiency achieves 73% at the resonant frequency and stays above 70% from 5.28 GHz to 6.37 GHz, which is a very good result for printed graphene antennas considering the inevitable mismatch and lower conductivity comparing to metal structures. The peak realized gain occurs at 5.8-6 GHz with a comparatively high value of 4.5 dB (Fig. 4-4.), even including the effect of mismatch. More importantly, it remains above 3 dB from 4.74 GHz to 6.91 GHz, ensuring continuous communication

quality.

From observation, this graphene nanoflakes printed array antenna exhibits the same

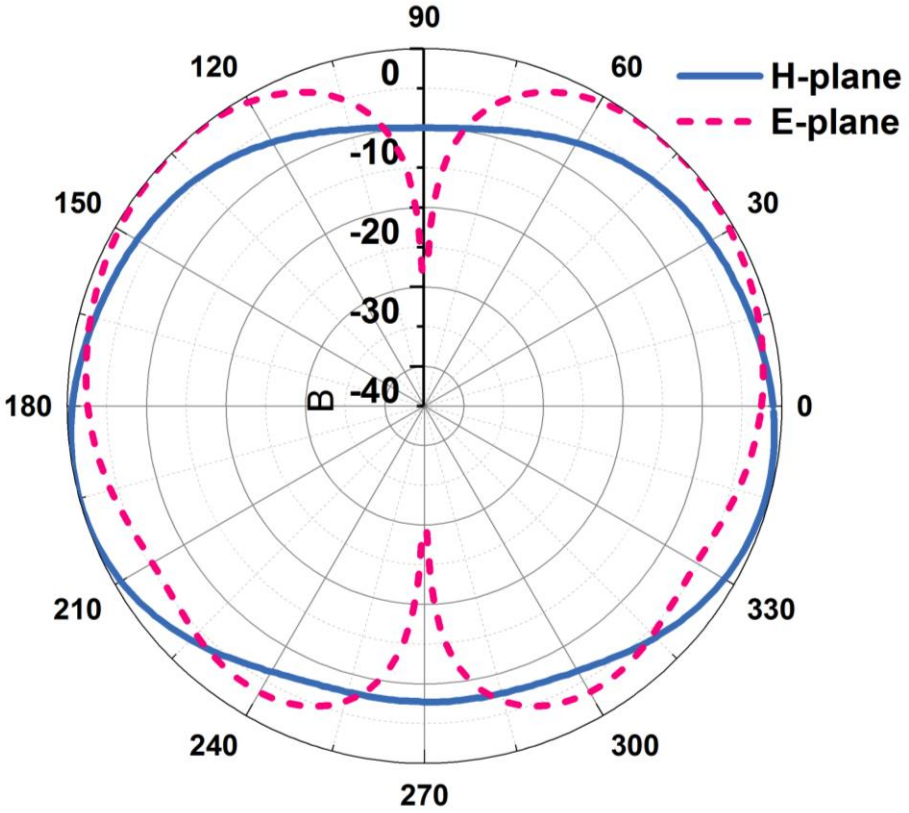

Fig. 4-5. Simulated radiation pattern of the graphene printed antenna array on both E-plane and H-plane.

shape as a typical patch antenna array in far field region without any evident deformation, proving the performance of the antenna, as seen in Fig. 4-5, the radiation pattern of the antenna in both E- and H-plane.

4.4 Conclusion

In this work, a graphene printed, compact, conformal, disposal, environmental friendly and low cost antenna array has been first successfully simulated and then fabricated with expected sheet resistance. 4.5 dBi gain and 73% efficiency has been shown in the simulation at its resonant frequency 5.8 GHz. The bandwidth of the array covers x band satellite communication, 4.8-5 GHz 5G portable networks, and 5.8 GHz upper WLAN. Screen printing has been used to fabricate the design. The good performance outcome in simulation and its very low cost imply a promising application prospect in graphene printed electronics, especially in the field of flexible and wearable electronic devices. The performance of the fabricated antenna as well as its flexibility will be tested in anechoic chamber to further validate the simulated outcome.

References

[1] K. Suganuma, Introduction to printed electronics. New York: Springer, 2014.

[2] W. Whittow et al., "Inkjet-Printed Microstrip Patch Antennas Realized on Textile for Wearable Applications", *IEEE Antennas and Wireless Propagation Letters*, vol. 13, pp. 71-74, 2014. Available: 10.1109/lawp.2013.2295942.

[3] R. J. Vyas, A. Rida, L. Yang, and M. M. Tentzeris, “Design and development of the first entirely paper-based wireless sensor module,” in *IEEE Antennas Propag Soc*. Int. Symp., Jul. 5–11, 2008, pp. 1–4.

[4] T. Leng et al., "Screen-Printed Graphite Nanoplate Conductive Ink for Machine Learning Enabled Wireless Radiofrequency-Identification Sensors", *ACS Applied Nano Materials*, 2019. Available: 10.1021/acsanm.9b01034.

[5] W. Lin, M. Hsu and C. Chiang, "17.2: New Decorative Patterning Technology and Materials on 3-Dimensional Surfaces for Bendable Display", *SID Symposium Digest of Technical Papers*, vol. 49, pp. 185-187, 2018. Available: 10.1002/sdtp.12675.

[6] I.S. Jacobs and C.P. Bean, “Fine particles, thin films and exchange anisotropy,” in *Magnetism*, vol. III, G.T. Rado and H. Suhl, Eds. New York: Academic, 1963, pp. 271-350.

[7] S. Zhao and R. Zhu, "Electronic Skin: Electronic Skin with Multifunction Sensors Based on Thermosensation (Adv. Mater. 15/2017)", *Advanced Materials*, vol. 29, no. 15, 2017. Available: 10.1002/adma.201770099. R. Nicole, “Title of paper with only first word capitalized,” J. Name Stand. Abbrev., in press.

[8] R. Hoffmann, S. Dilfer and J. Schneider, "Transparent indium tin oxide as inkjet-printed thin film electrodes for organic field-effect transistors", *physica status solidi* (a), vol. 208, no. 12, pp. 2920-2925, 2011. Available: 10.1002/pssa.201127362.

[9] Z. Zhang, X. Zhang, Z. Xin, M. Deng, Y. Wen and Y. Song, "Synthesis of monodisperse silver nanoparticles for ink-jet printed flexible

electronics", *Nanotechnology*, vol. 22, no. 42, p. 425601, 2011. Available: 10.1088/0957-4484/22/42/425601.

[10] Kamyshny, A. & Magdassi, S. Conductive nanomaterials for printed electronics. *Small* 10, 3515–3535 (2014).

[11] Lamminen, A. et al. Graphene-flakes printed wideband elliptical dipole antenna for low-cost wireless communications applications. *IEEE Antennas Wirel. Propag. Lett*. 16, 1883–1886 (2017).

[12] S. Taioli, P. Umari and M. De Souza, "Electronic properties of extended graphene nanomaterials fromGWcalculations", *physica status solidi* (b), vol. 246, no. 11-12, pp. 2572-2576, 2009. Available: 10.1002/pssb.200982339.

[13] Yamada, T. et al. A stretchable carbon nanotube strain sensor for humanmotion detection. Nat. Nanotechnol. 6, 296 (2011).

[14] S. Saeed, C. Balanis and C. Birtcher, "Inkjet-Printed Flexible Reconfigurable Antenna for Conformal WLAN/WiMAX Wireless Devices", *IEEE Antennas and Wireless Propagation Letters,* vol. 15, pp. 1979-1982, 2016. Available: 10.1109/lawp.2016.2547338.

[15] M. Tyona, "A comprehensive study of spin coating as a thin film deposition technique and spin coating equipment", *Advances in materials Research*, vol. 2, no. 4, pp. 181-193, 2013. Available: 10.12989/amr.2013.2.4.181.

[16] I. M. Graz, D. P. J. Cotton, and S. P. Lacour, "Extended cyclic uniaxial loading of stretchable gold thin-films on elastomeric substrates",*Applied Physics Letters*, Vol. 94, No. 7, Feb. 2009.

[17] D. Anagnostou, A. Gheethan, A. Amert and K. Whites, "A Direct-Write Printed Antenna on Paper-Based Organic Substrate for Flexible Displays and WLAN Applications", *Journal of Display*

[18] K. NAMIKI, X. CHENG and H. TAKAHASHI, "Indirectly Reactive Sputtering Coater for High Quality Optical Coatings", *IEICE Transactions on Electronics*, vol. 91-, no. 10, pp. 1673-1674, 2008. Available: 10.1093/ietele/e91-c.10.1673.

[19] H. Khaleel, H. Al-Rizzo, D. Rucker and S. Mohan, "A Compact Polyimide-Based UWB Antenna for Flexible Electronics", *IEEE Antennas and Wireless*

Propagation Letters, vol. 11, pp. 564-567, 2012. Available: 10.1109/lawp.2012.2199956.

[20] K. Pan et al., "Sustainable production of highly conductive multilayer graphene ink for wireless connectivity and IoT applications", *Nature Communications*, vol. 9, no. 1, 2018. Available: 10.1038/s41467-018-07632-w.

[21] T. Leng, X. Huang, K. Chang, J. Chen, M. Abdalla and Z. Hu, "Graphene Nanoflakes Printed Flexible Meandered-Line Dipole Antenna on Paper Substrate for Low-Cost RFID and Sensing Applications", *IEEE Antennas and Wireless Propagation Letters*, vol. 15, pp. 1565-1568, 2016. Available: 10.1109/lawp.2016.2518746.

Chapter 5 Graphene Printed Tri-band Flexible Antenna Array for Wireless Communication Applications

---

Xinyao Zhou, Ting Leng, Kewen Pan, Zhirun Hu

2021 IEEE International Symposium on Antennas and Propagation and USNC-URSI Radio Science Meeting, Singapore, 2022

My contributions:

I have prepared the graphene ink, designed, and fabricated the proposed device, performed all the measurements, calculated and analysed all the data, and drew all the graphs

Abstract

This paper presents a novel co-planar waveguide (CPW) fed tri-band graphene printed 1×2 planar array antenna for wireless communication use. The antenna is designed to support L band, the fifth generation (5G) sub-6 GHz band and 5.2 GHz wireless local area network (WLAN) communication applications with biodegradable and low-cost printed graphene. The graphene laminate which was screen-printed on paper substrate possesses a sheet resistance of 1.5 Ω /sq and a conductivity of 3.5×10^4 S/m. The peak gain of this antenna reaches 2.14 dBi at 3.8 GHz, indicating good power transmission.

5.1 Introduction

The demand for low-cost multiband antennas to transmit signals for different services has significantly increased over the decade. With the rapid development of 5G, the necessity of integrating various extensively used bands into modern compact portable wireless communication devices has raised even higher. A lot of work have been dedicated in recent years to designing dual-band and tri-band compact antennas with different methods, such as taking advantages of metamaterials aids and meandered lines for multiband operation, PIFAs, introducing slots to patch antennas,

adding C or L-shape strips to the structures [1-4]. For easier integration with 5G active devices and microwave integrated circuit amplifiers (MMIC), fully printable CPW-fed antennas are highly attractive to researchers due to the fact that all patterns can be put on the same plane. To reduce size of conventional microstrip patch antennas and at the same time achieve multiband signal transmission, meandered line design is often supported with CPW feed, obtaining large decrease in size, fully printable structure, and regular omnidirectional radiation patterns. Printed flexible antennas can be achieved in many ways, silver and gold inks are the most studied due to their mechanical stability and high conductivity. However, the extreme high cost greatly reduces the accessibility and sustainability for their commercial applications. Other conductive inks such as copper and aluminum are easily oxidized [5], the thermal annealing process narrows down the selection of substrates by a large margin. With its excellent electrical and mechanical properties, graphene is regarded as a sustainable substitution of metal with high electron transfer rate.

Many work involving graphene printed antennas has been reported, including dipoles, sensors, RFIDs and monopoles [5-7], exhibiting good radiation performance and proving the usability of graphene antennas.

In this work, we propose a novel tri-band CPW-fed graphene printed 1× 2 planar array designed with meandered line and ground extensions. The antenna is screen-printed on paper substrate with our highly conductive graphite ink. The simulation results are investigated to prove the design, measured results will be further presented in full paper.

5.2 Antenna fabrication

To produce highly conductive graphene ink, liquid-phase exfoliation method was used to disperse exfoliated graphite flakes in N-methyl-2-pyrrolidone (NMP) organic solvent. Then, 24-hour sonication and filtration were applied to the mixture to dispose unwanted large particles. The final conductive ink was tuned with Ethylene Glycol (EG) dispersant to 50 mg/mL. Screen printing procedure was implemented with a semiautomatic screen printer and a capillary film negatively patterned mesh screen. The printed sample was then dried and compressed with rolling machine (Agile F130 Manual Mill) to reduce resistance. The SMA connector was at last fixed to the CPW feeding point by using conductive epoxy. The average sheet resistance is measured as 1.5 Ω/sq. The conductivity is determined as 3.5×10^4 S/m using (5.1).

$$\sigma = \frac{1}{R_s t} \tag{5.1}$$

where σ is the conductivity, t is the thickness of the measured film and R$_S$ is the sheet resistance.

5.3 Antenna design and results

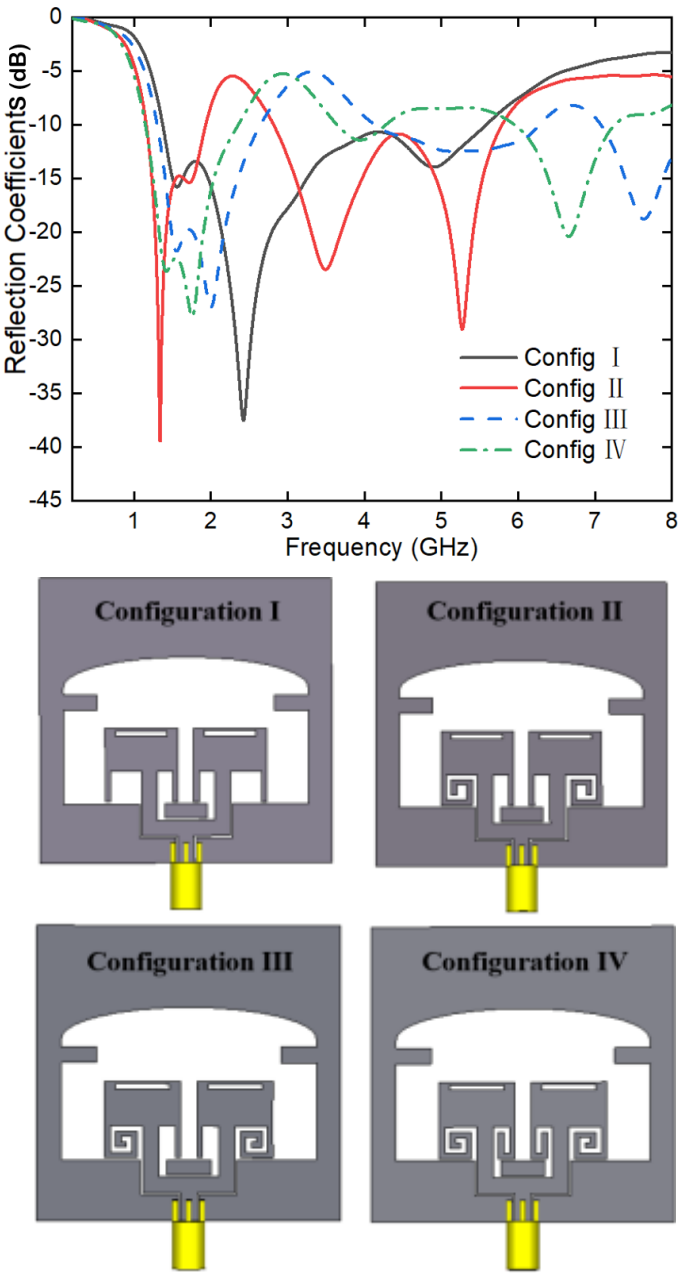

Fig. 5-1. Reflection coefficient comparison of the four configurations.

The ohmic sheet resistance of the printed graphene laminate is set to 1.5 Ω/sq. The paper substrate has a thickness of 0.1 mm and a relative permittivity of 2.31. The size of the whole structure is 56 mm×60 mm. The antenna array is implemented with a CPW feed (preventing ink penetration to the other side of paper) splitting into two branches. The inset of the patch brings the feed to a

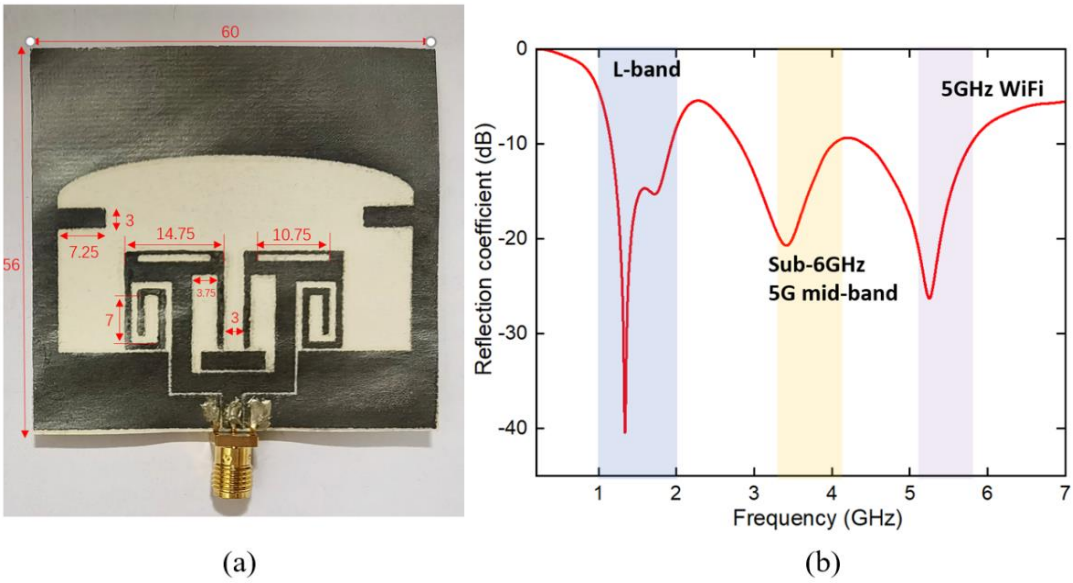

(a) (b)

Fig. 5-2. Fabricated prototype and detailed dimensions labelled in mm and (b) reflection coefficient of the proposed antenna.

higher point to improve input impedance matching, contributing to higher efficiency of the antenna. Four configurations of graphene array antennas are displayed in Fig. 5-1.

Configuration I shows the initial structure of an inset-feed CPW antenna array design with one rectangular slot on each element which has an ultra-wideband feature covering 1.2 GHz-5.9 GHz. Configuration II, III and IV are involved with different meandered line structures. The comparison of the return loss of four layouts can be observed in Fig. 5-1, where configuration IIshows three clear resonances at 1.35 GHz, 3.5 GHz and 5.25 GHz. For better

impedance matching at desired frequencies, configuration II is selected and further optimized to achieve the best result. The final geometry and detailed dimensions of the fabricated prototype are shown in Fig. 5-2 (a). Fig. 5-2 (b) shows the simulated return loss, three resonances can be observed at 1.4 GHz, 3.5 GHz and 5.2 GHz. The bandwidth of the antenna covers 1.2 GHz-1.9 GHz, 2.8 GHz-4 GHz and 4.5 GHz-5.8 GHz, realizing simultaneous signal transmission in L-band, 5G mid- band, and 5 GHz WiFi channels. Radiation patterns of the antenna at 1.4 GHz, 3.5 GHz and 5.2 GHz are exhibited in Fig.5-3. The patterns of 1.4 GHz and 5.2 GHz in H-plane indicates omnidirectional radiation performance. At higher resonance in E-plane, some deformation in shape can be spotted due to the change in surface current distributions. At 1.4 GHz, the surface current is focused on the ground extension, while at 3.5 GHz, the surface current is mainly distributed on the patch, and at 5.2 GHz, more power is radiated by the inner loop of the spiral meandered line. The peak realized gain of the antenna reaches 2.14 dBi at 3.8 GHz, verifying good power transmission.

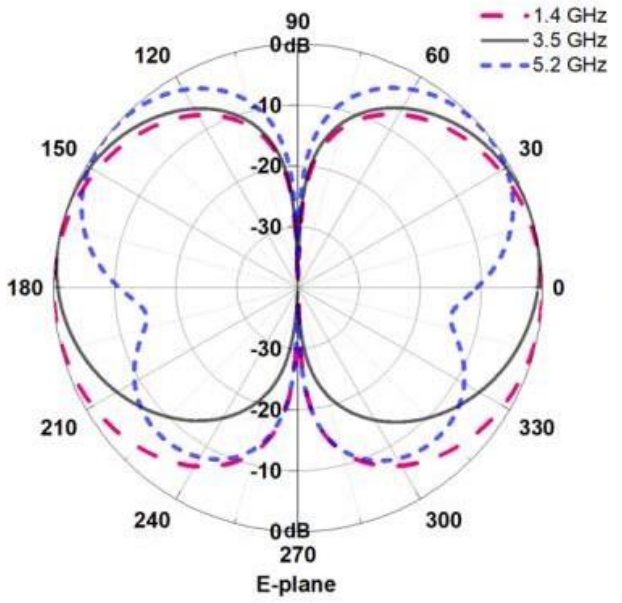

(a)

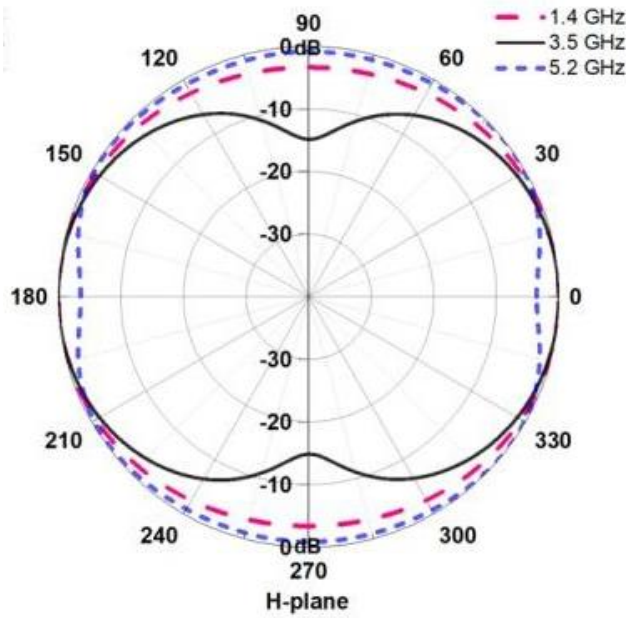

(b)

Fig. 5-3. Antenna radiation patterns in (a) E-plane and (b) H-plane at 1.4 GHz, 3.5 GHz and 5.2 GHz respectively.

5.4 Conclusion

A novel tri-band array antenna design was integrated with printed graphene technology to produce low-cost flexible antenna supporting simultaneous operation for multiple wireless services. The excellent bandwidth distribution and radiation pattern performance of this array antenna have exemplified that printed graphene-based antenna can take the place of high-cost conventional antennas consist of metallic structures and rigid substrates. Other measured results of this antenna will be further presented in full paper.

References

[1] Q. Zhao, S. Gong, W. Jiang, B. Yang and J. Xie, "COMPACT WIDE- SLOT TRI-BAND ANTENNA FOR WLAN/WIMAX APPLICATIONS", *Progress In Electromagnetics Research Letters*, vol. 18, DOI 10.2528/pierl10081601, pp. 9-18, 2010.

[2] Wei Hu, Ying-Zeng Yin, Peng Fei and Xi Yang, "Compact Triband Square-Slot Antenna With Symmetrical L-Strips for WLAN/WiMAX Applications", *IEEE Antennas and Wireless Propagation Letters*, vol. 10, DOI 10.1109/lawp.2011.2154372.J, pp. 462-465, 2011.

[3] D. Naji, "Design of Compact Dual-band and Tri-band Microstrip Patch Antennas", *International Journal of Electromagnetics and Applications*, vol. 8, DOI 10.5923/j.ijea.20180801.02, no. 1, pp. 26-34, 2018.

[4] T. Ali, M. Khaleeq, S. Pathan and R. Biradar, "A multiband antenna loaded with metamaterial and slots for GPS/WLAN/WiMAX applications", *Microwave and Optical Technology Letters*, vol. 60, DOI 10.1002/mop.30921, no. 1, pp. 79-85, 2017.

[5] K. Pan et al., "Sustainable production of highly conductive multilayer graphene ink for wireless connectivity and IoT applications", Nature Communications, vol. 9, DOI 10.1038/s41467-018-07632-w, no. 1, 2018.

[6] X. Huang et al., "Highly Flexible and Conductive Printed Graphene for Wireless Wearable Communications Applications", *Scientific Reports*, vol. 5, DOI 10.1038/srep18298, no. 1, 2015.

[7] T. Leng et al., "Printed graphene/WS2 battery-free wireless photosensor on papers", *2D Materials*, vol. 7, DOI 10.1088/2053-1583/ab602f, no. 2, p. 024004, 2020.

Chapter 6 A Dual-band Flexible Printed Graphene Antenna Array for 2.4 and 5 GHz WLAN Applications

---

Xinyao Zhou, Ting Leng, Kewen Pan, Zhirun Hu

2021 51st European Microwave Conference (EuMC), London, UK, 2022

My contributions:

I have prepared the graphene ink, designed, and fabricated the proposed device, performed all the measurements, calculated and analysed all the data, and drew all the graphs.

Abstract

In this paper, a 70×210 mm dual-band screen-printed graphene flexible antenna array designed for 2.4 GHz and 5 GHz wireless local area network (WLAN) communication is presented. The flexibility of the antenna is achieved using Co-Planar Waveguide (CPW) feed and screen-printing highly conductive graphene ink on extremely low-cost and disposable paper substrate. The proposed antenna consists of two elements and a stepped ground integrated with side stubs, supporting 2.4 GHz (802.11b/g/n) and 5 GHz (802.11a/n/ac) WLAN communication networks, with bandwidths of 1.74-2.72 GHz (55.96%) and 3.44–6.26 GHz (81.98%), achieving peak gains of 2.37 dBi and 2.55 dBi at 2.05 and 5.06 GHz, showing outstanding power transmissions and radiation performance at both frequencies, guaranteeing strong and stable wireless connections.

6.1 Introduction

The field of printed electronics has bloomed and brought a new era to wireless communications due to its advantage in simple fabrication process, compact size, and its unique compatibility with bendable substrates. To implement the mass deployment of (Internet of Everything) IoE applications spurred by the rapid evolution of 5G wireless communications, flexibility of devices is a clear need for enhancing the integration and incorporation with a variety of systems, especially for applications such as body centric networks, RFID systems, health, and military monitoring systems, etc. The development of printed electronics technology for the fifth-generation wireless communications offers favorable circumstances and

an abundance of opportunities for novel IoE applications.

Various conductive inks have been proposed for achieving flexibility in electronic devices, such as inkjet printing silver nanoparticle ink on paper substrate [1] and textiles [2], evaporating gold on micro structured PDMS substrate [3]. Although silver nanoparticle ink has been most intensively researched in the past due to its high conductivity and chemical stability, the extremely high cost of silver greatly limits its industry production. Also, metallic conductive ink printed conformal devices inevitably generates cracks while being bent to a large angle, which not only limits the sustainability, also significantly degrades the performance.

With high electrical conductivity, robustness, strength, and excellent electron transfer rate, graphene, a monolayer of carbon atoms, has been considered as a promising substitution of metal [4] for better integration into systems that require flexibility, light weight, and low cost since it was first isolated from Graphite [5]. Different methods of printing graphene conductive ink have been reported over the years [6], among them all, inkjet printing and screen printing surpass other approaches for their higher accuracy of pattern and no need for thermal or acid processing, which accounts for better compatibility with heat sensitive substrates such as paper, polymers, and textiles [7]. Paper substrate is often selected with screen printing technique to achieve cheap transmission lines, antennas, and capacitors [8-10] for its flexibility, disposability, ease in large-scale manufacturing and fast biodegradation, regarded as a solution to the mass electronic waste accumulated worldwide.

With higher requirement of data transmission rate and system reliability in

modern mobile communications for IoE applications, it is crucial for antennas to operate at multiple frequency bands to implement strong and stable connections in locations where often difficult to reach. In this paper, a meandered line inspired, planar, flexible, printed graphene antenna array on paper substrate with dual resonance for commercial WLAN applications is developed using the binder-free screen-printing technique proposed in [11], suitable for industrial scale fabrication. In Section II, the geometry of the antenna and design of dual band are demonstrated, followed by the illustration of fabrication process of the antenna. Simulated and measured results are exhibited in Section III to justify the design, including S11, radiation pattern and gain plots. Finally, conclusions are presented in Section IV.

6.2 Antenna design and fabrication

6.2.1 Antenna Design

The geometry and its corresponding dimensions of the proposed antenna are shown in Fig. 6-1 (a) and Table 6-1 respectively, this 70×210 mm two elements antenna array is modeled and simulated by CST Studio Suite. Considering the skin depth of graphene is much larger than the printed layer, the printed layer of graphene nanoflakes was modelled as ohmic sheet with a sheet resistance of 1.2 Ω/sq. Normal paper substrate of 2.31 dielectric constant and 0.1 mm thickness was chosen for its flexibility, biodegradability, low cost and environmental amity. Planar CPW feeding structure was selected to prevent the effect of ink penetration

to the other side of the substrate, also to guarantee easier integration into various systems. A stepped ground with side stubs was designed to improve impedance matching and suppress the radiation in horizontal axes hence enhance gain at operation frequencies [12].

The meandered line structure with different radiating elements is inspired by [13] and [14], spacing of the lines are specifically adjusted for matching. The small L-shape is designated to resonate at 5 GHz and the larger shape is for 2.4 GHz. A notch in the small L-shape can be observed at the feeding point, which can be regarded as an inset feed, bringing the feeding point closer to the center to improve input impedance. The T-shape coupling component above the structure is for gain enhancement at lower frequency range. A 50 Ω SMA connector is placed at the port to include impedance mismatch in simulation results. Fig. 6-1 (b) shows the flexibility of the antenna array.

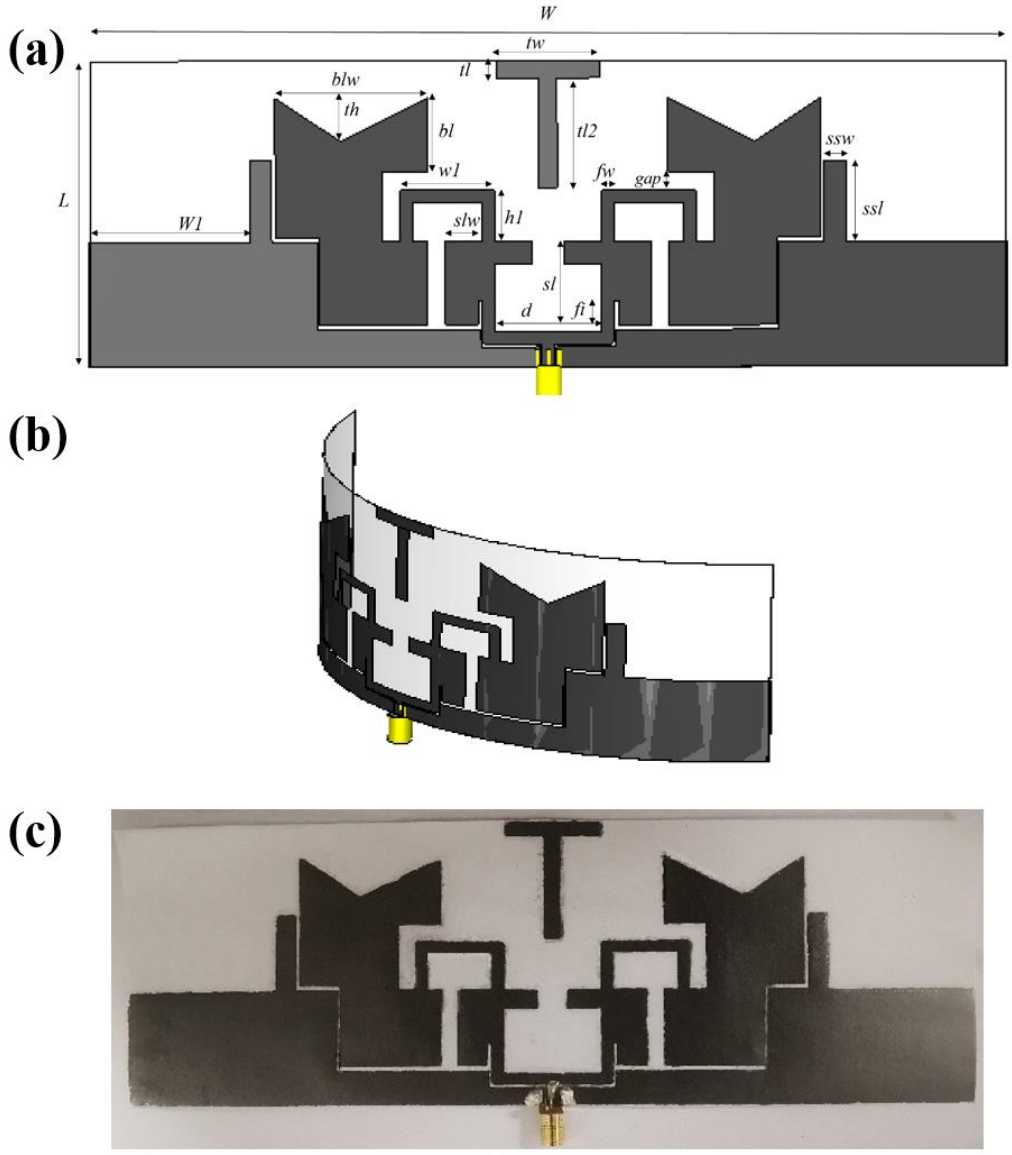

Fig. 6-1. Geometry of the proposed antenna: (a) CST model; (b) flexible antenna array; (c) fabricated prototype.

6.2.2 Antenna Fabrication

To fabricate the antenna, in this work, the graphene conductive ink was produced using the method reported by our group in [11]. First, graphite flakes were sheer mixed in N-methyl-2-pyrrolidone (NMP) for maximum dispersion. At the same time, applying a cooling system with circulating water to maintain the temperature at 20℃ and prevent overheating caused by graphene heat dissipation during sheer-mixing. After that, the mixture was sonicated and filtered to separate non-dispersible large particles and the solution. Another filtration process was then carried out to eliminate the solvent and re-disperse the solute in Ethylene Glycol and tuned to a certain concentrate.

Screen printing technology was employed with a semiautomatic screen printer and a negatively patterned 24T mesh screen. The screen was first prepared by exposing capillary film using an exposure machine with vacuum pressure regulating valve to prevent pattern displacement. The conductive ink was then printed on paper substrate (Xerox Performer A4 Paper 80 gsm), taking advantage of paper's porosity property. After that, the printed antenna was heated up to volatilize the Ethylene Glycol dispersant. Due the high resistance caused by the porous feature of printed graphene layer, a rolling compression was further applied to force well-aligned face-to-face contact of laminated graphene nanoflakes and smoothen the surface of printed graphene conductor [11], and thus contributes to significant improvement of surface current flow and increasement of film conductivity. The thickness of the final printed graphene layer is measured as 19 μm, much lower than graphene's skin depth at our desired frequencies [15].

The SMA connector was finally attached to the feeding point using conductive

epoxy. Fig. 6-1(c) shows the fabricated prototype.

The average sheet resistance of the final prototype, as shown in Fig. 1c, is measured as 1.5 Ω/sq. The conductivity is calculated as3.51×10^4 S/m using (1).

$$\sigma = \frac{1}{R_s t} \tag{6.1}$$

where σ is the conductivity, t is the thickness of the film and R_s is the sheet resistance.

6.3 Results and discussion

6.3.1 Reflection Coefficient Characteristics

Fig. 6-3 shows the comparison of the simulated and measured reflection coefficients of the proposed antenna, the resonant frequencies of the proposed antenna array are 2.4 and 5.8 GHz from the simulation, and 2.15 and 5.4 GHz from the measurement, justifying the design. The small discrepancy in frequency may be caused by the uneven surface produced in fabrication processes and higher than expected sheet resistance of the printed graphene layer.

Its bandwidth ranges, 1.744-2.72 GHz and 3.44–6.26 GHz, can be observed with $|S11| < 10$ dB, supporting both 2.4 GHz and whole coverage of 5 GHz

WiFi and WLAN networks, enhancing the transmission efficiency significantly for point-to-point links than single band antennas.

Table 6-1 Optimized dimensions of the dual band antenna array.

Parameters	**mm**	**Parameters**	**mm**
W	210	gap	4
L	70	fi	5.5
W1	37	sl	19
blw	35	d	24.2
th	10	bl	17
tl	3.82	h1	11.4
tw	12	slw	8.5
tl2	25.13	ssw	5
fw	2	ssl	18.66
w1	21.41		

6.3.2 Far-Field Radiation Characteristics

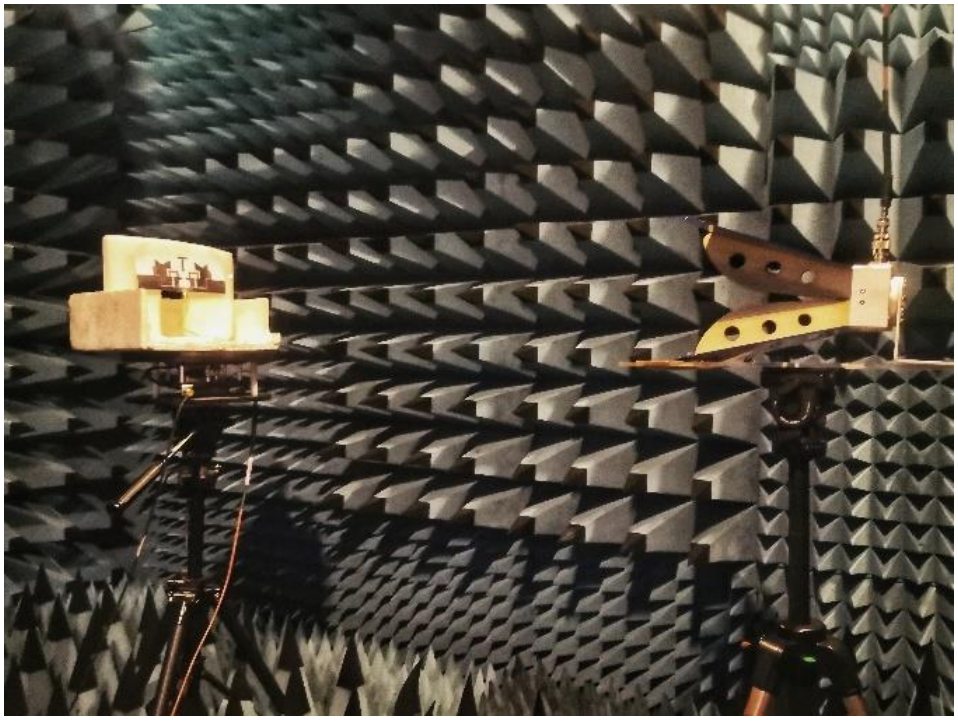

Fig. 6-2. Fabricated prototype measured in the anechoic chamber.

The far-field radiation performance of the proposed dual-band flexible antenna array was observed by measuring the antenna in an anechoic chamber with a calibrated E5071B VNA and a horn antenna connected to the other port, as shown in Fig. 6-2. The gain plotted in Fig. 4 shows a stable performance, above 0 dBi, for both frequency bands of WLAN applications, guaranteeing continuous connectivity. It is also worth mentioning that the peak gain 2.37 dBi and 2.55 dBi occur at 2.05 and 5.06 GHz respectively, close to the expectations from simulation result, obtaining signal reliability. From 2.6-4.8 GHz, the measured gain is remained below 0 dBi, verifying the stopband of the antenna and giving the antenna anti-interference feature in this frequency range. It can also be observed

that the gain from measurement decays faster than simulation result, this is due to more power loss is generated during measurement.

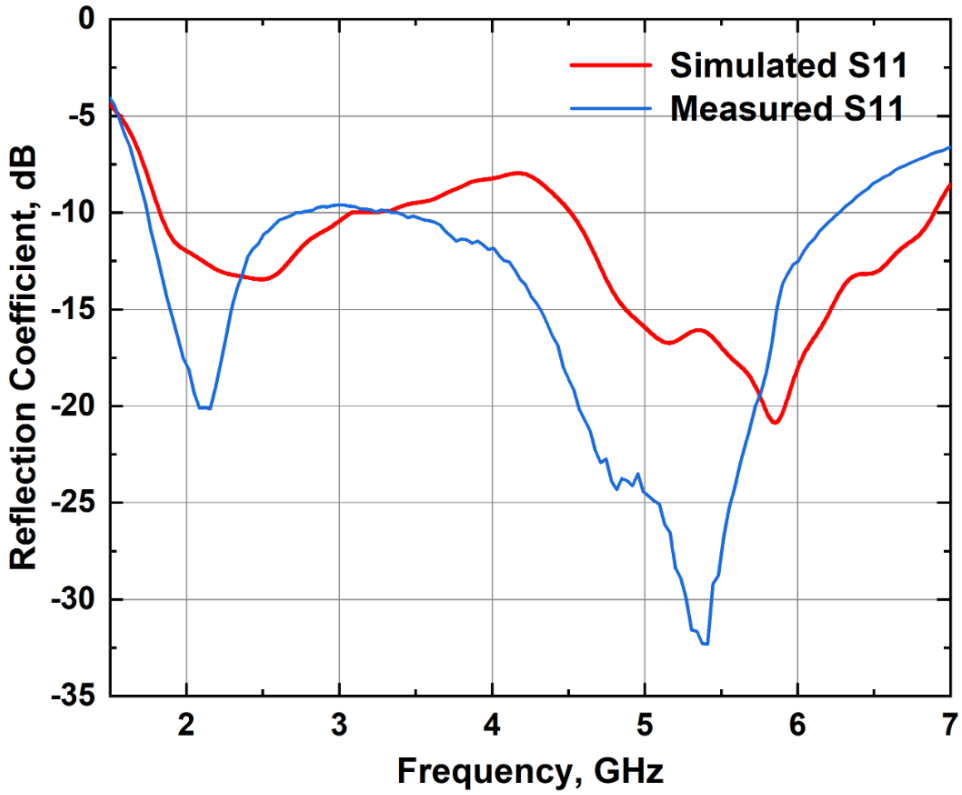

Fig. 6-3. Simulated and measured reflection coefficients of the proposed antenna array.

The measured and simulated far-field radiation patterns at 2.4 GHz and 5.1 GHz are presented in Fig. 6-5 in both E- and H- planes, where an even front and back radiation distribution can be observed. The shapes of the measured radiation patterns agree well with the simulation result. More distortion can be found in 5.1 GHz, as radiations in 5.1 GHz require higher precision of antenna shape than 2.4 GHz.

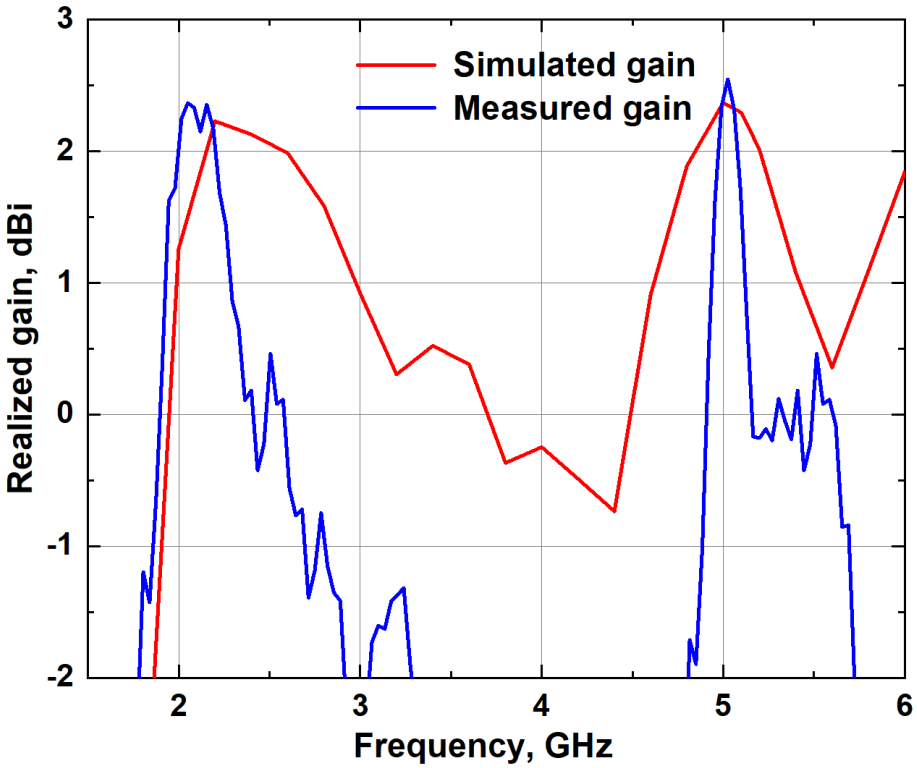

Fig. 6-4. Simulated and measured realized gain of the antenna.

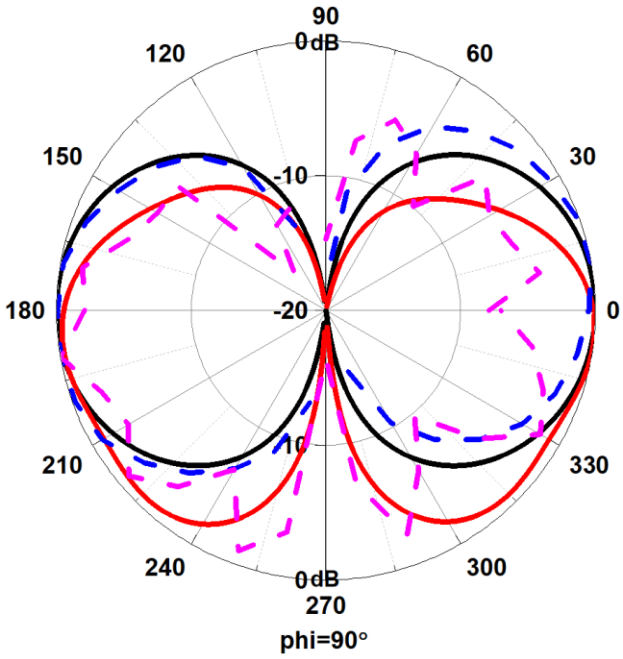

(a)

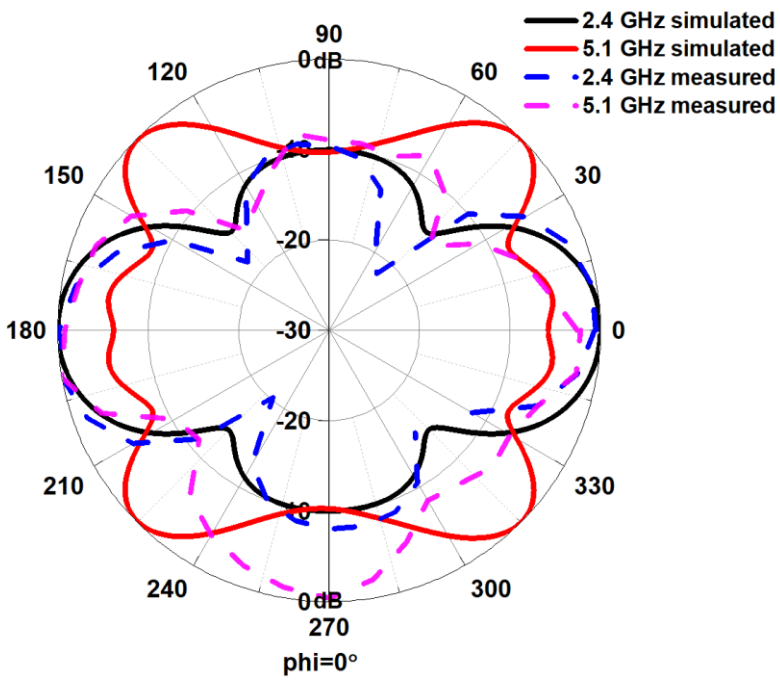

(b)

Fig. 6-5. Simulated and measured far field radiation patterns on different planes at 2.4 and 5.1 GHz: (a) phi = 90°; (b) phi = 0°.

6.4 Conclusion

In this work, a dual-band flexible and disposable printed graphene antenna array, consists of two antenna elements and meandered line structure, is designed, fabricated, and presented. The simulation results verify its multiple wide operating bands and stable gain performance. The flexibility, low-cost and environmental amity of the antenna exhibits its potential in WIFI and WLAN mobile communication applications in both 2.4 GHz and 5 GHz bands, consequently revealing it as a good candidate for high data rate IoE system use, especially for systems require high signal transmission reliability such as health and military monitoring.

References

[1] Z. Zhang, X. Zhang, Z. Xin, M. Deng, Y. Wen and Y. Song, "Synthesis of monodisperse silver nanoparticles for ink-jet printed flexible electronics", *Nanotechnology*, vol. 22, no. 42, p. 425601, 2011. Available: 10.1088/0957-4484/22/42/425601.

[2] W. Whittow et al., "Inkjet-Printed Microstrip Patch Antennas Realized on Textile for Wearable Applications", *IEEE Antennas and Wireless Propagation Letters*, vol. 13, pp. 71-74, 2014. Available: 10.1109/lawp.2013.2295942.

[3] I. M. Graz, D. P. J. Cotton, and S. P. Lacour, "Extended cyclic uniaxial loading of stretchable gold thin-films on elastomeric substrates", *Applied Physics Letters*, Vol. 94, No. 7, Feb. 2009.

[4] K. Novoselov, V. Fal′ko, L. Colombo, P. Gellert, M. Schwab and K. Kim, "A roadmap for graphene", *Nature*, vol. 490, no. 7419, pp. 192-200, 2012. Available: 10.1038/nature11458.

[5] K. Novoselov, "Electric Field Effect in Atomically Thin Carbon Films", *Science*, vol. 306, no. 5696, pp. 666-669, 2004. Available: 10.1126/science.1102896.

[6] L. Ng et al., Printing of Graphene and Related 2D Materials. .

[7] X. Li et al., "Self-reinforcing graphene coatings on 3D printed elastomers for flexible radio frequency antennas and strain sensors", *Flexible and Printed Electronics*, vol. 2, no. 3, p. 035001, 2017. Available: 10.1088/2058-8585/aa73c9.

[8] X. Huang et al., "Highly Flexible and Conductive Printed Graphene for Wireless Wearable Communications Applications", *Scientific Reports*, vol. 5, no. 1, 2015. Available: 10.1038/srep18298.

[9] T. Leng et al., "Printed graphene/WS2 battery-free wireless photosensor on papers", *2D Materials*, vol. 7, no. 2, p. 024004, 2020. Available: 10.1088/2053-1583/ab602f.

[10] P. He et al., "Screen-Printing of a Highly Conductive Graphene Ink for Flexible Printed Electronics", *ACS Applied Materials & Interfaces*, vol. 11, no. 35, pp. 32225-32234, 2019. Available: 10.1021/acsami.9b04589.

[11] K. Pan et al., "Sustainable production of highly conductive multilayer graphene ink for wireless connectivity and IoT applications", *Nature Communications*, vol. 9, no. 1, 2018. Available: 10.1038/s41467-018-07632-w.

[12] S. Jilani, M. Munoz, Q. Abbasi and A. Alomainy, "Millimeter-Wave Liquid Crystal Polymer Based Conformal Antenna Array for 5G Applications", *IEEE Antennas and Wireless Propagation Letters*, vol. 18, no. 1, pp. 84-88, 2019. Available: 10.1109/lawp.2018.2881303

[13] M. E. Atrash, K. Bassem and M. A. Abdalla, "A compact dual-band flexible CPW-fed antenna for wearable applications," *2017 IEEE International Symposium on Antennas and Propagation & USNC/URSI National Radio Science Meeting*, San Diego, CA, 2017, pp. 2463-2464, doi: 10.1109/APUSNCURSINRSM.2017.8073274.

[14] W. K. Toh, X. Qing and Z. N. Chen, "A Planar Dualband Antenna Array," in *IEEE Transactions on Antennas and Propagation*, vol. 59, no. 3, pp. 833-838, March 2011, doi: 10.1109/TAP.2010.2103039.

[15] X. Huang et al., "Highly Flexible and Conductive Printed Graphene for Wireless Wearable Communications Applications", *Scientific Reports*, vol. 5, no. 1, 2015. Available: 10.1038/srep18298.

Chapter 7 A sustainable approach towards Graphene nanoflakes ink production for far field wireless RFID sensing applications

Xinyao Zhou, Ting Leng, Kewen Pan, Yang Liu, Kostya Novoselov, Zhirun Hu

(To be submitted to) ***IEEE Transactions on Industrial Electronics***, 2022

My contributions:

I have performed all the graphene ink preparation and circulations, measured all the ink parameters, calculated and analysed all the data of ink performance, measured and analysed the UHF RFID tag performance and drew all the graphs.

Abstract

A sustainable approach for preparing high conductive screen-printing graphene ink by recycling cellulose solvent has been proposed. The ink uses Cyrene solvent in circulation and produces highly concentrated and conductive graphene ink to conquer the limitation of graphene inks in massive industrial production brought by the very high cost of the cellulose solvents. The concentrated ink can then be formulated and diluted to desired concentration. Systematic study of sheet resistance variation with number of cycles has been carried out. The average conductivity of the ink can achieve 3.032×10^4 S/m, with only 2-hour shear exfoliation applied, which exhibits about the same conductivity of recent works (using toxic NMP solvent, centrifugation, ultrasonication, and high temperature annealing, etc.), but with much simpler fabrication. A recycled ink enabled screen-printed graphene far-field tag antenna is screen printed on paper substrate and integrated with printed Graphene Oxide (GO) and SL900a sensory chip to achieve battery-free wireless UHF RFID far field temperature sensing. The high responsiveness, accuracy and sensitivity of the RFID sensing tag were observed with instantaneous detection, accurate and reliable wireless data transmission. The high conductivity graphene nanoflakes ink allows the screen-printed graphene tag to wirelessly harvest sufficient power from the reader for supplying the sensor IC chip. This work demonstrates a forward-looking approach to producing low-cost sustainable Cyrene graphene inks in which mass production of printed electronics can be achieved, revealing an extremely simple and low-cost industrial manufacturing method that is compatible with flexible substrates.

7.1 Introduction

The implementation of the Internet of Things (IoT) and its extension concept, the Internet of Everything (IoE), stimulated by the 5G and followed by the 6G revolutions, has greatly increased the yield requirements for conformal printed electronics applications including energy storage and conversion, flexible screens, sensors, antennas, optical detectors, electronic paper, radio frequency identification (RFID) tags, and wearable electronics, etc. [1-6]. Intense efforts have been put in developing more time and cost-efficient fabrication process for these flexible printed electronics with lower cost and higher feasibility in order to meet the urge of the blooming market.

The critical property of printed electronics relies on the presence of highly conductive tracks connected to each other. Thus, developing high-performance inks for printing electronics with high conductivity and low cost is therefore very crucial to the implementation of industrial scale printed electronics as a practical manufacture process. A promising electrically conductive ink should address the following requirements: excellent printability, stability over time, low cost, compatible with a range of substrates, and good tolerance of bending and strain.

Efforts have been intensively focused on providing highly conductive metallic nanoparticle inks for the high demanding market. Dispersed silver nanoparticle ink [8-10] has been regarded as a good candidate by researchers for its high conductivity, yet, the high cost of silver severely limits its application, especially where low-cost and sustainable electronics are constantly in dire need. However, the adoption of silver nanoparticle inks entails a sintering process for reinforcing the bonding of the deposit to the substrate and for eliminating undesirable solvents

[11] which strictly limits the selection of heat-sensitive substrates. High conductivity can also be implemented with other commonly used metallic conductive nanoparticle inks such as copper and aluminum [12]. However, using metallic structures, even with minor deformations, could easily result in irreversible cracks and electron transport discontinuities, not to mention the associated costs applied to high temperature annealing for preventing metal oxidation [13].

Of all printable conductive inks that have been developed for industrial manufacturing to date, graphene, with its exceptional characteristics granted by its 2-dimensional crystalline structure [14], such as high current-carrying mobility, conductivity, and strength, as well as its low manufacturing cost, is the most extensively investigated cost-effective and emerging material which is recognized as the promising alternative to metals when it comes to printable flexible electronics. Many methods of fabricating printed graphene have been reported, involving spraying, doctor blading inkjet printing, and screen printing. Since spray coating is not likely to produce a smooth surface of films and doctor blading suffers from a deficiency in pattern precision, inkjet printing and screen printing techniques have been adopted for most jobs [11, 15-20]. At the mass industry level, screen printing is the most extensively investigated and well-established printing technology, supporting a broad range of substrates [21-24], from glass, paper, metals, and textiles to polymers, and providing high precision manufacturing of printed electronics where complex designs are required, greatly enhances the ability to scale up manufacturing production.

Over the past decade, various methodologies have been proposed, reporting

on the synthesis and production of graphene conductive inks. To attain high yields of graphene, liquid phase exfoliation of graphite flakes [25] outperforms other methods such as dispersion and exfoliation of graphene oxide (GO), micro-mechanical cleavage, growing graphene on metals or annealing on Silicon Carbide (SiC) substrates because of its high productivity and ability to preserve the electronic structure of graphene. Exfoliation efficiency is closely correlated with the proportion of the solvent's surface tension component and the surface tension component of the material to be exfoliated [26]. Many compatible solvents have been studied for processing screen-printable graphene inks with good stability and low residual, including N-methyl-2-pyrrolidone (NMP), dimethylformamide (DMF), Cyrene (dihydrolevoglucosenone), water-surfactant solutions and water−IPA mixture [11, 27-31]. However, NMP and DMF solvents can only achieve low concentrations, more importantly, they suffer from high boiling points (>200 °C), and are often toxic [32], hindering their potential in industrial scale electronic applications. Water-based solutions with surfactants and water-IPA mixture could be sustainable alternative preparation methods with low cost, low boiling point and low harm which do not require annealing or chemical post treatments [29-31, 33]. A formulation of producing graphene slurries in aqueous solution with an exceptionally high concentration (50 mg ml^{-1}) and a low shear viscosity (0.064 Pa·s at 50 s^{-1}) has been presented in [33], yet the presence of the graphene flake edge oxidation still diminishes its electrical conductivity. To enable the efficient industrial production of highly conductive graphene inks at high yield, lowering the defect density as well as the degree of oxidation has become a clear demand.

So far, the graphene ink conductivity reported without thermal annealing can

be as high as 7.13×10^4 S m^{-1} with the use of bio-based Cyrene (CAS: 53716-82-8) solvent in a recent work [11], which was extracted from cellulose and first identified as excellent solvent for graphene dispersion in 2017 [34]. The optimization of the processing time and other factors for best performance (highest conductivity) has been investigated. It has been proved that, under the same bath ultrasonication exfoliation treatment, the sheet resistance of graphene laminate processed with Cyrene solvent instantly drops within the first 8 hours, whereas it takes about 20 hours with NMP for reaching the lowest sheet resistance (which is still higher than Cyrene). Thus, Cyrene is of higher cost, but proved a cleaner, environmentally friendly, and even better-performing alternative to hazardous organic solvents for graphene inks due to the particular surface tension and polarity it possesses, as well as the stability it offers at high concentration.

To further eliminate the limitations imposed by the high price and enhance the potential of Cyrene for industrial scale graphene ink production, the cost of solvents must be taken into account, which means that in order to realize substantial usage of Cyrene for large-scale ink production, it is essential that a sustainable approach be taken in order to allow an effective and feasible industrial production to finally be realized.

In this work, a sustainable ink production method is proposed which takes advantage of recycled Cyrene in circulations, The effect of recycled Cyrene on the properties of shear exfoliated graphene nanoflakes ink has been investigated. By recycling the solvent, the high price of Cyrene graphene ink can be greatly reduced by at least a tenth, while maintaining the superior electrical conductivity, defect-free, high concentration, and stability of the resulting graphene ink, enabling the

use of Cyrene in scalable industrial productions. A highly conductive graphene ink enabled printed graphene RFID far-field sensor is developed and tested, demonstrating high responsivity and sensitivity, allowing antenna to withdraw sufficient power wirelessly from the reader to power the sensor IC chip and transmit the data back to the reader. More importantly, we are finally able to bypass the chemical oxidation process of graphene conductive ink production, obviate the necessity of extensive use of toxic solvents, and resolve the critical issues associated with sustainable industrial use.

7.2 Material Preparation and Characteristics

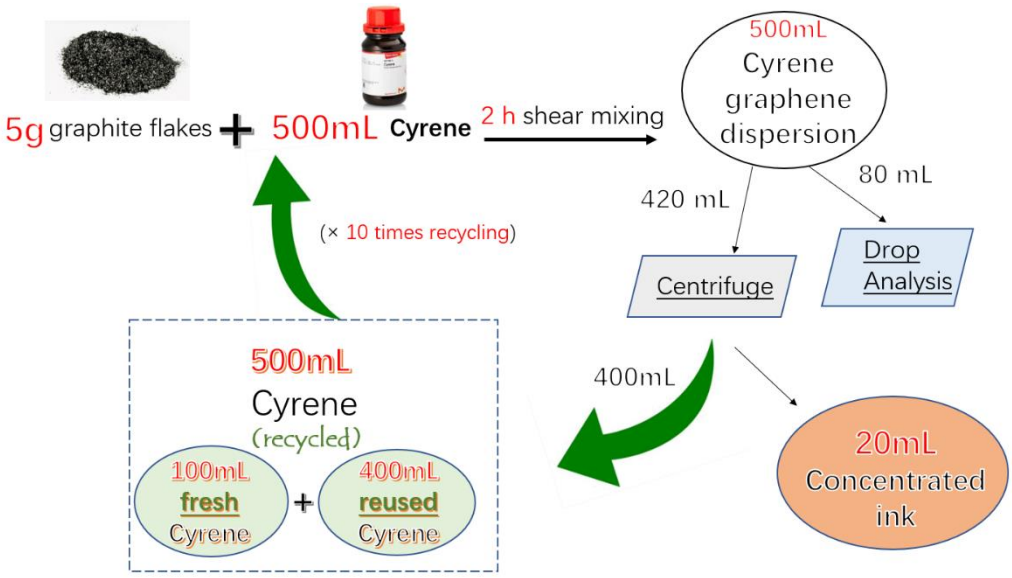

Fig. 7-1. The sustainable method to allow large-scale graphene ink dispersed in Cyrene solvent. 10 cycles have been performed and tested in this work.

By adding expandable graphite into Cyrene solvent and using only shear exfoliation, high-quality graphene nanoflakes were obtained. In our previous work, the ultrasonication exfoliation time of the graphene ink prepared using Cyrene solvent was examined and proved a much more efficient and time-saving method in comparison with NMP [11]. However, to implement large-scale ink production, the expense of solvents is an inevitable concern in the case of high-volume production of inks involving Cyrene. In this work, Cyrene was recycled and reused for 10 circulations, the exfoliated flakes produced after each cycle were sampled and further investigated for characterization. Furthermore, to further reduce the cost and achieve great sustainability in fabrication process, only shear mixing (2 hours) was used for exfoliation.

In order to prepare graphene inks, an amount of 5 g of expandable graphite flakes (purchased from Sigma-Aldrich) with the flake size >50 mesh (a -50 mesh powder has the size of particles that measure less than 297 microns) was slowly added to 500 mL Cyrene (dihydrolevoglucosenone, >99%, Circa Group Pty Ltd). The shear mixing process was then implemented with a modified shear mixer (L4R, Silverson) with square hole high shear screen, which sheared each sample 2 hours with 8000 RPM. A water-cooling system was applied to keep the temperature at 10 ℃. After that, the 500 mL dispersion was transferred into test tubes. As shown in Fig. 7-1, an 80 ml sample was extracted at each cycle to perform drop analysis so to investigate the ink's properties. The remaining 420 mL was proceeded to centrifugation at 12,000 rpm with the temperature being maintained at 10 ℃ for an hour. After centrifugation, the upper layer supernatant of the mixture should appear translucent yellow towards light, whereas the bottom layer is the dark concentrated ink. The 400 mL upper layer was then collected and poured into a clean glass bottle for the next cycle of Cyrene use, where 100 mL fresh Cyrene and 5 g graphite flakes were added to the circulation. The whole process was repeated for 10 times, with a usage of 1400 mL of Cyrene solvent only, while by conventional method, it will need about 6 L, reducing the amount of Cyrene usage by 76.67%.

After filtering the extracted ink samples through a 300-mesh stainless steel screen, 100 μL of the collected sample was dropped onto a filter paper (Whatman qualitative filter paper, Grade 5) which was placed on a glass funnel (140 mL Aldrich Buchner funnel), vacuum pumped in order to prevent the coffee ring effect. Following this, the filter papers were annealed in an oven for 6 h (160 °C) and compressed with a hydraulic compressor (Durston, DRM SS F130) with constant

strength.

The sheet resistance for each sample is obtained by measuring 6 different positions in the middle of the dropping area using a four-point probe station (Jandel, RM3000) and semiconductor characterization system (Keithley, 4200C). 6 printed samples were measured for each cycle. Scanning electron microscopy (SEM, MIRA3 TESCAN) was conducted for the 1st, 5th and 10th cycle to specifically visualize the surface and cross sections of the graphene sheet in order to allow detailed observation of the thickness of the printed layers and the sizes of the flakes after compression. As shown in Fig. 7-2, the SEM surface topology of the graphene laminate samples for the three cycles are presented with 10 k × magnification, with the 1 μm scale bar labeled for better observation.

It can be seen that after the completion of the 1st cycle, the flakes are of relatively bigger size comparing with the 5th and the 10th cycles, a more porous stacking structure can also be observed from the surface, resulting in degradation of the contact between flakes. Around the interspaced pores, the flow of current between the graphene flakes is directed to their tips and edges, giving rise to a potentially higher sheet resistance. After the 5th cycle, a smooth surface was attained (Fig. 7-2 (b)), which implies that a better overall stacking was obtained with the aid of the thinner and smaller flakes that were retained in the recycled Cyrene solvent during the past few cycles, acting as a connection between the large flakes. The flakes of larger size serve as the backbone, while the smaller pieces fill the voids. In Fig. 7-2 (c), after 10 cycles, a significant increase in the number of flakes with smaller size can be spotted, and the surge of such flakes would eventually lead to a massive increase in the interconnecting contacts between the

flakes, thus raising the sheet resistance.

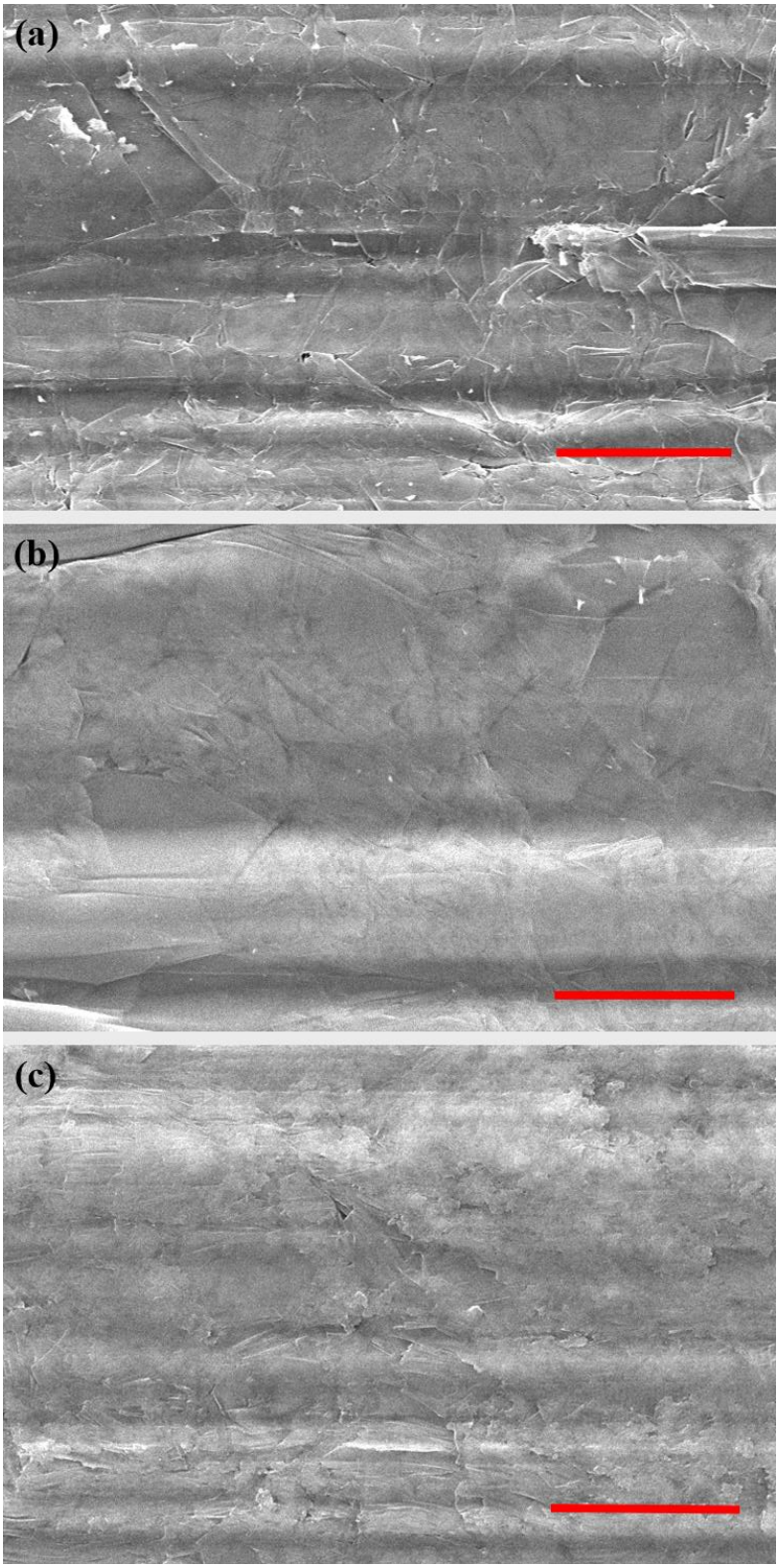

Fig. 7-2 SEM images of the surfaces of screen-printed graphene laminates (after compression) a) after the 1st, b) 5th, and c) 10th cycle with 10k × magnification; the scale bar labeled is 1 μm long.

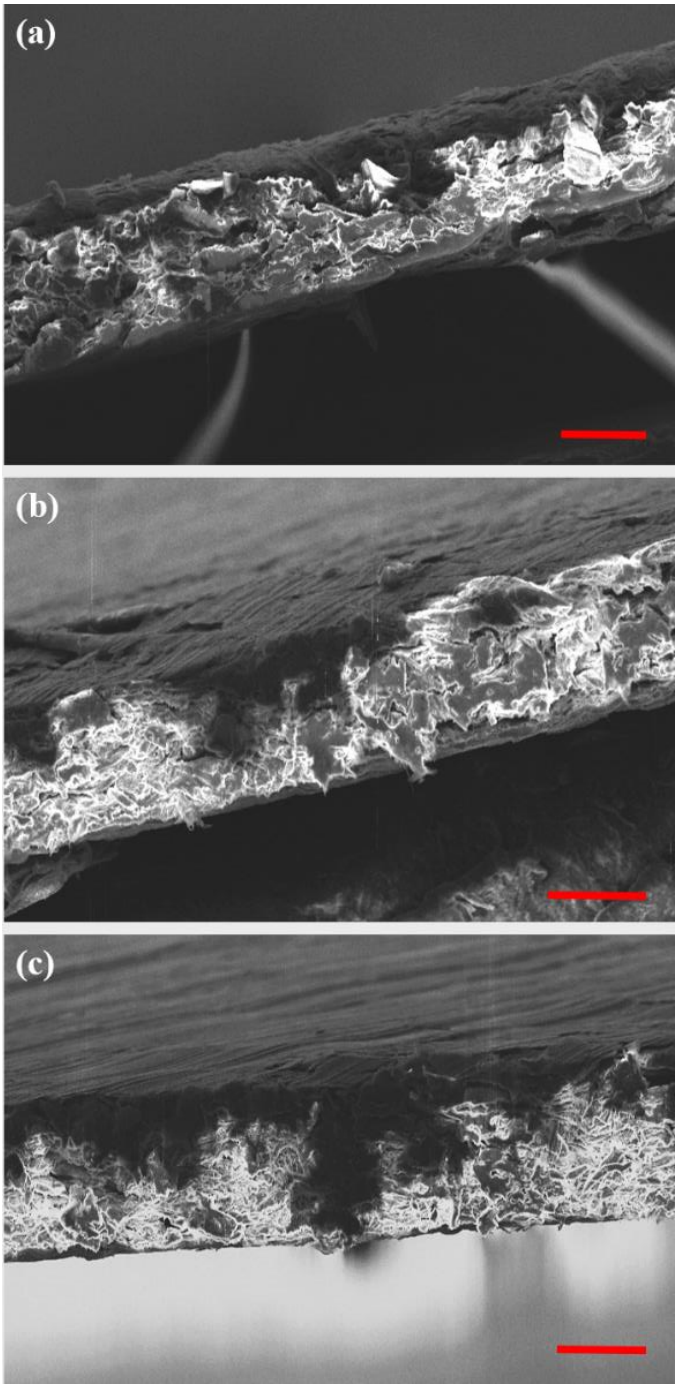

Fig. 7-3. The cross-section SEM images of the screen-printed graphene laminates (after compression) a) after the 1st, b) 5th, and c) 10th cycle with 500 X magnification; the scale bar labeled is 50 µm long.

The thickness of the printed laminates was determined by taking the average of measurements at 10 different locations on the cross-sectional SEM view of the compressed graphene sheets of each cycle. Fig. 7-3 displays the magnified SEM images of the 1st, 5th and 10th cycle conductive sheet samples with 500 x magnification. The average thickness of the 1st, 5th and 10th cycle samples are 62.12 μm, 53.2 μm and 69.6 μm. More condensed stacking can be observed in Fig. 7-3 (c), however, the increase of interfaces can contribute to higher resistance/thickness.

To evaluate the conductivity of the inks made in different recycling runs, the variation of the graphene sheet resistance is plotted in Fig. 7-4 with the fitted linear regression lines for standard errors. As shown in the plot, the sheet resistance of the samples decreases rapidly within the first 5 cycles. The lowest sheet resistance 0.624 Ω/sq appears at the 5th cycle, manifesting the previous assumption that best conductivity can be achieved by certain amount of smaller flakes filling in the void, establishing better interconnecting interfaces and allowing more fluent current flow.

The sheet resistance exhibits a tendency to rise at a fast rate between cycle 5 and cycle 7 since the longer shear mixing time leads to even smaller flake size, which induces a great increase in number of interfaces between graphene flakes. In addition, hydrodynamic processes can damage the graphene basal plane after long processing time, bringing down the conductivity of graphene flakes. After performing the loop for 7 times, a relatively steady state has occurred at around 0.79 Ω/sq, which indicates a balance between the rising trend of resistance brought by the increase of interfaces and the filling of gaps by smaller thin flakes. The

variation of the sheet resistance ranges from 0.967 Ω/sq to 0.624 Ω/sq for 10 recycling runs, indicating that the Cyrene can be recycled for graphene exfoliation to produce highly conductive graphene inks. The conductivity of the samples can be calculated using equation (7.1).

$$\sigma = \frac{1}{R_s t} \tag{7.1}$$

where R_s is the sheet resistance and t is the thickness of the sample.

For the 1st, 5th, and 10th cycles, the conductivity features 1.665, 3.032, and 1.866 $\times 10^4$ S/m respectively.

After ink fabrication and characterization, screen printing was carried out. Through exposing capillary films (ULANO, EZ50-Orange) on an exposure machine with a vacuum pressure regulation valve, a 24T mesh printing screen with a negative patterned antenna shape was prepared in advance. The developed ink was then screen printed on paper substrate using a semiautomatic screen printer (YICAI4060DV) with the assist of a slant squeegee moving at a chosen constant speed. Several parameters are decisive for sufficient ink depositing and hence lowering the sheet resistance, including the speed of the slant squeegee (50–100 mm s^{-1}), the angle of inclination of the squeegee (70°), the number of layers of the exposing capillary film (ULANO, EZ50-Orange) (4 layers in this work), and the mesh number of the selected screen (higher mesh contributes to higher resolution yet it impedes the ink from depositing). The final improvement of conductivity is done by rolling compression, which can greatly reduce the sheet resistance to its tenths [36], as seen in the SEM image in Fig. 7-2, graphene nanoflakes forming well-aligned laminated structure with face-to-face contact, allowing good flow of

surface current.

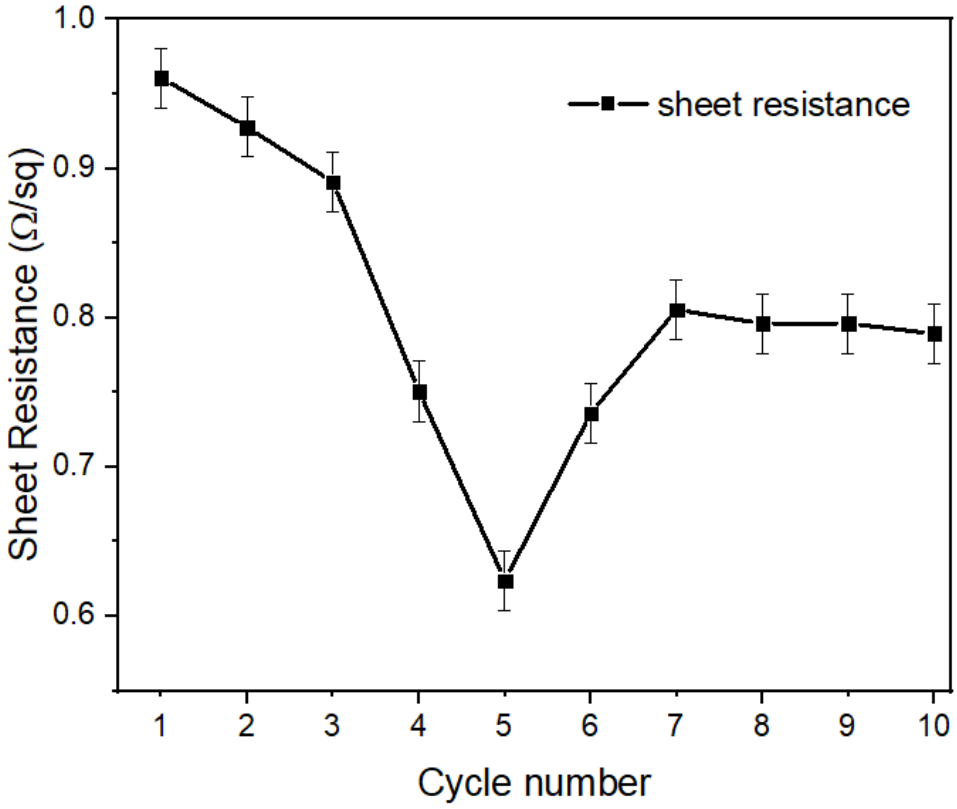

Fig. 7-4. Sheet resistance (Ω/sq) variation with increasing cycle numbers (measured 6 times per sample, 6 samples per point).

7.3 Recycled Cyrene Graphene Ink Printed Battery-Free Wireless UHF RFID Sensory Tag on Paper Substrate

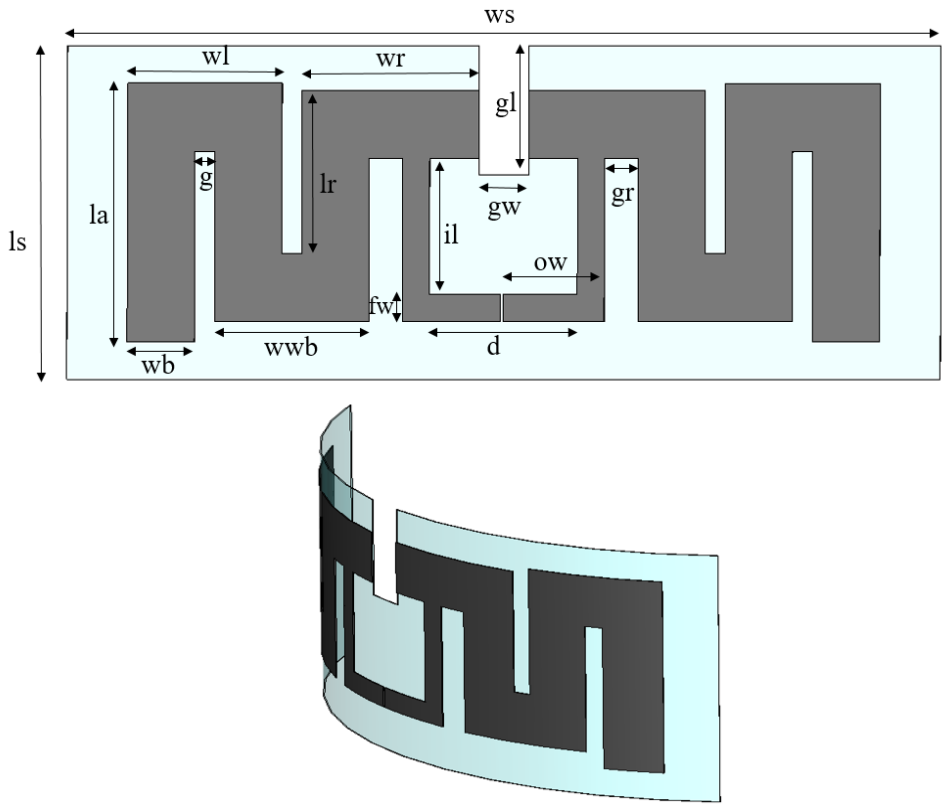

Fig. 7-5. Geometry of the proposed printed graphene UHF RFID tag on paper substrate.

The passive ultra-high frequency (UHF) RFID technology, operating at 860 MHz-960 MHz, has a long read range and throughput, allowing readability through a broad range of materials, and is extremely cost-effective, making it the most prevalent technology in all industries. For UHF RFID operations at ~900 MHz applications, the skin depth is about 80 μm. To prove the usability of the conductive ink, the prepared recycled Cyrene graphene ink has been used to produce far-field UHF RFID antennas on paper substrate. The layout of the

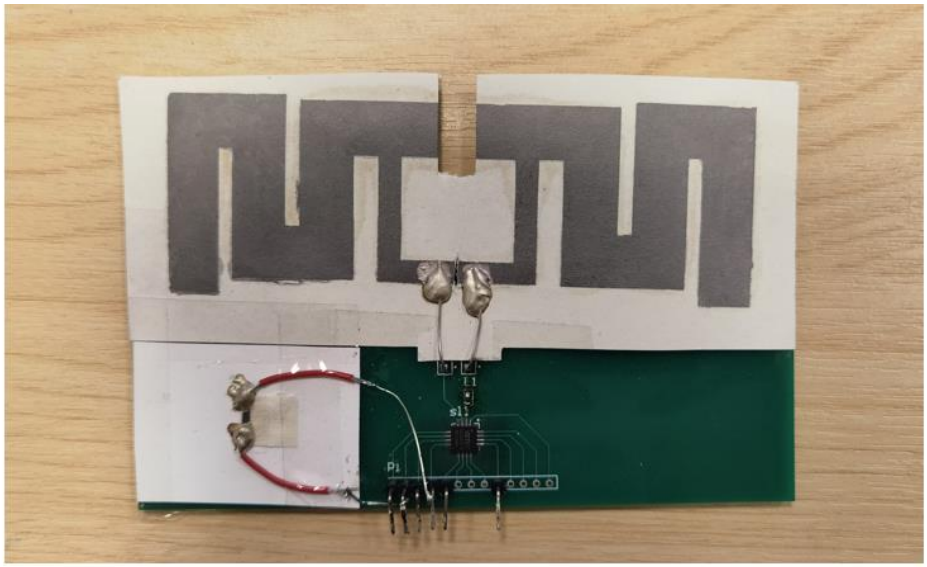

Fig. 7-6. The proposed tag antenna is integrated with an SL900A sensory chip on the designed PCB board to sense temperature and backscatter signals to readers.

designed tag is shown in Fig. 7-5, the pattern is used in the screen patterning in screen printing fabrication process.

The antenna is composed of a rectangular feeding loop and a meandered line radiating body with a size of 130 mm × 49 mm. CST Microwave Studios was used for the far-field tag antenna simulation [32]. The process can be briefly descripted as: the signal generator delivers a continuous wave, which travels through the circulator and is in turn emitted by the reader antenna. Then the tag antenna receives the power from the incident electromagnetic wave. This energy is utilized to power up the tag and activates its embedded RFID chip, which can further modulate the signal and backscatter it to the reader antenna. In order to design the antenna with optimal performance, a parametric study of the tag geometry has been performed and numerical analysis has been carried out. The printed graphene tag antenna was simulated under different geometrical parameters, involving number of turns of the meandered line, widths of the radiators, distance of the adjacent

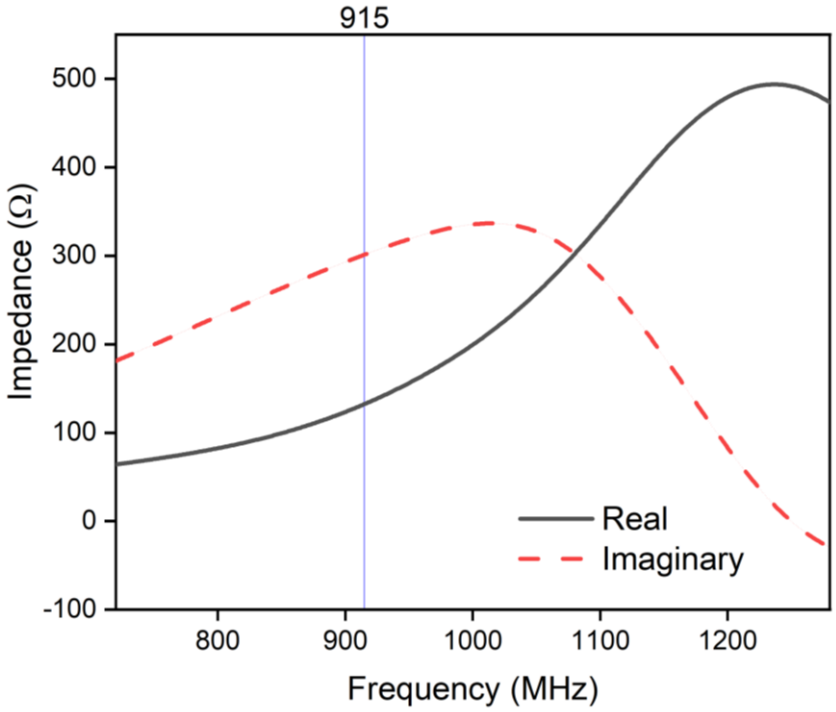

Fig. 7-7. The impedance variation with frequency of the tag. Conjugate match is achieved at 915 MHz.

structures, and dimensions of the middle gap, etc. The real and imaginary parts of the tag impedance at different frequencies can be obtained from the simulation. The printed graphene was modelled as ohmic sheet with a sheet resistance of 1.5 Ω/sq. The tag was then connected to SL900A sensory tag chip (AMSCO) for automatic data logging, as shown in Fig. 7-6. The chip is powered wirelessly by the RFID reader and contains a fully integrated temperature sensor with a temperature range from -29°C to +58°C.

To allow maximum power transfer to the chip, the input impedance of the antenna is designed to match the complex conjugate value of the chip input impedance. The detailed dimensions of the tag after optimization for the best conjugately matched performance are given in Table 7-1. The chip has a sensitivity threshold of -6.9 dBm, an impedance of (123-j303) Ω at 915 MHz, operating from 860-960 MHz, also features an accuracy of ±0.5 ℃ [37]. The impedance of the

optimized antenna at 915 MHz is achieved at (132.4+j301.3) Ω, as shown in Fig. 7-7, close to the conjugate match of the chip impedance.

In free space, the electromagnetic radiation that is incident on the RFID tag antenna has a power density (S) given by

$$S = \frac{P_t G_t}{4\pi r^2} \tag{7.2}$$

where P_t is the transmitted power, G_t is the power gain of the transmitting reader antenna, and r is the distance between the reader and tag antennas.

The minimum power needed to activate the tag can be expressed as [35]:

$$P_{tag} = \frac{P_{th}}{\tau G_r} = [P_t - L_{cable} + G_t - FSPL]_{dB} \tag{7.3}$$

where G_r is the gain of the antenna, P_{th} is the threshold of the power required to activate the embedded RFID chip, $FSPL$ is the free space loss , L_{cable} is the cable loss, τ is the matching factor, which has a range of $0 \leq \tau \leq 1$ and is 1 when the tag antenna and chip are perfectly matched.

Minimum power can be determined simply by raising the transmission power level to the point where the reader antenna is able to receive the backscattered signal generated from the tag.

The theoretical maximum reading range R_{max} of the tag directly relates to the EIRP (Effective Isotopically Radiated Power) as well as the minimum transmitted power required to activate the tag.

$$R_{max} = \sqrt{\frac{P_{max,EIRP}}{P_{tag}}} \cdot \frac{c}{4\pi f} \tag{7.4}$$

The radiation performance of the graphene RFID antenna at 915 MHz was measured by rotating the antenna in a step of 20° in both x- and y-planes, at the same time recording the backscattered power using calibrated Voyantic

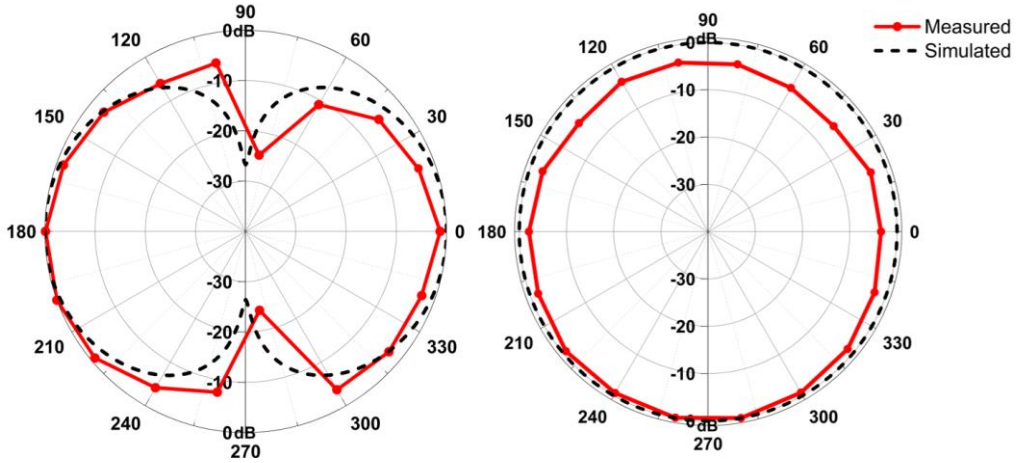

Fig. 7-8. Measured and simulated far-field RFID antenna radiation power density patterns in xz- (left) and yz- (right) planes.

Tagformance measurement system (with EIRP of 4 W), then normalized with the maximum received power. The RFID reader involves a signal generator, a transmitter, a power detector, and a receiver. The antenna was fixed at a distance of 26 cm (in far field region) with an adjustable foam holder and a rotatable holder with an embedded protractor and a pointer made of PET (Polyethylene Terephthalate) substrate.

The Tagformance measurement system employs a variable power output that sends a signal that activates the tag and measures the backscattered power from the tag. In Fig. 7-8, a similar radiation patterns to that of a dipole antenna can be observed from the measurements. The antenna is omnidirectional in the xz-plane and weakly directional in the yz-plane, verifying effective radiation of the printed RFID tag. Only small discrepancy can be observed from the comparison of

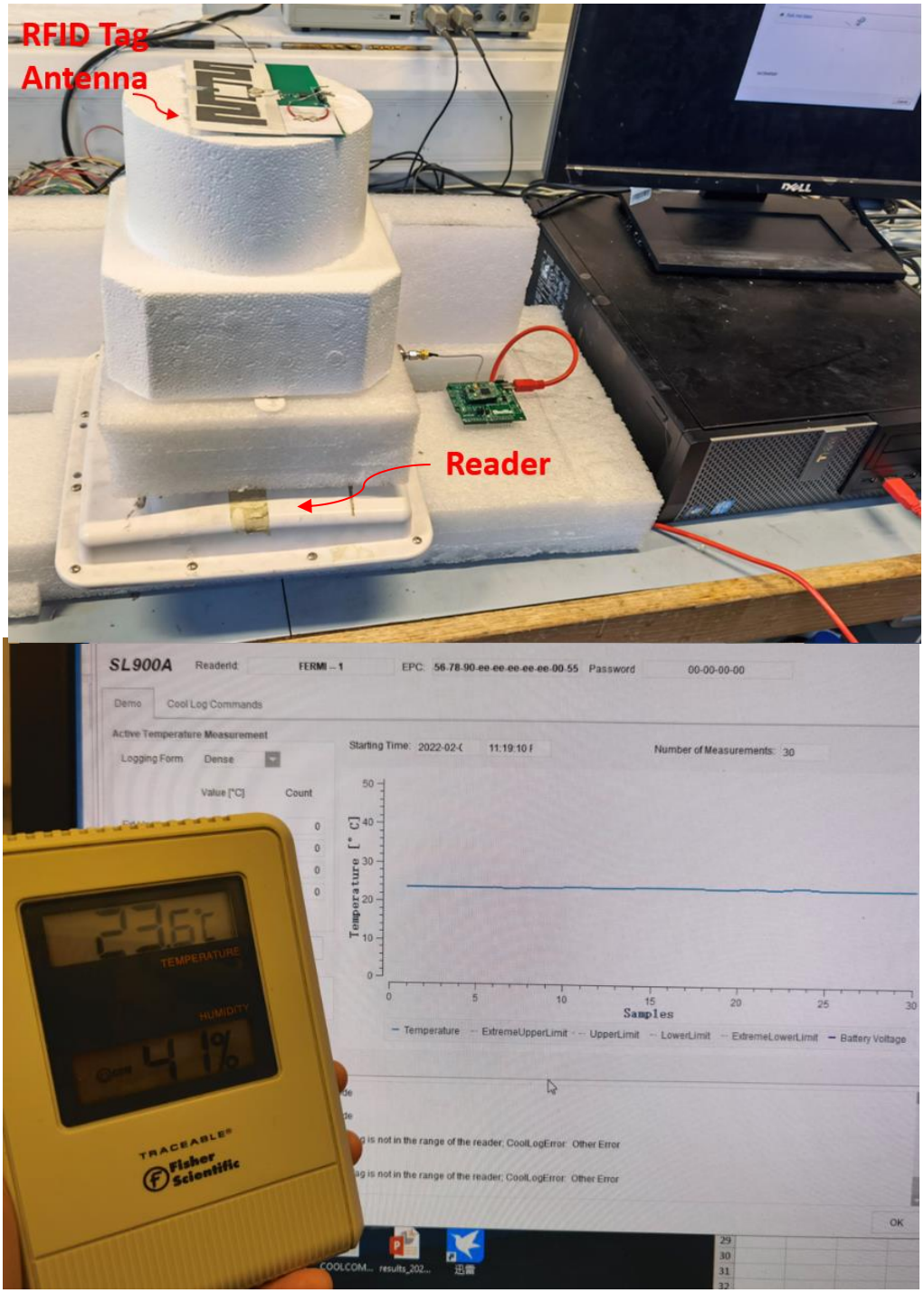

Fig. 7-9. Measurement setup for RFID tag performance test. A commercial thermometer was used for comparison, showing temperature values similar to those of the results of the RFID tag.

simulated results and measured results in both planes, which may be affected by the conductive epoxy which connects the tag to the chip, the uneven surface of the

printed graphene laminate, and the influence of angular position deviation.

For estimating the reading range, frequency was swept from 860 MHz to 960 MHz in a step of 5 MHz. By increasing the input power in a step of 0.1 dBm, the minimum transmitted power for powering up the tag can be obtained. With 4 W maximum radiated power, the maximum read range is calculated using (4). The maximum read range of the tag is 42.09 cm at 865 MHz. The printed graphene RFID tag antenna has a steady read range above 20 cm in the whole RFID band, showing its satisfactory behavior for RFID signal transmission.

The sensing performance of the proposed sensory tag was tested by taking the average value of 30 indoor temperature samples every 20 minutes from 13:00 to 17:00 in British winter time, as shown in Fig. 9. ST25RU3993 Reader Suite was used to measure the tag performance by recording the received backscattered signals and demodulating them, which provides multi-protocol support for the 840-960 MHz UHF communications and shows the processed data on the corresponding software. Another set of data was obtained from a commercial thermometer at the same time as the ongoing test of the sensor. The performance of the tag has been characterized in the far field by fixing the position of the reader and the sensor tag with a distance of 25 cm and orientation in the orientation of maximum gain. Two foam holders with low permittivity and loss were used to separate the RFID sensor and the reader.

The results acquired from the sensors were then compared with the results measured with the commercial thermometer. ~320 read count can be achieved in 20 seconds. Similar values of temperature change over the hours can be observed, as demonstrated in Fig. 9, with a maximum absolute error of 0.7 ºC, highly consistent with the temperature sensory accuracy of ± 0.5 ºC stated in the

datasheet of the chip, showing excellent sensitivity and valid performance of the graphene printed tag. The obvious change in temperature over time illustrates prompt response of the RFID sensor antenna, providing strong evidence of instantaneous detection, accuracy, and reliable wireless data transmission, verifying the promising potential of graphene printed electronics in terms of extremely low-cost, industrial scale, and fully sustainable wireless sensing IoT applications.

Table 7-1. Optimized dimensions of the designed RFID tag.

Parameters	**mm**	**Parameters**	**mm**
ws	130	wr	26.3
ls	49	fw	4
la	38	gw	7.4
wb	10	ow	15
wwb	23	d	22
wl	23	gl	19
g	3	gr	5
lr	24		

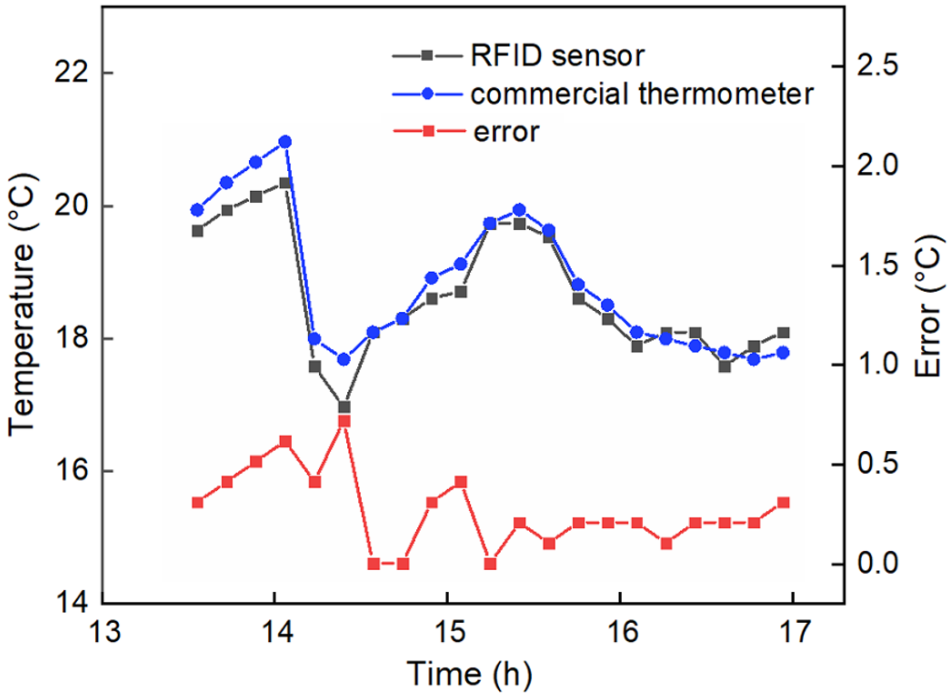

Fig. 7-10. Graphene printed UHF RFID tag temperature sensing performance compared with a commercial thermometer.

7.4 Conclusion

This proposed sustainable method based on recent research about highly conductive (7.13×10^4 S m^{-1}) and stable Cyrene graphene ink has brought the graphene ink industrial production to the next level by investigating the feasibility of Cyrene ink circulation method and the change in sheet resistance after every shear exfoliation operation cycle. By using this sustainable method, the severe limitations brought by the very high price of Cyrene can be eliminated by reusing the ink after centrifugation, separating the supernatant liquid and the highly concentrated graphene slurry. It has been proved that, with an increasing cycle number, the sheet resistance decreases within the first 5 cycles until reaching the lowest sheet resistance 0.624 Ω/sq, then rises to a steady state 0.79 Ω/sq, indicating

a balance between the rising trend of resistance brought by the increase of interfaces and the declining trend caused by filling of gaps by small thin flakes can be achieved in the end. The small change in sheet resistance of this method demonstrates that recycling Cyrene can be used for large-scale industrial production of flexible electronic devices from MHz to tens of GHz. To prove the industrial applications, a recycled Cyrene graphene ink printed battery-free wireless UHF RFID temperature sensing tag on flexible paper substrate has been successfully realized and tested. Its reliability, sensitivity, low cost and easy manufacture demonstrate a promising future of this technique for industrial use. It is conceivable that with this sustainable technology, printed graphene electronics can play a significant role in applications where massive production and high performance are urgently needed, such as soft robotics, bio-medical systems, wearable devices, and structural health monitoring systems.

References

[1] D. Anagnostou, A. Gheethan, A. Amert and K. Whites, "A Direct-Write Printed Antenna on Paper-Based Organic Substrate for Flexible Displays and WLAN Applications", *Journal of Display Technology*, vol. 6, no. 11, pp. 558-564, 2010. Available: 10.1109/jdt.2010.2045474.

[2] F. Aieta, P. Genevet, M. Kats and F. Capasso, "Aberrations of flat lenses and aplanatic metasurfaces", *Optics Express*, vol. 21, no. 25, p. 31530, 2013. Available: 10.1364/oe.21.031530.

[3] S. Zhao and R. Zhu, "Electronic Skin: Electronic Skin with Multifunction Sensors Based on Thermosensation (Adv. Mater. 15/2017)", *Advanced Materials*, vol. 29, no. 15, 2017. Available: 10.1002/adma.201770099.

[4] A. Ono, M. Takishita, M. Sumiyoshi and V. Mizeikis, "Laser Induced Photoreduction for Metal Based Flexible Transparent Electrode", *Proceedings of the International Display Workshops*, p. 939, 2020. Available: 10.36463/idw.2020.0939.

[5] Hu L, Hecht DS, Gruner G. Carbon nanotube thin films: fabrication, properties, and applications. Chem Rev 2010;110:5790–844.

[6] C. Huo, Z. Yan, X. Song and H. Zeng, "2D materials via liquid exfoliation: a review on fabrication and applications", *Science Bulletin*, vol. 60, no. 23, pp. 1994-2008, 2015. Available: 10.1007/s11434-015-0936-3

[7] I. M. Graz, D. P. J. Cotton, and S. P. Lacour, "Extended cyclic uniaxial loading of stretchable gold thin-films on elastomeric substrates",*Applied Physics Letters,* Vol. 94, No. 7, Feb. 2009.

[8] D. Anagnostou, A. Gheethan, A. Amert and K. Whites, "A Direct-Write Printed Antenna on Paper-Based Organic Substrate for Flexible Displays and WLAN Applications", *Journal of Display Technology*, vol. 6, no. 11, pp. 558-564, 2010. Available: 10.1109/jdt.2010.2045474.

[9] H. Khaleel, H. Al-Rizzo, D. Rucker and S. Mohan, "A Compact Polyimide-Based UWB Antenna for Flexible Electronics", *IEEE Antennas and Wireless Propagation Letters*, vol. 11, pp. 564-567, 2012. Available: 10.1109/lawp.2012.2199956.

[10] N. Riaz, M. Faheem and A. Riaz, "Surfactant-modified silver nanoparticle ink for high-resolution ink-jet printed narrow-gaped organic electrodes", *Materials Express*, vol. 7, no. 2, pp. 113-122, 2017. Available: 10.1166/mex.2017.1354.

[11] K. Pan et al., "Sustainable production of highly conductive multilayer graphene ink for wireless connectivity and IoT applications", Nature Communications, vol. 9, DOI 10.1038/s41467-018-07632-w, no. 1, 2018.

[12] A. Rida, L. Yang, R. Vyas and M. M. Tentzeris, "Conductive Inkjet-Printed Antennas on Flexible Low-Cost Paper-Based Substrates for RFID and WSN Applications," in *IEEE Antennas and Propagation Magazine*, vol. 51, DOI 10.1109/MAP.2009.5251188, no. 3, pp. 13-23, June 2009.

[13] T. Campbell, R. Kalia, A. Nakano, P. Vashishta, S. Ogata and S. Rodgers, "Dynamics of Oxidation of Aluminum Nanoclusters using Variable Charge Molecular-Dynamics Simulations on Parallel Computers", *Physical Review Letters*, vol. 82, no. 24, pp. 4866-4869, 1999. Available: 10.1103/physrevlett.82.4866.

[14] K. Novoselov, V. Fal′ko, L. Colombo, P. Gellert, M. Schwab and K. Kim, "A roadmap for graphene", *Nature*, vol. 490, DOI 10.1038/nature11458, no. 7419, pp. 192-200, 2012.

[15] X. Huang, T. Leng, T. Georgiou, J. Abraham, R. Nair, K. S. Novoselov, and Z. Hu, “Graphene oxide dielectric permittivity at GHz and its applications for wireless humidity sensing,” *Scientific reports*, vol. 8, no. 1, p. 43, 2018.

[16] X. Huang et al., "Highly Flexible and Conductive Printed Graphene for Wireless Wearable Communications Applications", *Scientific Reports*, vol. 5, DOI 10.1038/srep18298, no. 1, 2015.

[17] T. Leng et al., "Printed graphene/WS2 battery-free wireless photosensor on papers", *2D Materials*, vol. 7, DOI 10.1088/2053-1583/ab602f, no. 2, p. 024004, 2020.

[18] T. Leng, X. Huang, K. Chang, J. Chen, M. Abdalla and Z. Hu, "Graphene Nanoflakes Printed Flexible Meandered-Line Dipole Antenna on Paper Substrate for Low-Cost RFID and Sensing Applications", *IEEE Antennas and Wireless Propagation Letters*, vol. 15, DOI 10.1109/lawp.2016.2518746, pp. 1565-1568, 2016.

[19] P. Pataniya and C. Sumesh, "WS2 Nanosheet/Graphene Heterostructures for Paper-Based Flexible Photodetectors", *ACS Applied Nano Materials*, vol. 3, DOI 10.1021/acsanm.0c01276, no. 7, pp. 6935-6944, 2020.

[20] A. Capasso, A.E. Del Rio Castillo, H. Sun, A. Ansaldo, V. Pellegrini, F. Bonaccorso, “Ink-jet printing of graphene for flexible electronics: An environmentally-friendly approach”, *Solid State Communications*, vol 224, DOI 10.1016/j.ssc.2015.08.011, pp 53-63, ISSN 0038-1098, 2015.

[21] J. Metters, R. Kadara and C. Banks, "Fabrication of co-planar screen printed microband electrodes", *The Analyst*, vol. 138, DOI 10.1039/c3an00268c, no. 9, p. 2516, 2013.

[22] M. Li, Y. Li, D. Li and Y. Long, "Recent developments and applications of screen-printed electrodes in environmental assays—A review", *Analytica Chimica Acta*, vol. 734, DOI 10.1016/j.aca.2012.05.018, pp. 31-44, 2012.

[23] W. Hyun, E. Secor, M. Hersam, C. Frisbie and L. Francis, "High-Resolution Patterning of Graphene by Screen Printing with a Silicon Stencil for Highly Flexible Printed Electronics", *Advanced Materials*, vol. 27, DOI 10.1002/adma.201404133, no. 1, pp. 109-115, 2014.

[24] L. Ng et al., *Printing of Graphene and Related 2D Materials*, SPRINGER, DOI 10.1007/978-3-319-91572-2, 2018.

[25] A. Alaferdov, A. Gholamipour-Shirazi, M. Canesqui, Y. Danilov and S. Moshkalev, "Size-controlled synthesis of graphite nanoflakes and multi-layer

graphene by liquid phase exfoliation of natural graphite", *Carbon*, vol. 69, pp. 525-535, 2014. Available: 10.1016/j.carbon.2013.12.062.

[26] V. Nicolosi, M. Chhowalla, M. Kanatzidis, M. Strano and J. Coleman, "Liquid Exfoliation of Layered Materials", *Science*, vol. 340, no. 6139, 2013. Available: 10.1126/science.1226419.

[27] A. Najafabadi and E. Gyenge, "High-yield graphene production by electrochemical exfoliation of graphite: Novel ionic liquid (IL)–acetonitrile electrolyte with low IL content", *Carbon*, vol. 71, pp. 58-69, 2014. Available: 10.1016/j.carbon.2014.01.012.

[28] A. O'Neill, U. Khan, P. Nirmalraj, J. Boland and J. Coleman, "Graphene Dispersion and Exfoliation in Low Boiling Point Solvents", *The Journal of Physical Chemistry C*, vol. 115, no. 13, pp. 5422-5428, 2011. Available: 10.1021/jp110942e.

[29] S. Vadukumpully, J. Paul and S. Valiyaveettil, "Cationic surfactant mediated exfoliation of graphite into graphene flakes", *Carbon*, vol. 47, no. 14, pp. 3288-3294, 2009. Available: 10.1016/j.carbon.2009.07.049.

[30] S. Łoś, L. Duclaux, L. Alvarez, Ł. Hawełek, S. Duber and W. Kempiński, "Cleavage and size reduction of graphite crystal using ultrasound radiation", *Carbon*, vol. 55, pp. 53-61, 2013. Available: 10.1016/j.carbon.2012.12.005.

[31] T. Leng et al., "Screen-Printed Graphite Nanoplate Conductive Ink for Machine Learning Enabled Wireless Radiofrequency-Identification Sensors", *ACS Applied Nano Materials*, vol. 2, no. 10, pp. 6197-6208, 2019. Available: 10.1021/acsanm.9b01034.

[32] D. Systèmes 2019 CST Microwave Studios 2017 (Vélizy-Villacoublay: Dassault Systèmes)

[33] L. Dong et al., "A non-dispersion strategy for large-scale production of ultra-high concentration graphene slurries in water", *Nature Communications*, vol. 9, no. 1, 2018. Available: 10.1038/s41467-017-02580-3.

[34] H. Salavagione et al., "Identification of high performance solvents for the sustainable processing of graphene", *Green Chemistry*, vol. 19, no. 11, pp. 2550-2560, 2017. Available: 10.1039/c7gc00112f.

[35] K. Pan, L. Teng, L. Ting, **X. Zhou**, A. Stokes and Z. Hu, "Soft Wireless Battery-free UHF RFID Stretchable Sensor based on Microfluidic Technology", *IEEE Journal of Radio Frequency Identification*, vol. 3, no. 4, pp. 252-258, 2019. Available: 10.1109/jrfid.2019.2912959.

[36] X. Huang et al., "Binder-free highly conductive graphene laminate for low cost printed radio frequency applications", *Applied Physics Letters*, vol. 106, no. 20, p. 203105, 2015. Available: 10.1063/1.4919935.

[37] "SL900A EPC Class 3 Sensory Tag Chip - For Automatic Data Logging", *Ams.com*, 2018. [Online]. Available: https://ams.com/documents/20143/36005/SL900A_DS000294_5-00.pdf/d399f354-b0b6-146f-6e98-b124826bd737. [Accessed: 04- Aug- 2021].

Chapter 8: Conclusion and Future works

The thesis focused on integrating printed graphene technology into different antenna designs to conquer the most concerned surge in electronic waste caused by the mass production of antennas spurred by the mass deployment of IoT applications, achieving flexible, biodegradable, and low-cost antennas suitable for the implementation of next-generation communication networks. In Chapter 3, the graphene flakes were exfoliated in NMP solvent with no binder added, obtaining a conductivity of 3.68×10^4 S/m. A novel wideband (2.22 GHz to 3.85 GHz, 53.71% fractional bandwidth), $110\,mm \times 110\,mm$ 4x4 MIMO antenna has been constructed and fabricated using this ink, with four single antennas perpendicularly placed to each other for orthogonal polarization diversity. This specially designed antenna has been proved with extraordinary flexibility (160° bending limit), effective radiation, and minimized ECC (0.2×10^{-6}), demonstrating the capability of stable and high-power applications of the antenna. This first-ever graphene-printed MIMO antenna, whose success takes graphene antenna applications beyond low power radiation dipole antennas and RFID, has demonstrated its promising potential for systems where timely response and high data throughput are required.

In Chapter 4, by using the graphene ink prepared with the same method, a flexible array antenna on paper substrate was designed and fabricated. This antenna was aimed for 5.8 GHz radars, portable electronic devices, and commercial wireless LAN applications. The outstanding radiation performance of the array antenna was verified by its 73% total radiation efficiency (stays above 70% from 5.28 GHz to 6.37 GHz) and peak gain value of 4.5 dBi at 5.8 GHz, with

its bandwidth ranges from 4.6 GHz to 7.9 GHz (52.8%). Comparing to a conventional half-wave dipode with a gain of 2.15 dBi, typical graphene printed dipole with a gain of -0.6 dBi, this compact graphene printed array antenna is well-designed and realising excellent beamforming.

The research in Chapter 5 extended the design to the implementation of a 56 mm×60 mm graphene printed tri-band antenna which can support communication applications in a larger range of commercial bands: L band, the fifth generation (5G) sub-6 GHz band and 5.2 GHz wireless local area network (WLAN). The bandwidth of the antenna covers 1.2 GHz-1.9 GHz, 2.8 GHz-4 GHz and 4.5 GHz-5.8 GHz, realizing simultaneous signal transmission in different bands. The evolution of the antenna structure was carried out, involving different meandered line structures. At different resonance, the antenna would radiate with different designated structures. The peak gain of this antenna reaches 2.14 dBi at 3.8 GHz, indicating valid power transmission, but this is not stable as the gain cannot stay above 0 dBi for the entire three desired frequency ranges.

Another dual-band array antenna was further proposed with bandwidths of 1.74-2.72 GHz (55.96%) and 3.44–6.26 GHz (81.98%), consequently revealing it as a good candidate for high data rate IoE system in both 2.4 GHz and 5 GHz WiFi and WLAN mobile communication use. The peak gains of this antenna are 2.37 dBi and 2.55 dBi at 2.05 and 5.06 GHz, respectively, showing remarkable power transmissions and radiation performances at both frequencies, strong and stable wireless connections can therefore be guaranteed, but with the increase in size (70×210 mm) for sacrifice.

The work in Chapter 7 took the graphene ink industrial production to the next level by investigating the feasibility of Cyrene ink circulation method and the

change in sheet resistance after every shear mixing operation cycle. This method is based on a recent research about highly conductive (7.13×10^4 S m^{-1}) and stable Cyrene graphene ink. By using this sustainable method, the severe limitations brought by the very high price of Cyrene can be eliminated by reusing the ink after centrifugation, separating the supernatant liquid and the highly concentrated graphene slurry. It was found that, with an increasing cycle number, the sheet resistance decreases first, then rises to a steady state, indicating a balance between the rising trend of resistance brought by the increase of interfaces and the declining trend caused by filling of gaps by small thin flakes can be achieved in the end. The performance of the recycled cyrene graphene ink printed battery-free wireless UHF RFID sensory tag has successfully verified the ink quality for valid power transmission.

Within this field, further research can be focused on:

- Actual application tests of the designed antennas, i.e., on curved walls, pillars, or human body, can be further investigated, as the change in substrate would likely cause degradation of radiation. If necessary, a tunable metasurface layer can be added on top to enhance the directivity of the antenna and realize higher gain, or put in between to reflect the signals in the opposite direction to the degrading substrate.
- The efficiency boost of adding shear mixing exfoliation before ultrasonication bath treatment should be evaluated. It is known that adding shear mixing would increase exfoliation efficiency, but no systematic optimization process has been done. The conductivity and concentration of two set of ink samples can be compared, with one set of them processed with certain shear mixing time then ultrasonication treatment, the other set taken straight to

ultrasonication with the same bath sonication time. This should show how shear mixing procedure helps enhancing graphene ink fabrication efficiency.

- The dual- and tri-band antennas in Chapter 5 and 6 are either too big for portable devices or suffering from instability of radiation performance. To achieve better integration with the vast development of 5G technology, compact antennas with reliable power transmission functionalities are needed. Alterations in design structures should be carried out to improve.
- The major cause of the discrepancy between simulation results and experimental data lies in the unevenness of the printed graphene layer. The sheet resistance of printed graphene layer can range from 0.3-3.5 Ω/sq, which means some structural designs may not function as what we expect. An improved method for smoother, controllable, and more precise graphene printing should be developed and evaluated.